THESIS FOR THE DEGREE OF DOCTOR OF PHILOSOPHY

Identical emitters of light in open quantum systems

THERESE KARMSTRAND

Department of Microtechnology and Nanoscience
Applied Quantum Physics
Chalmers University of Technology
Göteborg, Sweden, 2024

Identical emitters of light in open quantum systems
THERESE KARMSTRAND
ISBN 978-91-8103-063-1

Doktorsavhandlingar vid Chalmers tekniska högskola
Ny serie nr 5521
ISSN 0346-718X

Applied Quantum Physics
Department of Microtechnology and Nanoscience
Chalmers University of Technology
SE–412 96 Göteborg
Sweden
Telephone +46 (0)31-772 1000

Chalmers Digitaltryck
Göteborg, Sweden, 2024

Identical emitters of light in open quantum systems
THERESE KARMSTRAND
Applied Quantum Physics
Department of Microtechnology and Nanoscience
Chalmers University of Technology

Abstract

The development of quantum mechanics has drastically changed the perspective on how we perceive the world. This has created a world that is now racing for the next new quantum technology. Accompanying this racing is an explosion of technological advancements that have facilitated experimental studies of light and matter interactions with unprecedented control down to the nanoscale. Improved experimental control and resolution, as well as the demonstration of strong light-matter interactions in new platforms, open the possibility of discovering unconventional phenomena that previously have been overlooked. This thesis explores light and matter phenomena with identical emitters of light and light confined in a cavity. The work is divided into two parts. The first part looks at the correlations that can arise between two-level emitters and a cavity field, and the complex behaviors arising from the competition between coherent driving, collective coupling, and dissipation. The second part revolves around the intriguing properties of polaritons formed due to the interaction between a microcavity and the collective bright mode in an array of harmonic nanoresonators, sustaining surface plasmon modes. The effects of dissipation is an important recurring theme.

Keywords: Open Quantum Systems, Quantum Optics, Quantum Plasmonics, Cavity QED, Collective effects, Nonequilibrium Critical Phenomena, Polaritons, Strong Coupling, Ultrastrong Coupling, Tavis–Cummings model, Hopfield Model

Acknowledgments

All the incredible people in my life have made this thesis possible.

My first acknowledgment goes to my patient supervisor, Göran Johansson. My Ph.D. experience has been similar to growing up as a teenager and preparing for an independent life as an adult, but now in a scientific context. Thus, it is good that you are not only a great scientist but also have parenting skills. Thank you for encouraging me, accepting my journey, and trusting me to find my own path. I am grateful for your support and guidance and our many inspiring discussions.

My next thank you goes to my co-supervisor, Timur Shegai. I am deeply grateful for your scientific guidance, which has been a great source of inspiration throughout my Ph.D. I also admire your eagerness to learn and improve yourself both as a scientist and a leader. Thank you for pairing me with Adriana, which led to a very successful collaboration that has given me a great start on my scientific career. And, lastly, thank you for adopting me as a side character in your group. Thanks to your open doors, I have had the opportunity to meet and learn from all the excellent people you attract.

I am also grateful for the support of all my co-authors, who have made the work presented in this thesis possible. All of you have taught me different skills that I will carry with me on my scientific journey.

Adriana Canales Ramos, I don't even know where to begin. You are one of the most inspiring people I have met. You radiate, and your passion for physics makes everyone excited. I am so grateful for all our discussions and all your support. It has really been a pleasure to learn together with you.

Maryam Khanahmadi, you are a brilliant quantum scientist, and I am sure you will achieve greatness. I am happy to have the opportunity to learn from you.

Timo Hillman and Théo Sépulcre, thank you for always having time to discuss dissipative phase transitions with me.

Christian Spånslätt Rugarn, thank you for being a great office mate and for sharing your experiences as an early-career scientist. Your advice will greatly help me navigate life as a postdoc.

Lastly, to Oliver, the love of my life. I would never have made it without you.

Therese Karmstrand, Göteborg, May 2024

List of publications

This thesis is based on the following papers:

A *Unconventional saturation effects at intermediate drive in a lossy cavity coupled to a few emitters*
Therese Karmstrand, Benjamin Rousseaux, Anton Frisk Kockum, Timur Shegai, and Göran Johansson,
Phys. Rev. A **108**, 053706 (2023)

B *Characterization of the output field in the driven-dissipative Tavis–Cummings model*
Therese Karmstrand, Maryam Khanahmadi, Zeidan Zeidan, and Göran Johansson
In preparation

C *Successive quasienergy collapse and breakdown of photon blockade in the few-emitter limit*
Therese Karmstrand, Göran Johansson and Ricardo Gutierrez-Jauregui
J. Opt. Soc. Am. B **41**, C38-C47 (2024)

D *Polaritonic linewidth asymmetry in the strong and ultrastrong coupling regime*
Adriana Canales, **Therese Karmstrand**, Denis G. Baranov, Tomasz J. Antosiewicz, and Timur O. Shegai
Nanophotonics **12**, 4073–4086 (2023)

The following paper was published during my doctoral studies but is out of the scope of this thesis.

I *Fabrication and chemical lift-off of sub-micron scale III-nitride LED structures*
Lesley Chan, **Therese Karmstrand**, Aaron Chan, Pavel Shapturenka, David Hwang, Tal Margalith, Steven P. DenBaars, and Michael J. Gordon
Optics Express **28**, 1094-4087 (2020)

Contents

Chapter 1

Introduction

The advancement of science can be seen as a feedback loop between three equally important units: (i) theoretical hypotheses and predictions, (ii) experimental realization and observations, and (iii) new technology (generalization). Through bidirectional feedback, discoveries in one trigger new developments in the other two, and so, the wheel of science widens our understanding of the world and revolutionizes the society we live in.

A recent example of such cycle is the development of quantum mechanics at the beginning of the twentieth century. Driven by an urge to understand experimental and real-world observations, a new mathematical theory involving noncommuting operators was formulated. This new mathematical formulation of physics, *Quantum mechanics*, led to fundamental microscopic theories on the scale of single atoms and subatomic particles that revolutionized the basic understanding of the physics around us, and inspired inventions such as the transistor and the laser, igniting an explosion of technological advancements including the computer. Now, a century later, classical computation is racing with the rapid developments of quantum computation to claim the first place as the most powerful. And, generations are born that will learn and view the laws of quantum mechanics as naturally as previous generations honored Newtonian mechanics. Technological advancements have also facilitated studying quantum systems in a completely new light with an unprecedented level of control. Therefore, exciting new physics and innovations are expected in the near future.

The theoretical explorations presented in this thesis are inspired by recent experiments with emitters of light interacting with light fields confined in an external structure, e.g., between two mirrors in what is called a cavity. Here, an emitter of light refers to any material resonance with an optically active dipole transition that emits photons. This includes everything from two-level atoms to excitons in quantum dots or molecules, or to the collective motion of electrons in metallic nanoparticles. The systems of partic-

ular interest are systems where the interaction between the emitter and the light field is strong, i.e., when nonperturbative methods are needed to describe the observed phenomena accurately. The field of physics focusing on the quantum description of such systems is known as *cavity Quantum Electrodynamics* (cavity QED) and it is the main topic of the thesis.

The great technological progress in the last decades has facilitated experimental studies of light and matter interactions between emitters and confined light with unprecedented control down to the nanoscale. Following these rapid developments, the research in this thesis has been developed along two parallel lines. The first line has taken inspiration from experiments that have demonstrated the ability to strongly couple small collections of two-level quantum emitters to a single cavity mode with incredible precision of positions, joined by an ability to probe their collective state via coherent driving fields. These experiments define a *few-body* regime of cavity QED that allows for monitoring the correlations that arise between the emitters and the light field. This line of research is also inspired by non-conventional cavity modes, such as plasmonic nanoresonators, as platforms for cavity QED. The second line of research focuses on strong and ultrastrong coupling with *harmonic* light emitters and also draws inspiration from plasmonic nanoresonators. In this case, the nanoresonators act as emitters that can be placed in cavities. This will lead to the formation of hybridized light-matter states called polaritons. Polaritons are intriguing quasiparticles that have gained significant attention due to their potential for engineering of new exotic properties, different from the properties of the bare constituents.

In the current era of quantum technology, it has also become evident that interaction with the environment is inevitable, no matter the attempts of shielding. In fact, the shielding in itself can change the properties of the system, as in the Purcell effect where the presence of two mirrors can change the radiative properties of a two-level atom. Therefore, the works of this thesis concern open quantum systems that include the effect of environmental interactions. Until recently, the common notion has been that this interaction typically induces decoherence, i.e., it destroys the quantum mechanical properties of the system. However, as the understanding of these incoherent interactions has grown, there are now many proposals for environmental engineering that harness interactions with the environment. The works presented in this thesis continue along these lines and showcase that the environment, indeed, plays an important role in stabilizing the system in steady states with specific properties.

1.1 What is light and matter?

As light-matter interactions are central components in all the appended works, let's start this thesis with a discussion on what is light and matter.

Historically, the classical description of physics has made a clear distinction between them: light is waves of electromagnetic radiation governed by Maxwell's equations, and matter is constituted by massive particles occupying space governed by Newton's laws. This distinction will agree with the intuitive picture of most readers of this thesis. The formulation of quantum mechanics changed this distinction by introducing wave-particle duality. In the quantum mechanical picture, light and matter alike can be ascribed to having wave and particle properties. In particular, quantum mechanics introduces the concept of wave functions to describe the state of a system which, for example, implies that states of matter also manifest interference effects. Moreover, quantum mechanics introduces the *photon* as a bosonic elementary particle. The photon is a single quantum of light with a well-defined energy and is used to describe the particle properties of light. The wave-particle duality fades the lines dividing light and matter. Nevertheless, a common distinction is that light is described by photons, while matter is not. Light-matter interaction, on the other hand, can blur the distinction between light and matter even further. Due to the formation of quasiparticles, new terms such as photon-like and matter-like, as well as photon/matter components, are introduced. Quasiparticles will be the topic of the next section which introduces the light-matter quasiparticles known as *polaritons*. Polaritons are, in many aspects, important for this thesis. Chapter 8 deals, for example, with the intriguing properties of plasmon-microcavity polaritons. And, as will be clear from the following section, polaritons play a fundamental role in this thesis both as a confined light-like mode and as a matter-like resonance playing the role of an emitter.

1.2 Light-matter hybridization: *Polaritons*

First, let's introduce the concept of quasiparticles. In simple words, a quasiparticle is a particle that includes the effects of an interaction with one or many other particles. Typically, they are found by diagonalizing the matrix representation of the system Hamiltonian including interactions. Then, knowing linear algebra, it is easy to see that the new quasiparticle description will contain a mixture of the bare components entering the Hamiltonian. The word "*bare*" here is used to emphasize that the particle is "un-dressed" by the interaction.

Polaritons are quasiparticles formed in a medium due to a strong interaction between photons and an active dipole transition in the material. These quasiparticles represent hybrid quantum systems that combine properties of both light and matter, often yielding

new intriguing characteristics. The most important types of dipole transitions for this thesis are the dipole-modes of *localized surface plasmon polaritons* and the dipole transition of effective two-level systems, which are components of the light-matter systems studied in this thesis. Plasmons are themselves quasiparticles formed due to interactions in the free electron plasma of metallic structures. This demonstrates how a quasiparticle description can reduce the physical description of the system by including the interaction in "new" particles which will carry the relevant properties of the system and which can interact with other elementary particles and quasiparticles in more complex compound systems.

1.2.1 Plasmonic nanoresonators

When a slab of metal or a metal nanoparticle is illuminated with an incident electromagnetic wave, a collective oscillation of the free charge density can be excited due to the interaction with the incident wave. As a result, the combined light-matter system forms hybridized states containing both light and matter components. At the metal-environment boundary, such a light-matter wave is closely related to a confined electromagnetic wave, similar to the internal field inside a cavity. This phenomenon is what is referred to as surface plasmon polaritons or SPPs [1, 2] In contrast to normal cavities, SPP modes have subwavelength confinement which can greatly enhance the interaction with two-level quantum emitters. Therefore, these hybrid light-matter cavities have gained a lot of attention recently for the realization of various phenomena in quantum optics [3–7].

The close analogy to confined electromagnetic waves allows for the adaptation of traditional cQED theory to these hybrid systems with SPP modes taking the roles of cavity modes [4, 7–11]. Even so, the matter part of these hybrid cavities gives them very different characteristics than traditional cavities. Besides breaking the diffraction limit with subwavelength confinement of the light component, these hybrid cavities have inherently broad line widths and are strongly dissipative [4]. This opens up for investigation of quantum-optical phenomena in a new regime that is so far not well explored. Interestingly, even the unusual ultrastrong-coupling regime[12] appears suitable for study with dissipative quantum systems [13–16].

So far, many observations of quantum-optical phenomena with plasmonic cavities have been limited to Rabi splitting in the spectrum [3, 17, 17–20]. Yet, the characteristic mode splitting referred to as Rabi splitting is equally well described by a classical coupled-oscillator model [21, 22]. Some difficulties with measuring quantum effects in these systems arise from the strong dissipation. For example, large power is needed for saturation of the emitters, and ultra-short lifetimes complicate the observation of nonclassical photon counting statistics. That being said, several works employing plasmonic nanoresonators have demonstrated quantum effects. One early work is found in

Ref. [23] which shows that plasmonic resonators can be used for transfer of entangled photons. Later, Ref.[24] demonstrated robust transfer of quadrature-squeezed states with SPPs in a gold waveguide. Another experiment measured single-molecule strong coupling at room temperature with a plasmonic nanocavity [25]. More recently, there have also been demonstrations of polariton condensation [26, 27].

Inspired by this new regime for quantum optics, our work in Paper A follows the direction set by Refs. [23–25] and challenges the idea that large dissipation always destroys quantum effects. By doing so, our explorations of the otherwise already well-studied Tavis–Cummings model for an ensemble of two-level emitters in a cavity unveil a nonlinear phenomenon under coherent driving that stands resilient to high cavity dissipation. Localized surface plasmons are also key components in the study presented in Paper D. There, they form plasmon-cavity polaritons with intriguing properties.

Chapter 2

Basics of light-matter interaction: from weak to ultrastrong coupling

After reading the introductory sections, it should be clear that the interaction between light and matter is an integral part of this thesis. Therefore, this section will introduce the basics of light-matter interaction and the different regimes categorized by coupling strength.

2.1 Classical description

In a classical description, light-matter interaction is governed by the Lorentz force

$$\mathbf{F} = q(\mathbf{E} + \mathbf{v} \times \mathbf{B}) \tag{2.1}$$

acting on a charged particle with charge q moving with the velocity $\mathbf{v}$ in an electric $\mathbf{E}$ and magnetic $\mathbf{B}$ field. While knowledge of the Lorentz force allows for deriving equations of motion for the particle in an electromagnetic field, Maxwell's equations instead relate the electric and magnetic fields with a given distribution of the charge ρ and current $\mathbf{J}$ densities in matter:

$$\nabla \cdot \mathbf{E} = \frac{\rho}{\varepsilon_0}, \tag{2.2}$$

$$\nabla \cdot \mathbf{B} = 0, \tag{2.3}$$

$$\nabla \times \mathbf{E} = -\frac{\partial \mathbf{B}}{\partial_t}, \tag{2.4}$$

$$\nabla \times \mathbf{B} = \mu_0 \left(\mathbf{J} + \varepsilon_\mathbf{0} \frac{\partial \mathbf{E}}{\partial_\mathbf{t}} \right). \tag{2.5}$$

The use of the vacuum permittivity ε_0 and permeability μ_0 in these equations reflects the fact that the material properties are included in the charge and current terms, describing *all* charges and currents in the material explicitly. Due to the latter, these equations can be applied to relate the electric and magnetic fields to the charges and currents down to the atomic limit (within the boundaries of classical mechanics). Therefore, this formulation is called the *microscopic* Maxwell's equations.

To describe the propagation of light in large structures of matter, it is often convenient to instead use the so-called *macroscopic* Maxwell's equations. The macroscopic Maxwell's equations differentiate between free and bound charges and currents in the material. This introduces two new fields: the displacement $\mathbf{D}$ and magnetic intensity $\mathbf{H}$ fields, which are related to the electric and magnetic fields through the constitutive equations

$$\mathbf{D} = \varepsilon_0 \mathbf{E} + \mathbf{P} = \varepsilon_0 \varepsilon_r \mathbf{E}, \tag{2.6}$$

$$\mathbf{H} = \mu_0 \mathbf{B} - \mathbf{M} = \mu_0 \mu_r \mathbf{B}. \tag{2.7}$$

In this way, material properties due to induced electric dipoles and magnetic moments bound in the material are included in terms of the polarization $\mathbf{P}$ and magnetization $\mathbf{M}$ fields. In linear media, $\mathbf{P}$ and $\mathbf{M}$ depends linearly on $\mathbf{E}$ and $\mathbf{B}$, respectively, making it possible to express the $\mathbf{D}$ and $\mathbf{H}$ fields through the relative permittivity ε_r and permeability μ_r. Generally, a macroscopic matter component is necessary to validate the underlying averaging of the microscopic processes that give rise to ε_r and μ_r. Hence, the name "macroscopic" Maxwell's equations. With the introduction of $\mathbf{D}$ and $\mathbf{H}$, Eqs. (2.2) and (2.5) above are replaced by the equations

$$\nabla \cdot \mathbf{D} = \rho_f, \tag{2.8}$$

$$\nabla \times \mathbf{H} = \mathbf{J}_f + \frac{\partial \mathbf{D}}{\partial_t}, \tag{2.9}$$

where the index f is now introduced to denote the free charges and currents in the material. An in-depth introduction to classical electrodynamics can be found in textbooks [28, 29].

The theoretical work of Paper D, led by A. Canales, employs a classical formulation of light-matter interaction to study polaritons from the weak- to ultrastrong-coupling regimes. In particular, a classical scattering matrix approach was used where the transmission and reflection coefficients are obtained with an effective permittivity for the nanoparticle arrays, found by fitting to numerical simulations of the reflection spectra. The reflection spectra were, in turn, obtained from numerical solutions of the macroscopic Maxwell's equations using tabulated experimental data for the relative permittivity ε_r in gold.

2.2 Quantum description

The physical picture underlying the construction of Maxwell's equations and Lorentz force law presented above is one about charged particles moving in potentials. Naturally, this picture is shared with the quantum-mechanical formulation of light-matter interactions, but the latter conversely relies on a Hamiltonian description with quantized fields.

The light-matter Hamiltonian derives from a Lagrangian formulation [30], employing the minimal coupling replacement $\mathbf{p} \rightarrow \mathbf{p} - q\mathbf{A}$ of the kinetic momentum for a charged particle with charge q interacting with an electromagnetic field described by the potential $\mathbf{A}$. In the simple case of a single electron moving in a one-dimensional potential, that couples to a single confined electromagnetic mode, the minimal-coupling replacement gives the following light-matter Hamiltonian in the Coulomb gauge [30, 31]

$$H_C = \frac{\left[\mathbf{p_e} + e\mathbf{A}(\mathbf{x_e})\right]^2}{2m_e} + V(\mathbf{x_e}) + H_f, \tag{2.10}$$

where H_f denotes the bare electromagnetic field Hamiltonian. Equation (2.10) could, e.g., describe a one-electron atom coupled to a single-mode cavity, where one electron has the predominant interaction with the field. Or, a complex many-particle system where the effect of the other particles/surrounding medium can be described as a one-dimensional potential in which the electron is moving. The square of the kinetic momentum $(\mathbf{p} + e\mathbf{A})^2$ describes the particle's kinetic energy including the interaction with the electromagnetic field and is the source of the familiar light-matter interaction term $\mathbf{p} \cdot \mathbf{A}$, and $\mathbf{A}^2$ term in the Coulomb gauge ($\nabla \cdot \mathbf{A} = 0$). Note that the corresponding Hamiltonian in the dipole gauge is easily obtained with the Power-Zienau-Woolley transformation [32].

So far, the principles introduced here are the same in the quantum mechanical and classical descriptions of light-matter interactions. Indeed, the classical Maxwell-Lorentz equations from the previous section can be derived from the minimal-coupling Lagrangian. The quantum-mechanical description is attained after a canonical quantization of the dynamical variables, which in the light-matter case are the position of the particle, the electromagnetic potential, and their conjugate momenta.

The (quantum) light-matter Hamiltonians of interest for this thesis are the famous Tavis-Cummings and Hopfield Hamiltonians. The former describes the collective interaction between an ensemble of quantum emitters, modeled as two-level systems, and a confined single-mode electromagnetic field under the dipole and rotating wave approximations. The few-emitter limit of this Hamiltonian is the theoretical foundation for Paper A-Paper C and it will be introduced in Chapter 4. The Hopfield Hamiltonian instead describes the coupling between a bosonic material excitation and the electromagnetic field. This Hamiltonian is introduced in Chapter 7 and is the center of attention

in the second part of the thesis that studies polaritons formed with the collective bright mode in an array of plasmonic nanoparticles and a single-mode microcavity.

2.3 Different regimes of light and matter coupling

The behavior of confined electromagnetic modes and resonant material excitations is heavily influenced by the strength of their interaction. Consequently, terminology such as *weak*, *strong* and *ultrastrong* has been coined to categorize the different observed behaviors in terms of the light-matter coupling strength. The categorization is not as straightforward as it may seem at first glance, however. During my Ph.D., I have encountered few other words with so many ambiguities about the connotation as the phrase "*strong coupling*". It seems that most light-and-matter scientists hold a clear idea of strong coupling in their minds, and still, their use of the phrase so often implies different things. The source of the confusion is that the definition of strong coupling is contextual. Certainly, losses and resolution are also important factors [21, 33–35].

This thesis is written in the context of modeling interacting light and matter systems. From this perspective, the categorization is rather straightforward and directly relates to the level of approximation made in the light-matter Hamiltonian. Taking the Hamiltonian as the foundation for the categorization instead of contextual observations gives a natural ordering of the different regimes, going from weak to strong to ultrastrong. The observations will, of course, be strongly tied to the predictions using a certain Hamiltonian, but taking the modeling as the base for the categorization provides a more transparent perspective on what physics underlies the expected characteristics of each regime. This perspective, moreover, circumvents the contradictory ordering in highly dissipative systems reaching ultrastrong coupling while not being in the conventional strong-coupling regime due to large losses [15].

The categorization and the main characteristics of the different regimes can be exemplified with the quantum-Rabi model [36], including losses. The Rabi model describes a two-level atom with transition frequency ω_0 in a single-mode cavity with resonance frequency ω_c. Losses can be introduced in a microscopic picture using an open-quantum-system approach, e.g., the Lindblad master equation, which will be discussed in more detail in Chapter 3. Here, we satisfy with phenomenologically introducing photon loss from the cavity with the decay rate κ, and spontaneous emission from the two-level atom with the decay rate γ. This approach suffices for the current discussion. The parameter governing the characterization is the light and matter coupling strength g. The system is shown schematically in Fig. 2.1(a), and a summary of the different regimes and their main characteristics are shown in Fig. 2.1(b)-(d).

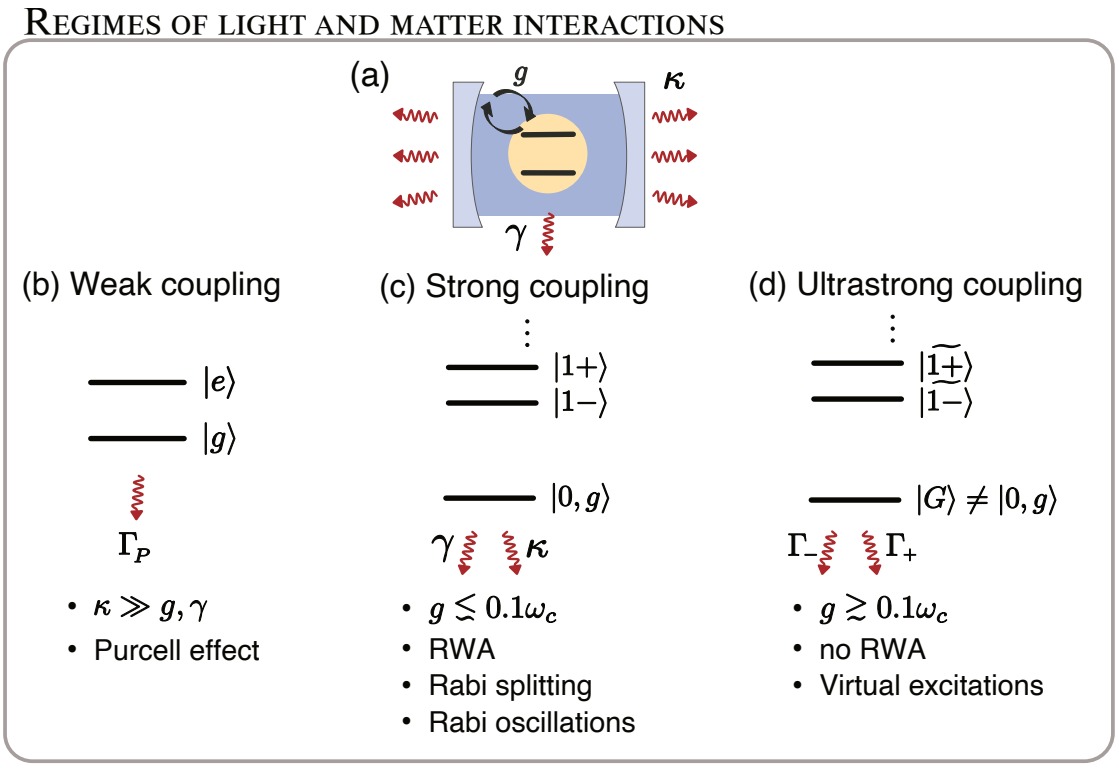

Figure 2.1: (a) Schematic illustration of a two-level system in a cavity with losses and its main characteristics in the (b) weak-, (c) strong-, and (d) ultrastrong-coupling regimes.

2.3.1 Weak coupling

The system is in the *weak-coupling regime* when the cavity's effect on the two-level atom can be considered a small perturbation. In this regime, the bare eigenstates of the two-level system are adequate to describe the system dynamics, and the effect of the cavity is cavity-enhanced or prohibited spontaneous emission due to the Purcell effect [37]. In a full quantum treatment, as is given by the Rabi Hamiltonian including losses, this regime allows for adiabatic elimination of the cavity. In a microscopic picture, the adiabatic elimination comes down to tracing out the cavity's degrees of freedom, giving an effective model for the two-level atom only, including the cavity's effects as parameters. An example is the elimination of a near-resonant cavity which opens up an extra decay channel for spontaneous emission. In this case, after tracing out the cavity's degrees of freedom, one finds the cavity-enhanced spontaneous emission rate $\Gamma_P = \gamma[1 + 4g^2/(\gamma\kappa)]$ [38]. The permission of adiabatic elimination of the cavity sets a practical condition for calculations which is $\kappa \gg g, \gamma$. This condition ensures that the cavity's linewidth can be approximated as a continuum of modes in the view of the two-

level atom. Physically, the condition means that the cavity's decay time is fast enough to dissipate an excitation transferred from the two-level system before it can be reabsorbed due to the light-matter coupling. Of course, one could also consider a reversed picture where the matter part is the lossy constituent acting as a small perturbation on the light mode.

2.3.2 Strong and ultrastrong coupling

The *strong-* and *ultrastrong-coupling* regimes are defined when the light and matter interaction can no longer be considered perturbative. Building on the definition of weak coupling stated above, this occurs when the probability for re-absorption of a photon exchanged with the cavity becomes non-negligible within the effective relaxation time of the system. At these coupling strengths, the effective model for the two-level system without the cavity breaks down, and both the cavity and the two-level system need to be included in the Hamiltonian for an accurate description of the dynamics. In this description, the bare states are no longer approximate eigenstates of the system. Instead, the light-matter interaction leads to the formation of dressed eigenstates – polaritons – which mix the light and matter degrees of freedom. This is true in both the strong- and ultrastrong-coupling regimes. From a modeling perspective, the difference between the strong- and ultrastrong-coupling regimes is the approximations made in the light-matter Hamiltonian.

In the dipole gauge, the Rabi Hamiltonian can be written as [39]

$$\hat{H}_{\mathrm{Rabi}} = \frac{\hbar\omega_0}{2}\hat{\sigma}_z + \hbar\omega_c\left(\hat{a}^\dagger\hat{a} + \tfrac{1}{2}\right) + i\hbar g\left(\hat{a} - \hat{a}^\dagger\right)(\hat{\sigma}_- + \hat{\sigma}_+), \tag{2.11}$$

where $\hat{\sigma}_z, \hat{\sigma}_+$, and $\hat{\sigma}_-$ are Pauli operators describing the two-level system and $\hat{a}, \hat{a}^\dagger$ are the standard bosonic annihilation and creation operators for the cavity mode. For this discussion, we are interested in the last term, which is the interaction part which describes the exchange of excitation between the cavity mode and the two-level system with the coupling strength g.

Here, we define the *strong-coupling regime* as the regime where the rotating-wave approximation (RWA) is permitted, thus, reducing the light-matter interaction part to[1]

$$\hat{H}_{\mathrm{RWA}} = i\hbar g\left(\hat{a}\hat{\sigma}_+ - \hat{a}^\dagger\hat{\sigma}_-\right). \tag{2.12}$$

The RWA takes the Rabi model to the familiar Jaynes–Cummings model [40, 41], for

[1] Going to a Heisenberg picture, it is easy to see that $\hat{a}^\dagger\hat{\sigma}_+$ and $\hat{a}\hat{\sigma}_-$ will be fast-rotating with double the frequency, while the other two terms $\hat{a}\hat{\sigma}_+$ and $\hat{a}^\dagger\hat{\sigma}_-$ will be approximately stationary and, thus, contribute significantly more to the dynamics of the system when g is not too large.

which the dressed eigenstates can be found analytically as

$$|n+\rangle = \sin(\theta_n)\,|n,\mathrm{g}\rangle + \cos(\theta_n)\,|n-1,\mathrm{e}\rangle\,, \tag{2.13}$$
$$|n-\rangle = \cos(\theta_n)\,|n,\mathrm{g}\rangle - \sin(\theta_n)\,|n-1,\mathrm{e}\rangle\,, \tag{2.14}$$

with $2\theta_n = \tan^{-1}[\sqrt{n}g/(\omega_0-\omega_c)]$. Note that these strong-coupling dressed states are excitation-number conserving and, in particular, the dressed ground state coincides with the bare ground state $|0,\mathrm{g}\rangle$. These properties are important for validating the use of the standard Lindblad operators in a microscopic treatment of dissipation in the strong-coupling regime. The corresponding eigenenergies,

$$\hbar\omega_{n,\pm} = \left(n+\frac{1}{2}\right)\hbar\omega_c \pm \frac{\hbar}{2}\sqrt{(\omega_0-\omega_c)^2+ng^2}, \tag{2.15}$$

display the $\sqrt{n}$-anharmonicity of the Jaynes–Cummings model and the characteristic vacuum Rabi splitting $(\omega_{1,+}-\omega_{1,-}) = 2\sqrt{(\omega_0-\omega_c)^2+g^2}$ at the single-excitation level.

Clearly, the strong-coupling description is sufficient to describe mode-splitting and exchange of excitation between the light and matter modes. For this reason, the *observation* of these effects is commonly regarded as signatures of strong coupling. From a modeling perspective, on the other hand, there are no hard limits defining the strong-coupling regime as it is defined based on approximations whose breakdowns are expected to appear gradually and depend on the specific system and observable in mind. As a guiding rule of thumb, the limit $g < 0.1\omega_c$, commonly found in the literature, can be considered as an upper limit *in the case of the Rabi model*, as the eigenfrequencies obtained with and without the RWA start to visibly deviate at that value in this model[2]. Nevertheless, in Paper D, we demonstrated that the dissipative properties in a polaritonic system described by the Hopfield model can be much more sensitive to changes in the light and matter coupling than the spectral properties. These results are discussed in Chapter 8.

The definition of the *ultrastrong-coupling regime* naturally follows from the above definition as the regime of coupling strengths where the RWA breaks down. One important feature of this regime is that the dressed and bare ground states no longer coincide. This occurs due to the inclusion of the fast-rotating terms $\hat{a}\hat{\sigma}_-$ and $\hat{a}^\dagger\hat{\sigma}_+$ which removes the excitation-number conserving symmetry inherent in the Janynes–Cummings Hamiltonian. Therefore, the dressed states, including the dressed ground state, will be mixed with states containing different numbers of excitations. To see this, consider the so-called Bloch-Siegert regime where $g \ll \omega_c+\omega_0$. In this regime, the ground state can be found perturbatively as [42]

$$|G\rangle = (1-\Lambda^2/2)\,|0,\mathrm{g}\rangle - \Lambda\,|1,\mathrm{e}\rangle + \sqrt{2}g\Lambda/(2\omega_c)\,|2,\mathrm{g}\rangle\,, \tag{2.16}$$

[2]See, e.g., Fig. 2 in Ref. [12]

to second order in $\Lambda \equiv g/(\omega_c + \omega_0)^3$. This mixing of states with different excitation numbers is the source of the debated virtual excitations in the ground state [12, 15]. This non-excitation-conserving mixing also has implications for how to treat dissipation in this regime. The standard Lindblad treatment used in the weak- and strong-coupling regimes does not accurately induce transitions between the dressed eigenstates, which can lead to surprising results. This will discussed more in Chapter 3.

The A^2-term

The different regimes of light-matter coupling introduced in this section were exemplified with a two-level system interacting with a single-mode cavity. The discussed concepts, however, hold for many interacting light-matter systems stemming from a minimal-coupling Hamiltonian analog to the single-particle version given in Eq. (2.10). This includes the Hopfield model discussed in Chapter 7, and other systems where the material component can be described by a quantized polarization field. Yet, it is important not to forget the $\hat{A}^2$-term in the ultrastrong-coupling regime when a Coulomb gauge formulation is employed. The $\hat{A}^2$-term arises from squaring the kinetic momentum in the Coulomb-gauge Hamiltonian shown in Eq. (2.10). Since the $\hat{A}^2$-term will be second-order in the electric charge, it can, in general, be neglected when considering a dipolar transition in the strong-coupling regime, but needs to be included in the ultrastrong-coupling regime. The main effect of the $\hat{A}^2$-term is to stabilize the dressed eigenenergies as the coupling strength increases [12]. The $\hat{A}^2$-term can also be absorbed into the field modes by a Bogolioubov rotation, as will be done in Chapter 7. This leads to a shift in the field resonance frequency, which generally is small under conditions validating the RWA, thus, motivating its exclusion in this regime. The example with the Rabi model above, on the other hand, is discussed in a dipole-gauge formulation. The dipole-gauge formulation also has a square term, analog to the $\hat{A}^2$-term in the Coulomb gauge. But, in the dipole gauge, the square term contrarily emerges in the material polarization field. In the current example, this term corresponds to an $\hat{x}^2$-term which only contributes with a constant shift of the two-level system's eigenenergies [39], that don't change the transition frequency. Hence, this term was omitted.

2.3.3 Different perspectives on strong coupling

The introductory clause to this section indicated that losses and resolution have been important factors behind inconsistent definitions of strong coupling. Inappropriately mixing concepts from quantum optics and classical descriptions of light-matter interactions is likely also a factor causing misconceptions. Above, a categorization based on a quantum modeling perspective was provided as an alternative. The definitions given

[3]The dressed eigenstates of the Rabi model can also be found analytically [43], but the expressions are complicated and provide little insight.

from this perspective deliberately avoid limits in terms of specific parameters. Instead, the level of approximations going into the light-matter interaction model is employed as a basis for the categorization. This approach emphasizes that the different regimes of light-matter interactions are contextual in the sense that the specific parameters of each platform and the specific observables determine the appropriateness of approximations. This way of differentiating between the different regimes provides a natural ordering going from weak to strong to ultrastrong coupling.

While the discussion about this categorization was made explicit by studying the quantum-Rabi model, the introduced concepts also transfer to other interacting light-matter systems that can be described by a light-matter interaction Hamiltonian on the form in Eq. (2.10). For example, systems where the material component can be described by a quantized polarization field [38], as demonstrated by Hopfield [44]. Much of the concepts also transfer to classical systems that can be described in terms of quantized fields, even though the displayed physics is essentially classical. The quantum mechanical description can then provide insights into the underlying processes that give rise to certain behaviors by offering means to turn on and off approximations, such as the RWA, which is not possible in a formulation based on Maxwell's equations. However, the direct adoption of quantum-optical concepts in a classical context should be avoided without a proper analysis of the underlying Hamiltonian, as has been noted in several areas of polaritonics [45, 46]. It should also be noted, that the perspective provided above is a quantum-optical perspective where the level of approximations governs what effects can be explained. From a classical perspective, these approximations have no meaning, as the solutions of Maxwell's equations do not make those distinctions. Most of the observations above – Purcell effect, mode splitting, and exchange of excitations – can equally well be described by classical models [21, 38] that inherently include all effects of the light-matter interaction through Maxwell's equations.

The rest of this subsection is dedicated to broadcasting two other perspectives on strong coupling that are relevant to this thesis. Both of them provide context to the discussion on decay rates in Paper D and Chapter 8. Let's begin with the strong-coupling limit $\Omega_R > (\kappa + \gamma)/2$ adopted in Paper D. This limit is defined in terms of the effective "Rabi" splitting [4], $\Omega_R \equiv (\omega_{\mathrm{eff},+} - \omega_{\mathrm{eff},-})$, where $\omega_{\mathrm{eff},\pm}$ are the effective polaritonic resonances including the effects of losses [5] . The reasoning behind this strong-coupling limit is that two distinct spectral peaks should be resolved. This generally occurs when the mode-splitting is larger than the average decay rate $(\kappa+\gamma)/2$, which approximately

[4]Quotation marks are used here as the Rabi model is not needed to observe mode splitting, but the terminology is still used as it is customary in many areas of nanophotonics.

[5]Expressions for the effective polaritonic resonance frequencies $\omega_{\mathrm{eff},\pm}$, which will be shifted compared to the bare frequencies due to the losses, can be found phenomenologically using a non-Hermitian Hamiltonian for two lossy coupled modes, see below. The same effective expressions for the resonances also show up in analytical calculations of the optical spectrum for spontaneous emission through the sides of the cavity in the quantum-Rabi model discussed above [38].

describes the polaritonic line widths in the strong-coupling regime. However, this limit is not fundamental and, in many situations, it is possible to observe two spectral peaks emerging before this point, as was demonstrated in Paper D[6].

Another perspective, which is consistent with our observations in Paper D, is provided by a non-Hermitian Hamiltonian formulation of two couled modes including losses. This approach is often employed phenomenologically in the strong-coupling community, but can also be derived from a Lindblad-master-equation approach by neglecting quantum jumps [47], see Section 3.4. Adopting the notation from the Rabi model above, but now for a generic light mode and material resonance, the matrix representation of a non-Hermitian-Hamiltonian description of the two coupled modes is given by

$$\mathrm{H}_{\mathrm{eff}} = \hbar \begin{pmatrix} \omega_c - i\frac{\kappa}{2} & g \\ g & \omega_0 - i\frac{\gamma}{2} \end{pmatrix}. \tag{2.17}$$

This effective Hamiltonian coincides with the matrix representations of the non-Hermitian Hamiltonians derived from the Lindblad master equation in the cases of a two-mode Hopfield model within the RWA, and the Jaynes–Cummings model at the single-excitation level. The eigenfrequencies of the Hamiltonian (2.17) are complex. Their real parts correspond to resonances and their imaginary parts correspond to decay. At zero detuning, $\omega_c = \omega_0$, the eigenfrequencies are given by

$$\omega_{\mathrm{eff},\pm} = \omega_0 - i\frac{\kappa+\gamma}{4} \pm \sqrt{g^2 - \left(\frac{\gamma-\kappa}{4}\right)^2}. \tag{2.18}$$

The expression under the square root displays that the eigenfrequencies will have an exceptional point [48, 49] at $g^2 = \left[(\gamma-\kappa)/4\right]^2$. Below this point, the real parts of the two solutions are degenerate as the square root is purely imaginary. This degeneracy is lifted at the exceptional point, and two different resonances can be observed.

Clearly, this result demonstrates another perspective on the emergence of two distinct spectral modes, that is based on the topology of the effective Hamiltonian and not the resolution of the measurement. If the existence of two distinct spectral modes is taken as the signature of strong coupling, this perspective gives the strong-coupling limit $g \geq |\gamma - \kappa|/4$, which is less restrictive than the limit based on resolution, stated above. This strong-coupling limit can also be related to the strong-coupling definition given in the example with the Rabi model. The connection is made via the non-Hermitian description of dissipation obtained by neglecting quantum jumps in the Lindblad master equation. The effective Hamiltonian given in Eq. (2.17) only coincides with the latter in the RWA. Thus, if one wants an explicit strong-coupling condition in terms of the losses, the limit presented here is a good candidate, even though the visibility of the

[6]See supplementary material, Figs. S5 and S6. Available at https://doi.org/10.1515/nanoph-2023-0492.

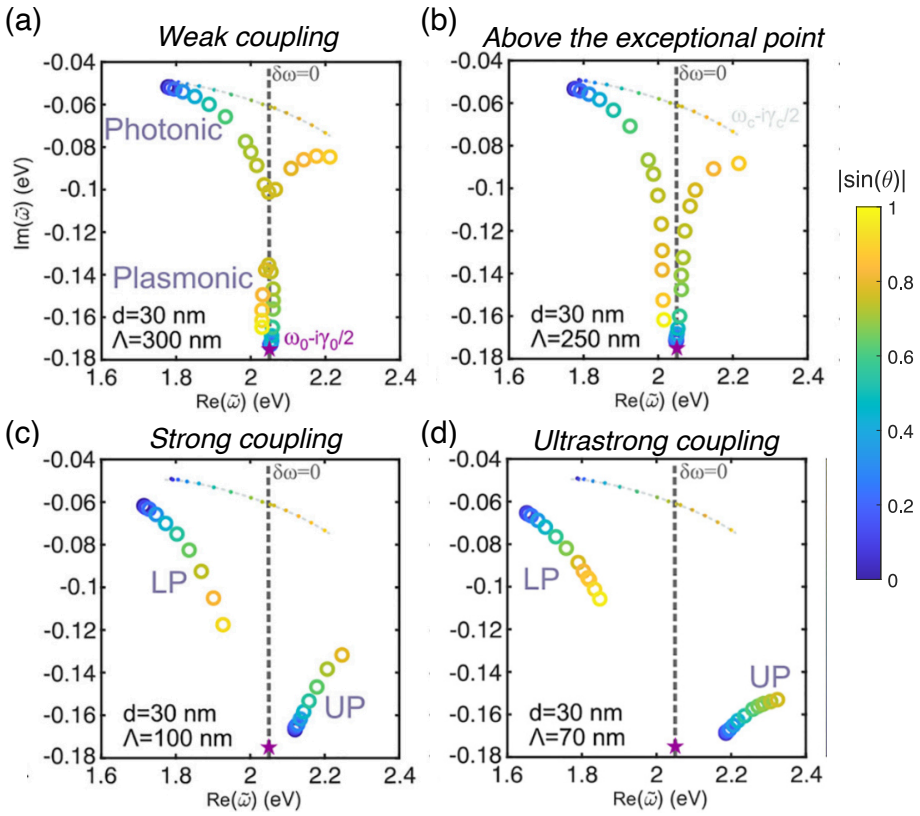

Figure 2.2: Eigenenergies in the complex-frequency plane are found as the poles of a classical scattering matrix. (a) At weak coupling strengths, there is a clear distinction between the photonic and plasmonic modes. (b) At the exceptional point, the real part of the trajectories split, demonstrating the appearance of two separate polaritonic resonances. (c),(d) At strong and ultrastrong coupling, there is a clear separation between the branches. The figure is adapted from Paper D [14] and the pole search was performed by A. Canales.

spectral modes close to the exceptional point can be limited, depending on the specific parameters of the studied system.

The non-Hermitian Hamiltonian description is a semiclassical approach to strong-coupling. In Paper D, A. Canales provided a classical analog to this description by performing an analysis of the poles to a classical scattering matrix in the complex-frequency plane. However, in contrast to the non-Hermitian Hamiltonian description, the scattering-matrix approach does not make any approximations on the regime of light-matter coupling, such as the RWA, nor is it introduced phenomenologically. The scattering matrix relates the incoming and scattered fields after the incoming field interacts with the system. In the complex-frequency plane, the real part of these poles

corresponds to resonances and the imaginary part to decay, $\tilde{\omega} = \omega - i\gamma$. Her results, adapted from Paper D, are shown in Fig. 2.2 and they display that the degeneracy of the resonances at zero detuning ($\delta\omega = 0$ in Fig. 2.2) in the weak coupling regime, is lifted above the exceptional point $g > |\gamma - \kappa|/4$. Thus, her results advocate a strong-coupling limit, which is in agreement with the non-Hermitian Hamiltonian description and is suitable in contexts where the light-matter system can be described classically.

Chapter 3

Open quantum systems

An open quantum system is a description of a quantum system that includes the interaction with the environment in which the system is embedded. The fundamental idea of an open-quantum-system description is a separation of all possible degrees of freedom into a few representing the system of interest, and "all the rest" representing the environment. After this separation, the principle is to derive effective equations of motion for the system's degrees of freedom, including the *effects* of the environmental degrees of freedom entering as parameters. This way, a probabilistic description of the time evolution of an otherwise large or, possibly, infinite physical system becomes tractable. How the derivation is carried out and the resulting equations of motion depend on the physical setting, and the methods used vary between different fields of research.

The effects of the environment are central themes in all the appended papers. In this work and all the appended papers, the well-established Lindblad master-equation formalism [50] is used. This formalism is the standard approach for treating weak interaction with the environment in cavity QED setups. The formalism is well explained in many textbooks on quantum optics [51–53]. Therefore, only the guiding principles and main approximations will be introduced. This will be done in Section 3.1. Section 3.2 will introduce the concepts of local and global environments, and Section 3.3 discusses different master equations suitable for the ultrastrong-coupling regime. Lastly, Section 3.4 briefly discuss the relation between Lindblad master equations and non-Hermitian Hamiltonians.

3.1 The Lindblad master equation

The Lindblad master equation treats the effects of the environment perturbatively and describes the dynamics of the reduced density matrix $\hat{\rho}_S$ for the system after tracing out the environmental degrees of freedom. The standard master equation in quantum

optics is obtained by modeling the environment as a reservoir of harmonic oscillators, representing the electromagnetic vacuum, and performing the *Born* and *Markov approximations*, as well as the *rotating wave approximation* [51–53]. The result of the derivation is an equation for the time evolution of the system's density matrix $\hat{\rho}_S$ which includes the effects of the environment as parameters. In the appended papers, we have additionally considered systems where thermal fluctuations can be neglected. Thermal fluctuations can, for example, be neglected at optical frequencies or at cryogenic temperatures. Neglecting thermal fluctuations gives a master equation in the following form,

$$\boxed{\dot{\hat{\rho}}_S(t) = -\frac{i}{\hbar}\Big[\hat{H}_S, \hat{\rho}_S(t)\Big] + \Gamma\bigg(\hat{L}\hat{\rho}_S(t)\hat{L}^\dagger - \frac{1}{2}\Big\{\hat{L}^\dagger\hat{L}, \hat{\rho}_S(t)\Big\}\bigg).} \tag{3.1}$$

Here, the first term describes unitary evolution with the system Hamiltonian $\hat{H}_S$ (including Lamb shifts) and the second and third terms describe incoherent evolution due to interaction with the environment. The inverse of Γ provides the characteristic timescale for the incoherent dynamics which is governed by the Lindblad jump operators $\hat{L}$. These operators are defined by the system operators involved in the system-environment interaction. A common example is single-photon loss with the annihilation operator for a leaky cavity mode.

The Born and Markov approximations

The derivation of the Lindblad master equation is performed with an undamped quantum system that is interacting weakly with a large environment, acting as a reservoir where information and energy from the system can be dissipated. The total system-reservoir Hamiltonian is

$$\hat{H} = \hat{H}_S + \hat{H}_R + \hat{H}_{SR}, \tag{3.2}$$

where $\hat{H}_S$ and $\hat{H}_R$ describe the bare system and reservoir, and $\hat{H}_{SR}$ decsribe the system-reservoir interaction. In quantum optics, the environment is commonly modeled as a large reservoir of harmonic oscillators, representing the continuum of modes in the vacuum electromagnetic environment. Though, other types of reservoirs are also possible [51]. It is, however, not important to specify the system and reservoir Hamiltonians explicitly to derive the general form of the Lindblad master equation, which in the interaction picture is written as

$$\boxed{\dot{\tilde{\rho}}_S(t) = -\frac{1}{\hbar^2}\int_0^t \mathrm{d}t'\ \mathrm{Tr}_R\bigg\{\Big[\tilde{H}_{SR}(t), \Big[\tilde{H}_{SR}(t'), \tilde{\rho}_S(t)\otimes\hat{\rho}_R\Big]\Big]\bigg\}.} \tag{3.3}$$

Here, the hats '$\hat{}$' on the operators are replaced with tildes '$\tilde{}$' to indicate interaction-picture operators and the reduced density matrix $\hat{\rho}_R$ for the reservoir is introduced.

Equation (3.3) is derived in the second-order *Born-Markov approximation*, starting from the interaction picture *Liouville-von Neumann equation*:

$$\dot{\tilde{\rho}}_{SR}(t) = -\frac{i}{\hbar}\Big[\tilde{H}_{SR}(t), \tilde{\rho}_{SR}(t)\Big]. \tag{3.4}$$

The Liouville-von Neumann equation is the analog of the Schrödinger equation for the density matrix and here it describes the time evolution of the total system-reservoir density matrix $\tilde{\rho}_{SR}$.

To make the Born- and Markov- approximations, it is important that the system-reservoir interaction is weak so that the effects of the environment can be treated perturbatively. In the second-order Born approximation, the weak interaction allows for neglecting terms higher than second-order in $\tilde{H}_{SR}$. It is also assumed that the reservoir is large (in comparison to the amount of dissipation, governed by the interaction strength), so the reservoir's statistical properties are only marginally affected by the interaction. The latter allows for taking the state of the reservoir $\tilde{\rho}_R$ to be approximately the same at all times, $\tilde{\rho}_R(t) \approx \hat{\rho}_R$. In the Markov approximation, it is assumed that the weak interaction allows for a separation of time scales, where the information that leaks out from the system is spread in the environment on a time scale that is much faster than the rate at which the information leaks out. In the derivation of the master equation, this assumption allows for making the replacement $\tilde{\rho}(t') \to \tilde{\rho}(t)$ in the integral Kernel. This replacement has the physical interpretation that the reservoir is memoryless in the sense that information leaks out from the system irreversibly and cannot be fed back to the system through the system-reservoir interaction.

The rest of the derivation, going from the general form in Eq. (3.3) to the standard Lindblad form master equation in Eq. (3.1), depends entirely on the specific system and reservoir. This is the cumbersome part of the derivation, involving the expansion of the commutator, evaluating reservoir correlation functions, and solving the resulting integrals. It is a good exercise to go through the math, but the standard derivation for common systems in cavity QED, including a lossy cavity, spontaneous emission from a two-level system, and collective dissipation from an ensemble of two-level systems, can be found in textbooks [52, 53] and is therefore not included here. Instead, the next section will discuss the concepts of local and global environments, which are important for modeling compound quantum systems but are often not explicitly discussed.

3.2 Local and global environments in complex quantum systems

Equation (3.1) above shows the Lindblad master equation for a single quantum system interacting, e.g., with the electromagnetic vacuum. To describe dissipation in the light-matter systems studied in this thesis, we need to extend this equation to compound quantum systems consisting of multiple subsystems. Dissipation for compound quantum systems can be treated in a *local* or *global* picture. In the local picture, each subsystem interacts independently with its local environment while, in the global picture, they interact collectively with a common global environment. The two scenarios are shown schematically in Fig. 3.1 and the two different types of master equations generated by these pictures are given in Eqs. (3.5) and (3.7) below. The two pictures can be combined to describe complex quantum systems composed of several different types of subsystems. For example, collective interaction with a common surrounding vacuum and local internal losses.

The *local* master equation in Eq. (3.5) has the same form as the standard master equation presented in Eq. (3.1), but now contains a sum over the local jump operators for the N subsystems. This treatment of local dissipation is motivated if the interaction between the subsystems is not too strong, as the local jump operators induce transitions between the bare states. An alternative approach to treating local dissipation, suitable for increasingly large coupling strengths as in the ultrastrong-coupling regime, is given below in Section 3.3.

Local master equation:

$$\dot{\hat{\rho}}_S(t) = -\frac{i}{\hbar}\Big[\hat{H}_S, \hat{\rho}_S(t)\Big] + \sum_{i=1}^{n} \Gamma_i \left(\hat{L}_i \hat{\rho}_S(t) \hat{L}_i^\dagger - \frac{1}{2}\Big\{ \hat{L}_i^\dagger \hat{L}_i, \hat{\rho}_S(t) \Big\} \right). \tag{3.5}$$

(3.6)

The master equation for n subsystems interacting with a *global* environment is given in Eq. (3.7). Due to the interaction with the same environment, the Lindblad term now mixes jump operators $\hat{L}_i$ and $\hat{L}_j$ for different subsystems with indices i and j. The physical interpretation of this mixing is that the global environment generates a dissipative coupling between the subsystems. The famous superradiance effect [54] demonstrates how such dissipative coupling can build up correlations between the subsystems that drastically change their behavior.

Global master equation:

$$\dot{\hat{\rho}}_S(t) = -\frac{i}{\hbar}\Big[\hat{H}_S, \hat{\rho}_S(t)\Big] + \sum_{i,j=1}^{n} \Gamma_{ij} \left(\hat{L}_i \hat{\rho}_S(t) \hat{L}_j^\dagger - \frac{1}{2}\Big\{ \hat{L}_j^\dagger \hat{L}_i, \hat{\rho}_S(t) \Big\} \right). \tag{3.7}$$

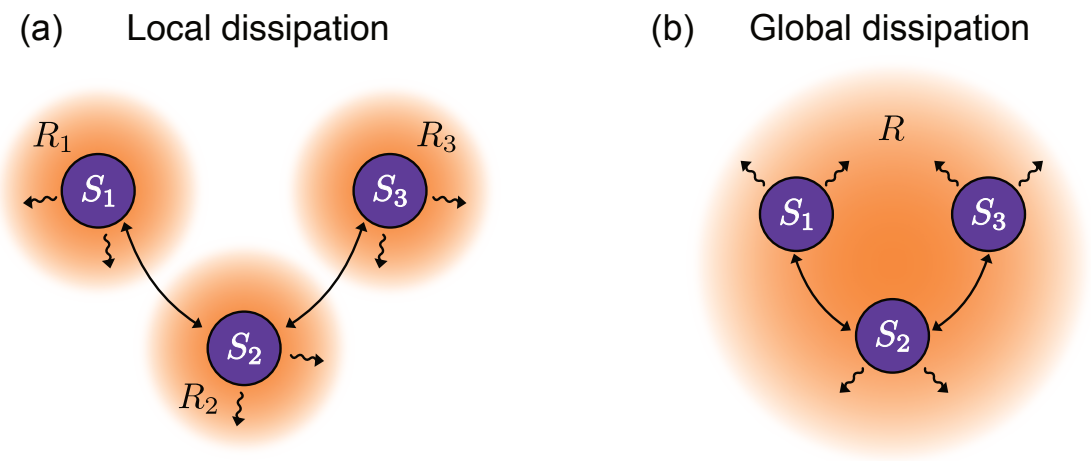

Figure 3.1: Dissipation in an interacting compound system $\hat{H}_S = \hat{H}_{S_1} + \hat{H}_{S_2} + \hat{H}_{S_3}$ can be (a) local, or (b) global. Local dissipation generally breaks collective symmetries of compound systems. Global dissipation, on the other hand, can create correlations between the subsystems due to the collective interaction with the same reservoir.

3.3 Losses in ultrastrongly coupled systems

The standard approach to model losses in a coupled system is to derive a local master equation, considering transitions between the bare, uncoupled states in each subsystem. This approach works well in most situations when the coupling is weak or strong. However, as the coupling strength increases, this treatment breaks down and can lead to erroneous predictions of measurable excitations in the ground state. The reason for the failure of the standard approach is that the coupling between the two subsystems cannot be treated perturbatively in the ultrastrong-coupling regime. Thus, the ground state of the bare system is not necessarily the dressed ground state of the coupled system, as demonstrated in Eq. (2.16) in the discussion on light-matter coupling regimes. Since the standard approach gives jump operators that induce transitions between the bare states, this approach fails to bring the system to the dressed ground state. Consequently, the standard master equation can predict excitations in the ground state, even at zero temperature [42]. The large spectral separation of the modes in the ultrastrong coupling regime also challenges the white noise approximation of the standard master equation.

A correct treatment of dissipation in ultrastrongly coupled systems should contrarily generate jump operators that induce transitions between the dressed states. A suitable master equation for this purpose was derived for the open Quantum-Rabi model

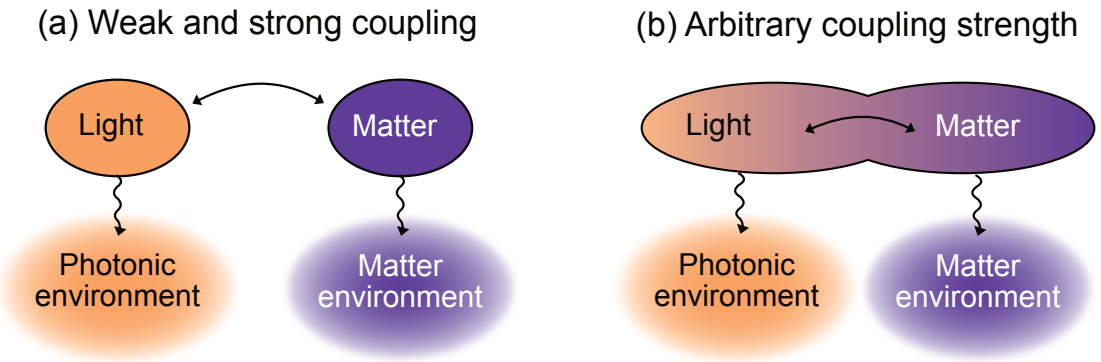

Figure 3.2: Illustration of two approaches to describe dissipation in compound quantum systems with local environments such as the coupled light-matter systems considered in this thesis. (a) When the interaction of the coupled system can be treated perturbatively, it is often justified to describe dissipation for the bare subsystems separately. (b) As the coupling strength increases, it becomes important to describe the interaction with the environment by the dressed eigenmodes of the system.

in Ref. [42]. Their derivation is based on first expressing the bare system operators in the (local) system-reservoir interaction Hamiltonian in terms of the dressed eigenstates of the coupled system, and then proceeding according to the standard Lindblad master equation derivation. Figure 3.2 shows a schematic illustration of the differences between the two approaches.

Expressed explicitly for an arbitrary subsystem interacting with its environment via the operator $(\hat{s} + \hat{s}^\dagger)$, the projected operators going into the derivation are

$$\sum_{j,k} c_{jk} \, |j\rangle\langle k| \equiv \langle j|\hat{s} + \hat{s}^\dagger|k\rangle \, |j\rangle\langle k| \tag{3.8}$$

where $|j\rangle$ and $|k\rangle$ are eigenstates to the ultrastrongly coupled system. In the derivation of Ref. [42], they further use the conservation of parity inherent in the Rabi model and the *secular approximation*. The latter assumes each transition $k \to j$ to be spectrally well separated from all other transitions $k' \to j'$. Taken together, these properties lead to jump operators for effective two-level systems constituted by the parity-allowed transitions between rungs in the dressed-state ladder of the Rabi model. Their result is a dressed-state master equation, written in a general form for n interacting subsystems in Eq. (3.9) below. Lambshifts are absorbed into the Hamiltonian $\hat{H}_S$.

Dressed master equation within the secular appr.:

$$\dot{\hat{\rho}}_S(t) = -\frac{i}{\hbar}\Big[\hat{H}_S, \hat{\rho}_S(t)\Big] + \sum_n \sum_{j,k>j} \Gamma_n^{jk} \mathcal{D}\big[\hat{c}_{jk}\big]\hat{\rho}_S. \tag{3.9}$$

In Eq. (3.9), the first sum is over the n subsystems, $|j\rangle$ and $|k\rangle$ are dressed eigenstates of the system, and the superoperator $\mathcal{D}\big[\hat{c}_{jk}\big]\cdot = \hat{c}_{jk}\cdot\hat{c}_{jk}^\dagger - \frac{1}{2}\Big\{\hat{c}_{jk}^\dagger\hat{c}_{jk}, \cdot\Big\}$ is the Lindblad dissipator with the jump operators $\hat{c}_{jk} \equiv |j\rangle\langle k|$. The corresponding decay rates are given by

$$\Gamma_n^{jk} = \gamma_n(\omega_{jk}) |\, \langle j|\hat{s} + \hat{s}^\dagger|k\rangle \,|^2 \tag{3.10}$$

with $\gamma_n(\omega) = 2\pi D_n(\omega)|\kappa_n(\omega)|^2$, where $D_n(\omega)$ in the density of states, and $\kappa_n(\omega)$ the frequency-dependent coupling strength to the environment. At the bare resonance frequency ω_n, $\gamma_n(\omega_n) = \gamma_n$ gives the bare decay rate in the uncoupled system. The evaluation of the decay rate at the transition frequencies ω_{jk} requires the reservoir to be locally flat around the transition ω_{jk}. This corresponds to a local white noise approximation.

The secular approximation is very restrictive and has limited application to systems without large anharmonicity. Another approach is to consider the opposite limit: harmonic transitions. This limit is suitable, e.g., for coupled bosonic modes, whose dressed eigenstates also exhibit a harmonic spectrum. The result of a derivation analog to the one in Ref. [42], but now assuming harmonic transition frequencies $\omega_{jk} = \omega_m$, with ω_m being the resonance frequencies of the dressed modes, gives the harmonic dressed-state master equation for n interacting modes presented in Eq. (3.11). The assumption $\omega_{jk} = \omega_m$ relaxes the restriction of independent two-level transitions in the secular approximation, to transitions along harmonic ladders with frequencies ω_m. In the latter situation, it is only important that the harmonic dressed modes are well separated spectrally, such that $|\omega_m - \omega_{m'}| \gg 1$ for $m \neq m'$.

Dressed master equation within the harmonic appr.:

$$\dot{\hat{\rho}}_S(t) = -\frac{i}{\hbar}\Big[\hat{H}_S, \hat{\rho}_S(t)\Big] + \sum_{m=\text{dressed}} \sum_{n=\text{bare}} \gamma_n(\omega_m)\mathcal{D}[\hat{c}_{nm}]\hat{\rho}_S. \tag{3.11}$$

Here, the indices n and m denote the bare and dressed modes, respectively. As in the previous case, $\gamma_n(\omega) = 2\pi D_n(\omega)|\kappa_n(\omega)|^2$ is evaluated at the dressed resonance frequency ω_m, and it corresponds to the bare decay rate γ_n, when evaluated at ω_n. The jump operators are defined as

$$\hat{c}_{nm} = \sum_{\substack{j,k>j \\ \epsilon_{jk}=\hbar\omega_m}} \langle j|\hat{s}_n + \hat{s}_n^\dagger|k\rangle \,|j\rangle\langle k|\,, \tag{3.12}$$

where $|j\rangle$ and $|k\rangle$ are dressed eigenstates of the system, and $\hat{s}_n$, $\hat{s}_n^\dagger$ are the system operators involved in the system-environment interaction with the nth bare mode. The dressed states can be found numerically, which would also give the operators $\hat{c}_{nm}$. On the other hand, assuming coupled bosonic modes, the master equation (3.11) can be reduced to Eq. (3.13).

Dressed master equation for bosonic modes.:

$$\dot{\hat{\rho}}_S(t) = -\frac{i}{\hbar}\Big[\hat{H}_S, \hat{\rho}_S(t)\Big] + \sum_{m=\text{dressed}} \sum_{n=\text{bare}} \Gamma_n(\omega_m)\mathcal{D}[\hat{c}_m]\hat{\rho}_S. \tag{3.13}$$

This reduction uses the fact that n bilinearly coupled bosonic modes, described by a Hamiltonian that is at most quadratic, can be diagonalized analytically[1] and will present $m = n$ dressed bosonic modes in the diagonal basis. The jump operators $\hat{c}_m$ can, therefore, be identified as the bosonic annihilation operators for the dressed modes and they are related to the $\hat{c}_{nm}$ operators via the relationship

$$\hat{c}_{nm} = c_{nm}\hat{c}_n, \tag{3.14}$$

where the coefficients c_{nm} are defined as

$$c_{nm} \equiv \langle 0, m|\hat{s}_n + \hat{s}_n^\dagger|1, m\rangle\,, \tag{3.15}$$

with $|0, m\rangle$, and $|1, m\rangle$ being dressed states with 0 and 1 excitations in the mth dressed mode. In Eq. (3.13), the coefficients c_{nm} are absorbed in the decay rates

$$\Gamma_n(\omega_m) = \gamma_n(\omega_m)|c_{nm}|^2. \tag{3.16}$$

The c_{nm} can be found numerically, or be expressed in terms of the transformation coefficients that diagonalize the system Hamiltonian. In the context of the Hopfield model, the transformation coefficients are the so-called Hopfioeld-coefficients.

The interpretation of the dissipation term in Eq. (3.13) is that each dressed mode will experience an effective decay rate that is the interference between all the bare decay rates. Depending on the coefficients c_{nm}, the effective decay of the dressed modes will experience loss, gain, or remain neutral with respect to the average decay rates of the system. All this will be made explicit in Chapter 8, where the bosonic master equation (3.13) is applied to a two-mode Hopfield model in the ultrastrong coupling regime.

The harmonic approximation is similarly restrictive to the secular approximation but favors harmonicity instead of anharmonicity. Therefore, its application to non-harmonic dressed modes should be carefully considered. A more general master equation that could be applied to hybrid systems, that are neither harmonic nor appropriate for the

[1] These are the conditions for a bosonic Bogoliubov transformation, see Chapter 7 for more details.

secular approximation has been proposed in Ref. [55]. This generalized master equation provides a suitable tool, e.g., for studying the transitions from weak to strong, to ultrastrong, to deepstrong coupling, where the transition changes in character from anharmonic to harmonic, depending on the coupling strength. However, it suffers from not providing simple and transparent expressions for the decay process and often needs numerical filtering to deal with oscillating terms that do not converge [56]. Deepstrong coupling has not been introduced here as this coupling regime is irrelevant to this thesis. The interested reader can read about it in, e.g., Ref. [57].

As a final note, the two approaches: secular and harmonic approximations, are analogous to the Lindblad master-equation derivation for a single two-level system and a single cavity, respectively, but performed with the projected operators given in Eq. (3.8) instead of the bare operators.

Before we move on to the results part of this thesis, the connections between the Lindblad master equation and a non-Hermitian Hamiltonian formulation for systems including losses will be briefly discussed.

3.4 Effective non-Hermitian Hamiltonians

Equation (3.1) presented the standard master equation for a single quantum system experiencing dissipation due to the interaction with its local environment with the operator $\hat{L}$. The effects of the environment through the so-called jump operators $\hat{L}$ can be divided into *nonunitary dissipation* and *quantum jumps* [58]. The two categories are governed by the anticommutator and the jump term $\hat{L}\hat{\rho}_S(t)\hat{L}^\dagger$ in Eq. (3.1), respectively. As the name suggests, the latter is responsible for what is called a quantum jump, i.e, an abrupt change in the system's state due to dissipation. The effect can be thought of as a measurement-like action of the environment on the state of the system. On the other hand, the dissipative part describes the *continuous* and *irreversible* loss of information, energy, and coherence to the macroscopic environment. This effect is easy to see if one groups the anticommutator term with the Hamiltonian contribution. In that case, these two terms define a *non-Hermitian* Hamiltonian $\hat{H}_{\text{eff}} = \hat{H}_s - i\frac{\hbar\Gamma}{2}\hat{L}^\dagger\hat{L}$ [47] and the master equation (3.1) can be written as

$$\dot{\hat{\rho}}_S(t) = -\frac{i}{\hbar}\left[\hat{H}_{\text{eff}}\hat{\rho}_S(t) - \hat{\rho}_S(t)\hat{H}_{\text{eff}}^\dagger\right] - \Gamma\hat{L}\hat{\rho}_S(t)\hat{L}^\dagger. \tag{3.17}$$

If the effects of quantum jumps can be neglected, the evolution of the system is solely provided by $\hat{H}_{\text{eff}}$. This assumption is often made in quantum optics at weak-excitation conditions when quantum jumps are rare. The effective Hamiltonian can also be used for modeling post-selection schemes. A pedagogical explanation of the connections between evolution with non-Hermitian Hamiltonians and the full quantum dynamics described by master equations on Lindblad form can be found in Ref. [59].

For this thesis, the connection between the master equation and an effective non-Hermitian Hamiltonian brings context to the classical modeling of decay discussed in Paper D. In the field of nanophotonics, and especially in polaritonics, it is common to model the effects of dissipation by non-Hermitian Hamiltonians of the form defined above. The non-Hermitian Hamiltonian in Eq. (2.17) presents one explicit example for two coupled modes. This approach to including the effects of dissipation is, in many situations, sufficient to describe the phenomena observed experimentally. However, it is important to know the microscopic origin of $\hat{H}_{\text{eff}}$ to understand its validity.

Our work in Paper D demonstrated that the commonly used non-Hermitian-Hamiltonian approach for two coupled modes with losses, fails to describe the polaritonic linewidths. Even in the – conventional – strong-coupling regime [$g > (\kappa + \gamma)/2$], where it is often deemed appropriate. While the non-Hermitian Hamiltonian from Eq. (2.17) predicts linewidth averaging with equal linewidths at zero detuning between the coupled modes, our results in Paper D demonstrated a linewidth asymmetry at zero detuning that remained in the strong-coupling regime. The error in the predictions of the non-Hermitian Hamiltonian arises because of the light-matter interaction terms that are neglected in a strong-coupling treatment. This error is circumvented in Paper D by employing a transfer matrix method that, building on the solutions of Maxwell's equations, inherently includes all effects of the light-matter interaction. To see how the error arises due to an incorrect description of dissipation in the coupled system, a description that allows for distinguishing the contribution of different terms in the light-matter interaction is needed. The quantum model of the polaritonic decay rates given in Chapter 8 provides such a description based on the Lindblad formalism outlined here. The results of Chapter 8 demonstrate that the linewidth averaging predicted with the non-Hermitian Hamiltonian description is only found within the RWA approximation. This is not surprising as the non-Hermitian Hamiltonian (2.17) would only be obtained from a Lindblad master equation formulation when the RWA is applied. Thus, this example not only highlights the importance of knowing the approximations going into the modeling but also that the definition of strong-coupling in terms of the losses can be misleading.

Part I
Identical two-level emitters

The first part of this thesis focuses on small ensembles of identical two-level emitters interacting with a single-mode cavity. "Two-level emitter" is a collection term for emitters of light that can be modeled as a two-level system, including two-level atoms, artificial atoms, ions, excitonic molecules, and quantum dots. Historically, large ensembles of two-level atoms attracted attention due to intriguing cooperative phenomena such as superradiance [54, 60]. Over the last decade, this interest has renewed, but now in a *few-emitter* regime. Recent experiments have demonstrated an unprecedented level of control of individual emitters in various platforms, including neutral atoms [61, 62], artificial atoms [63, 64], ions [65], molecules [66–68], and quantum dots [69]. This allows for testing of the fundamental differences between a single and many emitters, as well as monitoring of cooperative effects in a controlled setup.

For this thesis, we are interested in the experiments that have demonstrated the ability to strongly couple small collections of emitters to a single cavity mode. These systems are well described by the Tavis–Cummings model, which is introduced in Chapter 4. In particular, Chapter 5 takes inspiration from strong coupling with plasmonic nanoresonators playing the role of the cavity [20, 25, 68–71]. This chapter summarizes the main findings of Paper A and the follow-up draft, Paper B. Chapter 6 contrarily studies cooperative phenomena in high-quality cavities [72–78], which is the topic of Paper C.

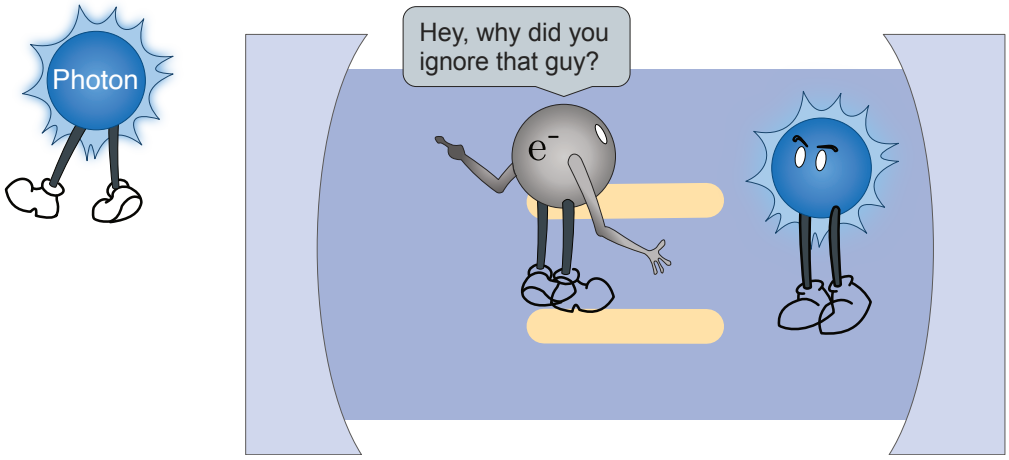

Chapter 4

The Tavis–Cummings model

The Tavis–Cummings model is a version of the Dicke model [60] for an ensemble of non-interacting identical emitters interacting with a common radiation field. Dicke's work highlighted the importance of treating a gas of radiating two-level atoms as a collective ensemble in this situation. As a result of not treating the atoms individually, a coherent spontaneous emission effect known as superradiance [54] could be shown. Hence, these works pioneered modern research on cooperative phenomena in light-matter platforms [79]. In 1968, about a decade after Dicke's work, Tavis and Cummings solved the Hamiltonian of N identical two-level emitters interacting with a single-mode radiation field in the RWA [80]. Therefore, modern literature normally refers to the Dicke model for the light-matter Hamiltonian with N two-level emitters without making the RWA and the Tavis–Cummings model for the same Hamiltonian but with the RWA.

The Tavis–Cummings Hamiltonian in the dipole gauge can be written as

$$\hat{H}_{\mathrm{tc}} = \hbar\omega_c \hat{a}^\dagger \hat{a} + \sum_{i=1}^{N} \left[\hbar\omega_0 \hat{\sigma}_{+i}\hat{\sigma}_{-i} + \hbar g \left(\hat{a}^\dagger \hat{\sigma}_{-i} + \hat{a}\hat{\sigma}_{+i} \right) \right]. \tag{4.1}$$

The operators $\hat{a}$ and $\hat{a}^\dagger$ are annihilation and creation operators for the cavity mode with resonance frequency ω_c, and the operators $\hat{\sigma}_{+i}$ and $\hat{\sigma}_{-i}$ are the Pauli raising and lowering operators, respectively, for the ith two-level emitter with transition frequency ω_0. The last term in Eq. (4.1) describes the dipole interaction between the cavity and emitters with the individual coupling strength $\hbar g = -\mu_{\mathrm{eq}} E_0$, with $\mu_{\mathrm{eg}} = \mu^*_{\mathrm{eg}} = \langle g|\hat{\sigma}_{-i} + \hat{\sigma}_{+i}|e\rangle$ being the emitters' transition dipole moment, and E_0 being the amplitude of the cavity field. Normally, the dipole interaction depends on the particles' positions. Here, we assume this coupling can be controlled deterministically. Alternatively, the emitters are localized in a small area compared to the cavity mode. With equal interaction rates g, the structure of the interaction term in the Tavis-Cummings Hamiltonian [Eq. (4.1)] leads

to the collective interaction strength $g_{\mathrm{col}} = \sqrt{N}g$ between the cavity and the collective bright mode of the emitter ensemble.

The Hamiltonian (4.1) is written in terms of Pauli operators for the individual two-level emitters. This formulation historically comes from describing spin-$\frac{1}{2}$ particles in magnetic fields [81]. Later, it was shown that any ensemble of non-interacting two-level systems, perturbed by an external field, obeys the same unitary transformations [82]. Followingly, the framework related to the addition of spins and total angular momentum states [83, 84] can be applied to generic two-level systems that are not necessarily spin systems. Employing the collective pseudospin operators, the Tavis–Cummings Hamiltonian in Eq. (4.1) can equivalently be written as,

$$\hat{H}_{\mathrm{tc,col}} = \hbar\omega_c \hat{a}^\dagger \hat{a} + \frac{\hbar\omega_0}{2}\hat{S}_z + \hbar g\Big(\hat{a}\hat{S}_+ + \hat{a}\hat{S}_-\Big), \tag{4.2}$$

where the collective operators are defined as

$$\hat{S}_k = \sum_{i=1}^{N} \frac{1}{2}\hat{\sigma}_k, \quad k = \{x, y, z\}, \tag{4.3}$$

$$\hat{S}_\pm = \sum_{i=1}^{N} \hat{\sigma}_\pm. \tag{4.4}$$

The collective pseudospin operators obey the angular momentum commutation relations $\left[\hat{S}_i, \hat{S}_j\right] = i\epsilon_{ijk}\hat{S}_k$, $\left[\hat{S}_+, \hat{S}_-\right] = 2\hat{S}_z$ and $\left[\hat{S}_z, \hat{S}_\pm\right] = \pm\hat{S}_\pm$.

In analogy with spin-$\frac{1}{2}$ particles, the pseudospins are associated with an SU(2) symmetry. Thus, their otherwise 2^N-dimensional tensor-product Hilbert space can be written as a direct sum of irreducible representations (irreps), in which the spin Hamiltonian has a block diagonal form. An illustrative textbook example is the addition of two spin-$\frac{1}{2}$ particles whose irreps are the singlet and triplet, with total spin 1 and 0, respectively:

$$\frac{1}{2} \otimes \frac{1}{2} = 1 \oplus 0. \tag{4.5}$$

In left-hand-side tensor-product representation, one keeps track of each individual emitter, and the states are expanded in the basis $\{|gg\rangle, |ge\rangle, |eg\rangle, |ee\rangle\}$, where g and e denotes the occupation of the ground and excited states, respectively. In the right-hand-side direct-product representation, the good quantum numbers are instead the total angular momentum S and the projection $m_S = -S, -(S+1), ..., S$, with $\hat{S}_z |S, m_S\rangle = m_S |S, m_S\rangle$. In the example above, this means that the bases $\{|1,-1\rangle, |1,0\rangle, |1,1\rangle\}$ and $\{|0,0\rangle\}$, expressed in the states $|S, m_S\rangle$, are good bases for the triplet ($S = 1$) and singlet ($S = 0$), respectively[1]. The states in the different bases can be related via

[1] Hence, then names triplet and singlet.

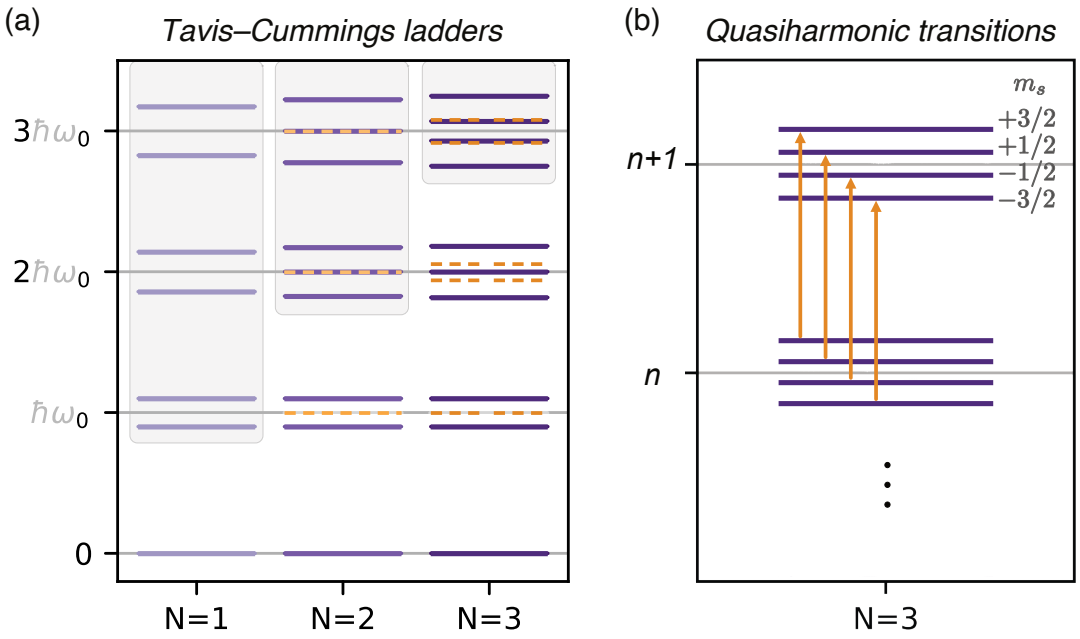

Figure 4.1: Eigenenergies of the Tavis–Cummings model for $N = 1, 2$, and 3 two-level emitters. (a) Solid lines denote energy levels in the full-spin sector ($S = N/2$), and dashed lines denote the other spin sectors ($S < N/2$). The shaded areas mark where the spectra regularize at $n \geq N$ number of excitations. (b) Close-up on the eigenenergies far up the Tavis–Cummings-ladder with $N = 3$, the different steps can be related to the different projections m_s. At high excitation, the transitions become quasiharmonic.

the Clebsch–Gordan coefficients that can be found in tables. For the example with two spin-$\frac{1}{2}$ particles, the states are related as

$$\begin{aligned} |1,1\rangle &= |ee\rangle\,, \\ |1,0\rangle &= \frac{1}{\sqrt{2}}\big(|ge\rangle + |eg\rangle\big), \\ |1,-1\rangle &= |gg\rangle\,, \\ |0,0\rangle &= \frac{1}{\sqrt{2}}\big(|ge\rangle - |eg\rangle\big). \end{aligned} \tag{4.6}$$

This example demonstrates the relation between the quantum number m_S and the total excited state occupation p, which is $p = N/2 + m_S$.

The collective operators introduced above do not mix states from different irreps, i.e., different spin sectors labeled by S. Therefore, the Tavis–Cummings Hamiltonian can be written in an infinitely block-diagonal form, expressed in terms of the collective emitter states $|S, m_s\rangle$ and the photon number states $|n\rangle$ describing the state of the cavity. The block diagonal form allows for diagonalization of each block separately to find the dressed states corresponding to each spin sector S [80, 85, 86].

The eigenenergies corresponding to the dressed states of the Tavis–Cummings model are shown up to the third rung of the Tavis–Cummings ladder for $N = \{1, 2, 3\}$ in Fig. 4.1. Solid purple lines show the eigenstates corresponding to the full-spin sector $S = N/2$. Dashed orange lines show the eigenstates corresponding to the other spin sectors, which are $S = 0$ and $S = \{1/2, -1/2\}$ for $N = 2$ and $N = 3$, respectively. The spectrum at low levels of excitation ($n < N/2$) has an irregular structure that grows in complexity with the emitter number N. Higher up the Tavis–Cummings ladder ($n \geq N$), the spectrum regularizes, and at high excitation levels $n \gg N$, the transitions become quasi-harmonic. The latter is illustrated for $N = 3$ in Fig. 4.1(b), where it is also shown how the parallel eigenvalue ladders can be associated with the projections m_S. In Paper C, we show how this underlying structure remains when including drive and dissipation in the cavity mode and imprints a correlation between the emitters and the cavity field, revealed in the cavity's phase-space distribution when it is driven to high excitation levels.

Chapter 5

Cavity QED with a lossy cavity without adiabatic elimination

Strong coupling between quantum emitters and plasmonic nanoresonators has opened up the possibility of exploring cavity QED in unusual parameter regimes. Despite the inherently lossy nature of plasmonic resonances, with lifetimes in the femtosecond regime, the subwavelength confinement of electromagnetic radiation facilitates strong coupling with a few quantum emitters. Moreover, operating at optical frequencies, these systems show potential for applications at non-cryogenic temperatures [68, 87]. For example, a room-temperature all-optical transistor at the single-photon level has been a longstanding goal [88, 89]. However, observing quantum effects with strongly dissipative cavities remains difficult.

These facts inspired the study that eventually led to Paper A, and the draft presented in Paper B. With the goal of exploring the potential for nonlinearities at the single-photon level in these types of systems, despite large losses, we investigated the response of a lossy cavity coupled to a few emitters under pulsed driving on the cavity mode. Interestingly, we found that the intensity response from a cavity with a single emitter was more than double that of two emitters when driving on resonance with the cavity and emitters. Switching to continuous-wave driving and studying the steady-state response, we found that the effect was even bigger, with the response from a cavity coupled to one emitter being an order of magnitude bigger than the response from a cavity coupled to two emitters. In particular, we identified that the cavity response would be proportional to the $2(N+1)$th power of the drive amplitude when it coupled to N two-level emitters. In Paper A, we analyzed this effect in detail, which we call *unconventional saturation*.

The identification of the unconventional saturation effect and a thorough analysis of its underlying mechanisms are the main contributions of Paper A. Section 5.2 below summarize the main characteristics of the effect and introduces the phenomenological model we developed to provide insights into the numerics. In our case, not eliminating

the cavity mode was an important part of our success in identifying the correlation between the emitter number and the cavity field in this regime. One implication of the observed nonlinear dependence on the driving intensity is a large bunching effect. Therefore, we are also interested in the photon statistics and the output states from a cavity displaying this effect. These are the topics of Paper B, whose preliminary results are summarized in Section 5.3.

Related works

The mechanism underlying the unconventional saturation effect bears similarities with electromagnetic-induced transparency (EIT) [90]. EIT refers to the opening of a narrow transparency window in the spectrum of a three-level system due to the interference between two allowed transitions. Typically EIT is observed with large ensembles of Λ-type atoms [91–93], that is, atomic systems that have an energy-level structure resembling the letter Λ. However, in our case, the response found at weak drive is rather that of two classical coupled oscillators, which display a classical analog of EIT [94]. The classical EIT effect is an interference effect between the normal modes of two coupled oscillators that can lead to a huge suppression of excitation at the frequency of the drive on resonance with the oscillators. From this perspective, the unconventional saturation effect can be interpreted as the breakdown of the harmonic-oscillator approximation for the ensemble of two-level emitters. The signatures of classical EIT[1], shown in the cavity's scattering spectra in Paper A, have been previously discussed within the context of a single exciton coupled to a classical radiation field. In this context, the narrow transparency dip in the cavity's spectrum has been referred to as *exciton-induced transparency* (ExIT) [95, 96] and has been interpreted as a fano resonace [97, 98]. Even though the saturation of the ExIT has been discussed in [98], this work and Refs. [95–98] were limited to semiclassical and classical descriptions of a single two-level system in a single-mode radiation field. Thus, the effect we observed in Paper A was not identified. However, the systems exhibiting ExIT [99] should be suitable for demonstrating unconventional saturation.

The literature on the Tavis–Cummings model is extensive and includes a thorough theoretical foundation developed over the second half of the 20th century. A full quantum description of ExiT was given in the case of a single two-level atom coupled to a cavity at the end of the 90s [100]. This time, it was referred to as cavity-induced transparency to differentiate it from EIT with three-level, Λ-type atoms. Yet, neither does this work analyze the drive-dependence of the cavity response, which is a key component of Paper A. On the other hand, the study in Ref. [101] observes a similar behavior of the cavity's response to external driving in the context of a cavity QED laser. Their rate-equation approach to finding the steady-state photon number and carrier occupation, i.e., the number of emitters in the excited state, showcases a similar nonlinear

[1] A narrow transparency dip at the resonance frequency.

transition between an empty and filled cavity solution with increasing pump power. In their case, their focus is on a "threshold-less" laser, where a single photon would induce the lasing condition and, thus, no transition would be observed as a function of pump power. Following that, they do not pay attention to the correlations between the emitter number and cavity response in the few-body-few-photon regime. Only in recent years have such correlations attained attention in light of state-of-the-art experiments with just a few emitters.

5.1 Model system

The model system of Paper A and Paper B is a coherently driven and lossy single-mode cavity coupled to a narrow linewidth two-level emitter, which can be well described by the Tavis–Cummings Hamiltonian. To include the effects of dissipation, we use the master equation

$$\dot{\hat{\rho}} = -\frac{i}{\hbar}\Big[\hat{H}_{tc,d}, \hat{\rho}\Big] + \gamma_c \mathcal{D}_{\hat{a}}[\hat{\rho}] + \sum_{i=1}^{N} \gamma_e \mathcal{D}_{\hat{\sigma}_{-i}}[\hat{\rho}], \tag{5.1}$$

where we include photon loss from the cavity with the decay rate γ_c and local spontaneous emission with the rate γ_e from the emitters. The superoperator $\mathcal{D}_{\hat{o}}[\cdot] = \hat{o}\cdot\hat{o}^\dagger - \frac{1}{2}\big\{\hat{o}^\dagger\hat{o}, \cdot\big\}$ is the standard Lindblad superoperator for dissipation associated with the operator $\hat{o}$. The unitary evolution described by the first term in Eq. (5.1) is governed by the Tavis–Cummings Hamiltonian introduced in Eq. (4.1) and a coherent drive on the cavity with amplitude $\Omega_d/2$ in the rotating wave approximation. In the rotating frame of the laser, this Hamiltonian takes the simple form

$$\hat{H}_{\mathrm{tc,d}} = \hbar g \sum_{i=1}^{N}\Big(\hat{a}^\dagger\hat{\sigma}_{-i} + \hat{a}\hat{\sigma}_{+i}\Big) + \frac{\hbar\Omega_d}{2}\Big(\hat{a} + \hat{a}^\dagger\Big), \tag{5.2}$$

when the drive is in resonance with the cavity and emitters.

Parameter regime

The considered parameter regime is a lossy cavity $\gamma_c \gg \gamma_e$ and strong collective coupling $g_{\mathrm{col}} = \sqrt{N}g \approx \gamma_c$, which means systems with large cooperativity:

$$C \equiv \frac{4g_{\mathrm{col}}^2}{\gamma_c\gamma_e}. \tag{5.3}$$

The effects observed in Paper A can also be observed for weaker collective coupling $g_{\mathrm{col}} \lesssim \gamma_c$, which corresponds to a smaller cooperativity C[2]. However, for stronger cou-

[2]The effects of varying spontaneous emission rate γ_e and coupling strengths g_{col} are shown in Figs. 12 and 13 in Appendix E of Paper A.

pling strengths $g_{\mathrm{col}} \gg \gamma_c$, the distinction between the dressed states above the single-excitation level becomes tractable. This changes the behavior of the driven and dissipative system drastically, as was demonstrated in Paper C. Collective versus individual emitter decay is also known to affect the behavior of spin ensembles [60, 102]. In Paper A, the effects of collective decay on unconventional saturation were investigated in Appendix D. Our comparison between the two descriptions showed that there were no qualitative differences in our few-emitter regime and a strongly dissipative cavity[3]. This was not surprising as the strong collective coupling to the cavity is the main decay channel for the emitters in this regime, and the effects we observe are not related to the symmetries of the spin ensemble, which would otherwise be affected by the local versus collective description of the dissipation. In our case, the main effect of emitter decay is stabilizing the photon number in the weak-drive regime. This gives the response along the lower asymptotical (dashed) line in Fig. 5.1.

5.2 Unconventional Saturation

The *conventional* saturation effect occurs when an emitter or nonlinear medium in a cavity cannot absorb more photons and, thus, has become saturated. In the spectrum, this is revealed as a merging of the Rabi doublet into a single Lorentzian peak at the cavity resonance when increasing the intracavity field [103]. From the perspective of the emitters in the steady state, saturation occurs when all emitters have an equal probability of being in the excited and ground states due to the stimulated Rabi flopping [41] induced by the driving from the cavity, thus giving the saturation expectation value $\sum_{i=1}^{N} \langle \hat{\sigma}_{+i}\hat{\sigma}_{-i}\rangle_{\mathrm{sat}} = N/2$. The conventional saturation effect is marked by dashed circles in Fig. 5.1, which plots the steady-state photon number $\langle \hat{a}^\dagger \hat{a}\rangle_{ss}$ and emitter population $\langle \hat{\sigma}_+\hat{\sigma}_-\rangle_{ss}^{\mathrm{ens}} \equiv \sum_{i=1}^{N} \langle \hat{\sigma}_{+i}\hat{\sigma}_{-i}\rangle_{\mathrm{ss}}$ as functions of the drive strength Ω_d. When the emitters saturate, their effect on the cavity averages out, and the cavity photon number regains a linear dependence on the external drive intensity $I \propto \Omega_d^2$. This is shown in the encircled area in Fig. 5.1(a), where the photon number follows the response $(\Omega_d/\gamma_c)^2$ of an empty cavity (dotted curve).

The *unconventional* saturation effect instead emerges in a regime of drive strengths before there are any signs of saturation in the steady-state population of the emitters, as is shown in the shaded areas in Fig. 5.1(a) and (b). The slopes of the photon numbers in this regime in the log-log plot reveal a $\Omega_d^{2(N+1)}$-dependence on the external drive, where N is the number of emitters coupled to the cavity. This corresponds to a power-of-$(N+1)$ dependency on the drive intensity, $I^{(N+1)} \propto \Omega_d^{2(N+1)}$, which is indicative of $(N+1)$-photon processes.

[3] See, e.g., Fig. 10 in Appendix D of Paper A.

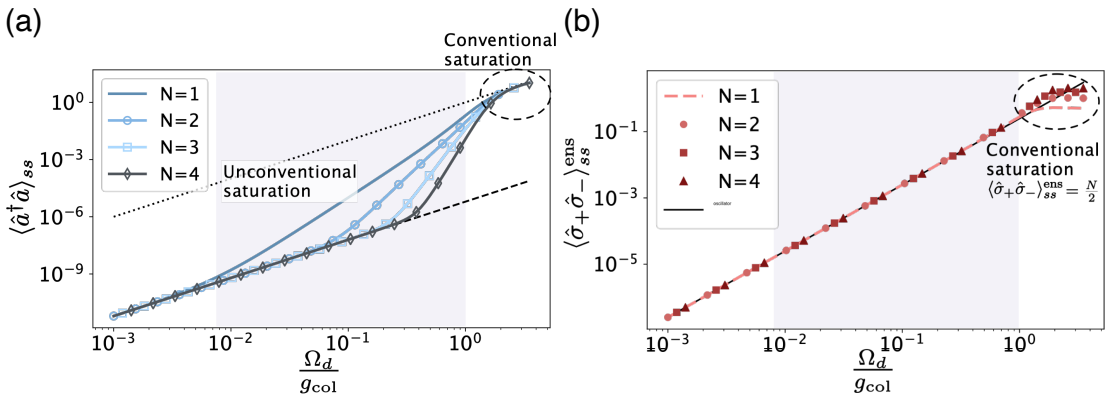

Figure 5.1: Log-log plots of the steady-state expectation values of the photon number and emitter population as a function of the normalized drive strength Ω_d/g_{col} for $N = 1 - 4$ emitters with the same collective coupling strength g_{col}. The shaded areas mark the driving regime displaying the unconventional saturation effect, where (a) the photon number display a clear dependence on the emitter number, while (b) the population of the emitters is still increasing linearly. The circles mark the conventional saturation effect where the emitter population saturates at $N/2$, and the response of the cavity again becomes linearly dependent on the driving intensity $I \propto \Omega_d^2$. The parameters used to produce this plot were $g_{\text{col}}/\gamma_c = 1$, $\gamma_e/\gamma_c = 0.01$.

To provide insights into these numerical results, we developed a phenomenological model that qualitatively captures the effects. This model is based on the good agreement between a coupled-oscillator model and the Tavis–Cummings model in the weak-drive regime and the fact that the emitter ensemble's eigenvalue structure resembles a harmonic oscillator up to the same order of excitation as the emitter number. By combining these two pictures we could explain the observed effect in the cavity as an effective drive on the cavity arising due to the destructive interference between the ensemble and the coherent drive up to the order N. A good intuition for the dynamics is provided by the picture of the emitter ensemble acting as a saturable mirror that only reflects photon states up to order N. Then, from this perspective, the unconventional saturation effect could be described as a competition of interaction rates that saturates when the ensemble cannot reflect more of the incoming light field as a consequence of its finite eigenenergy space. Therefore, this effect be seen as a dynamic counterpart to the conventional saturation effect. This perspective is illustrated as a comic in Fig. 5.2, where a single atom reflects single-photon states, but not two-photon states that can be directly absorbed in the cavity.

The effective drive on the cavity in this phenomenological description can be divided into three parts and is illustrated from the cavity's perspective in Fig. 5.3(b). Before a

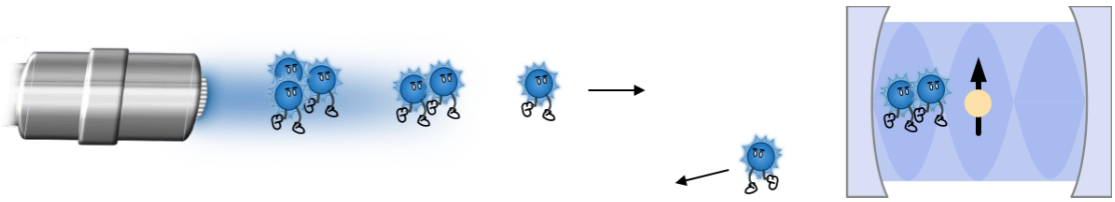

Figure 5.2: A comic illustrating the unconventional saturation effect with a single two-level emitter coupled to a lossy cavity. The system behaves as a saturable mirror where N emitters destructively interfere with the drive up to N photons. This interference breaks down at $(N+1)$ photons that are directly absorbed in the cavity instead.

multiphoton absorption event, the cavity has a small residual photon number $\langle\hat{n}\rangle_{\text{weak}}$ due to imperfect cancellation/reflection from the emitters. Then, at some time t $(N+1)$-photons come from the drive that are directly absorbed by the cavity. This step can be seen as intermittent saturation of the emitters. After that, the absorbed photons leak out of the cavity due to exponential decay. Time-averaging over such multiphoton absorption events in a classical master-equation formulation for the cavity populations gives the analytical expression for the photon number in the steady state,

$$\boxed{\langle\hat{n}_c\rangle_{ss} = \langle\hat{n}\rangle_{\text{weak}} + \frac{(N+1)P_{N+1}^{T}}{T\gamma_c}.} \tag{5.4}$$

The weak-drive photon number is given by the coupled-oscillator description in the weak-drive regime

$$\langle\hat{n}\rangle_{\text{weak}} = \frac{\Omega_d^2}{\gamma_c^2}\frac{1}{(1+C)^2}. \tag{5.5}$$

The parameter P_{N+1}^{T} is the probability of having $(N+1)$ photons in the external drive during the time T and is given by the Poisson distribution with the discrete-mode amplitude $\alpha_d = \Omega_d T$,

$$P_{N+1}^{T} = \mathrm{e}^{-|\Omega_d T|^2}\frac{|\Omega_d T|^{2(N+1)}}{(N+1)!}. \tag{5.6}$$

The time T must be related to the temporal mode matching between the external drive and the effective drive from the emitters. Thus it could be identified as $T = 1/g_{\text{col}}$.

The photon number obtaiend with Eq. (5.4) is plotted and compared with the numerical results in Fig. 5.3(a), cf. red-dashed and blue-solid curves, respectively. As can be seen, there is a good qualitative agreement between the phenomenological model and the exact numerical results. Hence, supporting the intuition given by the emitters-ensemble as a saturable mirror. We could also derive an expression for the critical drive

to enter the unconventional-saturation regime from the same phenomenological model. By posing the condition that the harmonic-oscillator description of the emitters breaks down at $(N+1)$ photons, we obtained the expression

$$\boxed{\Omega_{\mathrm{cr}}(N) = \left(\frac{N!\gamma_e^2 g_{\mathrm{col}}^{2(N-1)}}{16}\right)^{\frac{1}{2N}} \left(1+\frac{1}{C}\right)} \tag{5.7}$$

The critical drive Ω_{cr} for $N = 1-4$ is plotted as black stars in Fig. 5.3(a). As can be seen, it predicts the onset of unconventional saturation in the analytical model with high precision, and only slightly overestimates the onset seen in the numerical results.

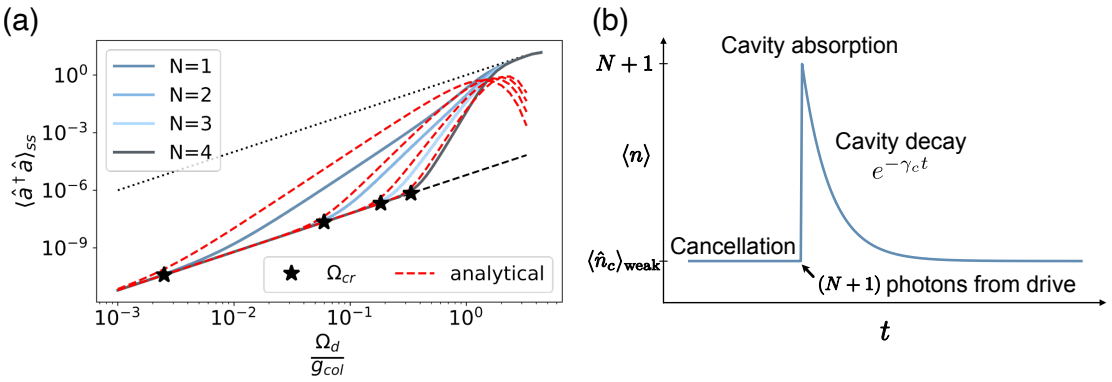

Figure 5.3: The unconventional saturation effect can effectively be understood as direct absorption of $(N+1)$-photon pulses in the cavity that subsequently leak out from the cavity through exponential decay. Panel (b) illustrates the time dynamics for one such absorption event. Time averaging over many $(N+1)$-photon absorption events gives the steady-state photon number $\langle \hat{n}_c \rangle_{ss}$, which is plotted as red dashed curves in panel (a). The analytical results show a good qualitative agreement with the numerical simulations plotted as blue solid curves. Including the absorption of higher numbers of photons ($> N+1$) removes the falling tails and captures the conventional saturation at higher driving strengths. The parameters used for panel (a) were the same as for Fig. 5.1.

To conclude, this section has shown you the main characteristic of the unconventional saturation effect, which is a photon number scaling with the drive as $\Omega_d^{2(N+1)}$ when it couples to N emitters. An intuitive picture of the effect as a destructive interference effect between the external drive and the emitters that break down at $(N+1)$-photons was also given. The next section will continue the investigations of the unconventional saturation effect on a more practical level. In particular, we are interested in the photon statistics, and the output from a cavity displaying the unconventional saturation effect, as they will uncover any potential for quantum state engineering.

5.3 Photon statistics and bundle generation

A multiphoton absorption process of order n will depend on the $(n+1)$th power of the optical intensity. Hence, our results from Paper A are indicative of $(N+1)$-photon absorption in the cavity. This statement is further supported by the phenomenological model presented in Paper A and summarized above, which showed a good qualitative agreement between an effective $(N+1)$-photon drive on the cavity and the exact numerical results. Multiphoton absorption in the cavity suggests an enhancement of multiphoton states in the cavity's photon number distribution. If this is the case, it should show up as a super-Poissonian photon-number distribution in the cavity field. A super-Poissonian photon-number distribution in the cavity is, in turn, indicative of photon bunching in the forward's scattered field. That is, photons are emitted grouped in bundles with higher probability than randomly distributed [104]. The main objective of Paper B is to characterize the emission properties of Tavis–Cummings systems in the unconventional saturation regime. Our preliminary results are summarized below.

Correlation functions

The photon-number distribution can be characterized through its photon statistics provided by the normalized two-time correlation functions for the cavity field [105]. The nth-order correlation function for the cavity field at zero-time delay has an easy formulation in the steady state, which can be expressed in terms of the cavity populations $\rho_m = \langle m|\hat{\rho}_c|m\rangle$ as

$$g^{(n)}(0) = \frac{\left\langle \left(\hat{a}^\dagger\right)^n (\hat{a})^n \right\rangle}{\left\langle \hat{a}^\dagger \hat{a} \right\rangle^n} = \frac{\sum\limits_{m\geq n} \frac{m!}{(m-n)!}\rho_m}{\left(\sum\limits_{m\geq 0} m\rho_m\right)^n}. \tag{5.8}$$

Photon bunching in the field will be signaled by $g^{(n)}(0) > 1$. Employing the phenomenological model developed in Paper A, we can additonally find analytical expressions $\bar{p}_m$ for the populations ρ_m. Taking these $\bar{p}_m$ for the cavity populations in Eq. (5.8), we get analytical solutions for the nth-order correlation functions:

$$\boxed{\bar{g}^{(n)}(0) = \frac{\sum\limits_{m\geq n} \frac{m!}{(m-n)!}\bar{p}_m}{\left(\sum\limits_{m\geq 0} m\bar{p}_m\right)^n}.} \tag{5.9}$$

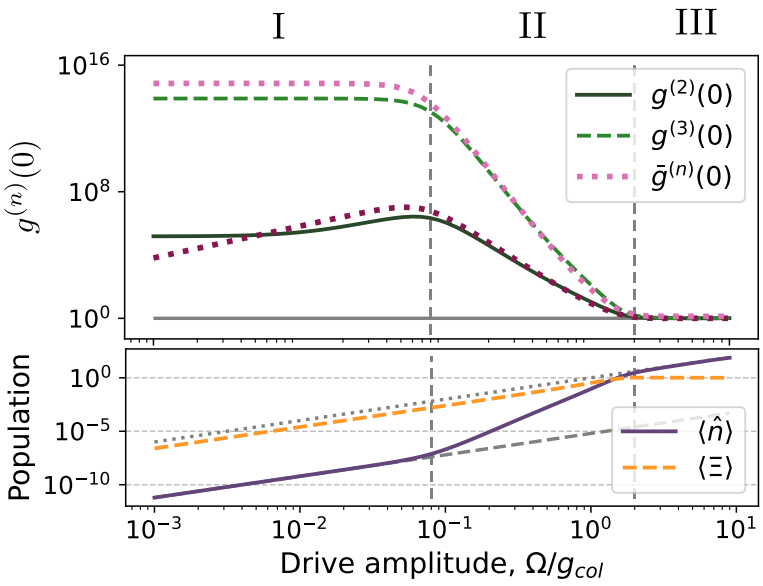

Figure 5.4: Zero-time-delay correlation functions [top panel], and cavity ($\langle\hat{n}\rangle_{ss}$]) and emitter ($\langle\Xi\rangle \equiv \langle\hat{\sigma}_+\hat{\sigma}_-\rangle_{ss}^{\text{ens}}$) populations [bottom panel], for increasing drive amplitude when the cavity contains two emitters. The response is characterized by three different regimes. For weak drive (I), the 3rd-order correlation function is constant as predicted for $(N+1)$-photon absorption in the cavity. As the drive increases, the cavity population displays the unconventional saturation effect, and the higher-order correlation functions start to decrease (II) until the emitters saturate in the strong-drive regime (I I I). The dotted curves show the correlation functions for an empty cavity driven by $(N+1)$-photon pulses. The parameters used to obtain this figure were $g_{\text{col}}/\gamma_c = 1$ and $\gamma_e/\gamma_c = 0.1$

By plotting the $g^{(n)}(0)$ as functions of the drive Ω_d, we confirm a huge bunching effect in the cavity field in the weak-drive regime, where all $g^{(n>1)}(0) \gg 1$. Moreover, we find that another signature of the unconventional saturation effect is $g^{(N+1)}(0) = constant$ in the weak-drive regime $\Omega_d/g_{\text{col}} \ll 1$. This claim is supported by the analytical expression $\bar{g}^{(N+1)}(0)$, which in the weak-drive regime can be found as

$$\bar{g}^{(N+1)}(0) = 1 + \frac{N!}{\gamma_c/g_{\text{col}}}\frac{K_2}{K_1}, \tag{5.10}$$

where K_1 and K_2 are constants determined by the system parameters.

Figure 5.4 demonstrates these findings for the case $N = 2$. In this figure, green solid and dashed curves plot the second $g^{(2)}(0)$ and third-order $g^{(3)}(0)$ correlation functions found by solving the master-equation, and pink dotted curves plot the analytical expressions $\bar{g}^{(2)}(0)$ and $\bar{g}^{(3)}(0)$. In particular, we can identify three different regimes at

weak (I), intermediate (II), and strong (III) drives with different characteristics. In the following, we're interested in the output from the system in regime (II), which has a larger average photon-number than in the weak-drive regime, while still demonstrating large bunching. This regime corresponds to the unconventional saturation regime, where $(N+1)$-photon processes are dominating the cavity's response to external driving.

Characterization of the output field

The output from the cavity can be characterized by photon-detection simulations. For this, we use a stochastic master equation [58] corresponding to the master equation (5.1). We assume all light emitted from the cavity is detected, while the weak emission from the emitters due to a small dissipation to modes other than the cavity is undetected. After the detection of a photon, we count the total number of excitations $\langle m \rangle_c = \langle m | \hat{\rho}_c | m \rangle$ remaining in the system at the next time step using the conditional density matrix $\hat{\rho}_c = \hat{a}\hat{\rho}\hat{a}^\dagger / \operatorname{Tr}\{\hat{a}\hat{\rho}\hat{a}^\dagger\}$. The remaining excitations $\langle m \rangle_c$ are used to characterize a photon bundle. After the identification of a bundle, the next photon bundle starts at the $(\langle m \rangle_c + 1)$th photon-detection event. The obtained distribution is then compared with the corresponding distribution for a coherently driven cavity with the same output flux of photons α, with conditional Poisson distribution $P_m(\alpha)$ after the detection of one photon.

The statistics of photon bundles characterized with $\langle m \rangle_c$ after ~ 5000 photon detection events are presented in Fig. 5.5. The corresponding bundle size will be $\langle m \rangle_c + 1$, as it is conditioned on the detection of a photon. The drive strengths are chosen within region (II), corresponding to the specific emitter number. As expected, the distribution with an empty cavity follows the Poisson distribution $P_m(\alpha)$ [Fig. 5.5(a)]. Including a single emitter in the cavity, we find a large enhancement of two-photon bundles ($\langle m \rangle_c + 1 = 2$) [Fig. 5.5(b)]. Similarly, we find an enhancement of three-photon bundles in the case with two emitters in the cavity [Fig. 5.5(c)]. These observations agree well with the picture of $(N+1)$-photon enhancement due to the unconventional saturation effect. The case with three emitters in the cavity also shows an enhancement of $(N+1)$-photon bundles. However, it is clear from Fig. 5.5(c) that the suppression of lower photon numbers ($n < N+1$) are less efficient in this case.

5.4 Outlook

So far, we have confirmed that a system displaying the unconventional saturation effect will have a large bunching of photons in the cavity field. We have also found that the photons leaking out of the cavity will have an enhancement of photon bundles compared to a coherent light source, which could find applications in post-selection schemes or multiphoton spectroscopy. In Paper B, we also employ a cascaded-quantum-system ap-

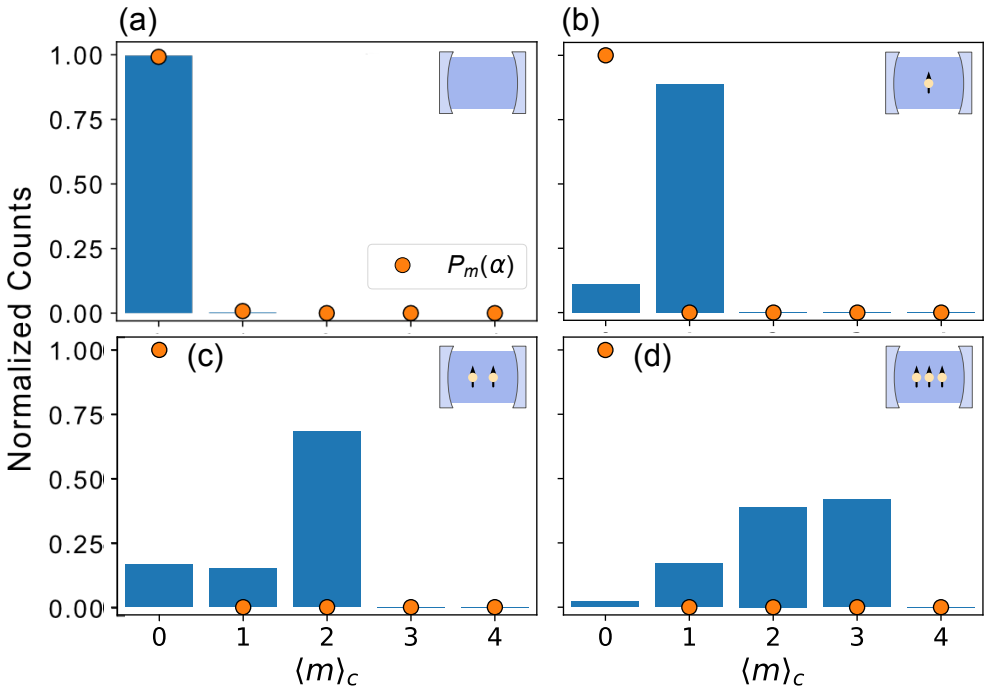

Figure 5.5: Remaining excitations in the cavity-emitter system after the detection of a photon for (a) an empty cavity and drive $\Omega_d/\gamma_c = 0.4$, and (b)-(d) a cavity containing $N = \{1, 2, 3\}$ emitters and drive amplitudes $\Omega_d/\gamma_c = \{0.3, 0.4, 0.8\}$. The orange circles mark the corresponding distribution for a coherently driven cavity with the same output flux α of photons. The data used to produce this figure consists of $\sim$ 5000 photon detection events.

proach to catch the output state with a boxcar filter. Catching states conditioned on a photon detection event display Wigner distributions corresponding to superpositions of fock states up to $\langle m \rangle_c$ photons. Thus, our preliminary results demonstrate the potential to harness this, previously overlooked, nonlinear effect emerging in lossy Tavis-Cummings systems. However, there is more work required to fully understand and characterize the output field in this regime. There are also open fundamental questions about how the competition between coherent and incoherent processes settles the system's behavior. Understanding the fundamental mechanism that governs the behavior of small emitter ensembles in driven cavities will help guide the development of new quantum technology.

Chapter 6

Photon blockade breakdown in the few-emitter limit

This chapter leaves the lossy cavity modes behind and focuses on Tavis–Cummings systems with a few emitters inside *high-quality* cavity, which is the model system in Paper C. However, even though the work of Paper C considers a low-loss cavity mode, the inspiration for this work came from where Paper A left off. The increasingly sharp transitions between the two linear regimes with increasing emitter number N, found in Paper A, suggest a critical behavior in the limit $N \to \infty$. My initial studies in the lossy cavity regime showed that the observed cavity response could be related to absorptive optical bistability [106] in the limit $N \to \infty$ in a low-photon density regim [107, 108]. Yet, at the same time as I observed the indications of optical bistability in the large N limit, I also found bimodal Wigner distributions, which is considered a signature of bistability, with only a few two-level emitters. The latter was surprising as previous studies on the extension of single-atom bistability [109] to the few-emitter regime [110] had ruled out the possibility of optical bistability with a few emitters with my set of parameters. This raised questions about the correlations that arise between the cavity field and the emitters that are imprinted in the cavity field and are tractable in the few-emitter regime. With my coauthors of Paper C, we set out to answer these questions, leading to the work presented in Paper C, which will be summarized in the following.

6.1 Model system

The notation in Paper C is slightly different from the previous chapter therefore, the Hamiltonian is repeated here for clarity,

$$\tilde{\mathcal{H}}_\varepsilon = \hbar\Omega(\hat{S}_+\hat{a} + \hat{S}_-\hat{a}^\dagger) + \hbar\varepsilon(\hat{a} + \hat{a}^\dagger). \tag{6.1}$$

This is again the driven Tavis–Cummings Hamiltonian in the rotating frame of the drive on resonance with the cavity and emitters. The coupling strength is now denoted Ω, and ε is the drive strength. Dissipation is included with the master equation

$$\dot{\hat{\rho}} = (i\hbar)^{-1}\left[\tilde{\mathcal{H}}_\varepsilon, \hat{\rho}\right] + 2\kappa\left(\hat{a}\hat{\rho}\hat{a}^\dagger - \frac{1}{2}\hat{a}^\dagger\hat{a}\hat{\rho} - \frac{1}{2}\hat{\rho}\hat{a}^\dagger\hat{a}\right), \tag{6.2}$$

where we consider photon loss with the decay rate κ as the only decay channel. As this master equation does not have any local emitter processes that mix states from different spin sectors, the total angular momentum S is a conserved quantity. Therefore, we can work with the total angular momentum states $|S, m_s\rangle$ with a fixed total angular momentum S. The results presented in Paper C are obtained within the full-spin sector $S = n_{at}/2$, where n_{at} is the number of emitters.

6.2 Successive quasienergy collapses

The work in Paper C emphasizes the role of the dressed states in the behavior of the driven-disspative Tavis–Cummings system. Through a systematic analysis, we could demonstrate a structure in the system, provided by the dressed states, that is maintained in the presence of cavity drive and dissipation.

The eigenenergies of the Tavis–Cummings Hamiltonian without drive and dissipation were shown in Fig. 4.1. Including a drive on the cavity shifts the attention from energies and eigenstates into quasienergies and time-periodic states that satisfy

$$\tilde{\mathcal{H}}_\varepsilon|\psi_\alpha\rangle = \tilde{E}_\alpha|\psi_\alpha\rangle. \tag{6.3}$$

When the drive is weak, it will only be a small perturbation to the undriven dressed states, and the corresponding quasienergies will have a discrete spectrum that resembles the undriven spectrum. In the rotating frame of the drive, these energies will be symmetrically split around 0. As the drive increases, the time-periodic solutions to Eq. (6.3) begin to spread along different excitation manifolds. These driven states have been found analytically for a single atom [111–113], and a similar mechanism is expected to follow for many atoms. Following the single-atom results, the quasienergies are found to maintain the discrete $\sqrt{n}$-anharmonic structure at weak drives but will become closer

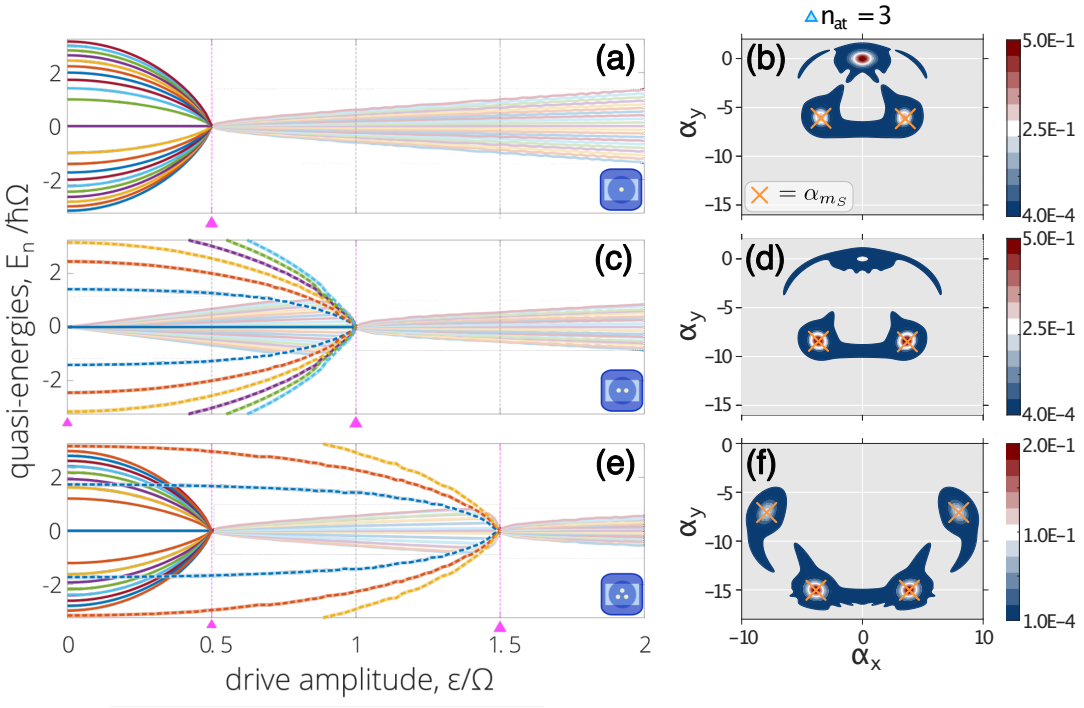

Figure 6.1: [(a),(c),(d)] Quasienergies of the driven Tavis–Cummings Hamiltonian for $n_{at} = \{1, 2, 3\}$ obtained via numerical diagonalization of Eq. (6.1). A discrete spectrum found at small drive amplitudes collapses at the critical drives $\varepsilon_{\text{col}}(m_s) = |m_S|\Omega$ with $m_S = 0, (\frac{1}{2}), 1, (\frac{3}{2}), \ldots, \frac{1}{2}n_{at}$ for even (odd) number of atoms. After each collapse (pink triangles), a continuous spectrum rises (shaded lines). These partial collapses allow for states to be organized into separate groups denoted by the cooperative number m_S, drawn here as solid and dashed lines. [(b),(d),(f)] Wigner distributions of the cavity field with $n_{at} = 3$. After each collapse point, two new peaks appear in the Wigner distributions. Orange crosses mark the approximate coherent states amplitudes α_{m_S}, obtained with the mean-field equations.

and closer in energy as the drive increases until they collapse into a continuous spectrum at the point $\varepsilon = 1/2$. Physically, we can understand this behavior as a photon-blockade effect [113], where the anharmonicity at low excitation levels prevents excitation of the system at weak drives, which is then broken through at high levels of excitation where the excitation paths become quasi-harmonic.

In Paper C, we numerically solved for the quasienergies with $n_{at} = \{1, 2, 3\}$, and found that the single-atom behavior is, indeed, maintained with many atoms, but now, the collapses occur successively. Moreover, following the approach of Ref. [112], we could find the collapse point of the successive collapses and relate it to the emitter projections m_S:

$$\boxed{\varepsilon_{\text{col}}(m_S) = \Omega|m_S|.} \tag{6.4}$$

The successive collapses of the quasienergies are shown in Fig. 6.1(a) that plots the quasienergies for $n_{at} = \{1, 2, 3\}$ as a function of the drive ε. The pink triangles mark the collapse points $\varepsilon_{\text{col}}(m_S)$. After each collapse point, there is a large degeneracy of states at the drive frequency. The shaded solutions in Fig. 6.1(a) are numerical artifacts arising from working in a truncated Fock-basis.

6.2.1 Multipeaked Wigner distributions

Next, we included the effects of photon loss described by the master-equation (6.2). Dissipation will, in general, stabilize a driven system in a steady state with a well-defined excitation number. However, in Paper C, we additionally found that photon loss in this system will stabilize the steady state in a superposition of coherent states that are correlated with the emitter projection m_S via the parallel quasiharmonic excitation paths, high up the Tavis–Cummings ladders. By plotting the steady-state Wigner distributions of the cavity field at increasingly strong drives, we could see these metastable coherent states emerge after each collapse point. Our results for $n_{at} = 3$ is shown in Fig. 6.1(b). The top panel is obtained close after the first collapse point $\varepsilon_{\text{col}}(1/2)$ and shows how the empty-cavity solution at $\alpha_x = \alpha_y = 0$ gives way to a double-peaked Wigner distribution. The empty-cavity solution vanishes as the drive increases (middle panel), and at strong drives, far beyond the second collapse point $\varepsilon_{\text{col}}(3/2)$, four well-separated peaks are found (bottom panel) corresponding to $m_S = \left\{-\frac{3}{2}, -\frac{1}{2}, \frac{1}{2}, \frac{3}{2}\right\}$.

The emergence of multiple peaks in the Wigner distributions can be associated with the coexisting dressed-state ladders (labeled by m_S) in a mean-field picture, where the cooperative response of the emitters can be seen as independent radiating dipoles radiating with the rate $|m_S|\Omega$. In this picture, the mean-field solution $\alpha_{m_S} = \langle \hat{a} \rangle_{m_S}$ above

$\varepsilon_{\text{col}}(m_s)$ can be found as

$$\alpha_{m_S} = -i\frac{\varepsilon}{\kappa}\left[1 + \frac{m_S\Omega}{\kappa|\alpha_{m_S}|}\right]^{-1}, \tag{6.5}$$

with

$$|\alpha_{m_S}|^2 = \left(\frac{\varepsilon}{\kappa}\right)^2\left[1 - \left(\frac{m_S\Omega}{\varepsilon}\right)^2\right]. \tag{6.6}$$

The mean-field amplitudes α_{m_S} display two opposite phases corresponding to the plus and minus rungs of the m_S-ladders in the Tavis–Cummings spectrum. The orange crosses in Fig. 6.1(b) show that these solutions coincide perfectly with the peaks in the Wigner distributions.

However, the excitation paths in the real system are not independent, and fluctuations will induce switching between them. Yet, the likelihood of switching decreases in the limit of large excitation, thus making it more likely for the system to remain inside a single m_S-ladder as the excitation number increases. In this limit, it is possible to create approximate eigenstates of the jump operator $\hat{a}$ within a single ladder. These approximate states will resemble coherent states with the amplitudes α_{m_S}, thus the success of the mean-field solutions. Moreover, as these states are approximate pointer states (eigenstates of the jump operator), they will act as attractors under time evolution with the master equation (6.2, which minimizes the rate at which the system loses its purity to the environment [114].

6.3 Outlook

Our work in Paper C is a generalization of the photon blockade breakdown with a single two-level atom to the few-emitter regime. The breakdown of photon blockade has been characterized as a 2nd-order dissipative phase transiton [113]. The thermodynamic limit in this system is defined by the limits $\varepsilon/\kappa \gg 1$ and $\Omega/\kappa \gg 1$, with $\varepsilon/\kappa = constant$, which corresponds to the limit where we see the individual m_S-ladders becoming more and more independent. The work in Ref. [115] showed that the photon blockade breakdown can be associated with a spontaneous breaking of an antiunitary particle-hole type of symmetry that is related to a sign change in the atomic operators $\hat{S}_{x,y}$ accompanied by one in the field quadratures $(\hat{a} \pm \hat{a}^\dagger)$. Our numerical study in Paper C supports their single-atom results, but in our few-emitter limit, the symmetry is broken in stages.

In particular, we looked for signatures of symmetry breaking in the Liouvillian spectrum [116, 117], which is indicated by multiple eigenvalues of the Liouvillian to approach 0 in the thermodynamic limit [116, 118, 119]. Our results displayed a complex

interplay of attraction and repulsion of the biggest[1] eigenvalues as the drive was increased. As our study was numerical, we were limited to finite-size systems, so our results are not more than indicative. Nevertheless, we could see a clear and sharp rise of $2s$ eigenvalues, related to the atomic number as $s = n_{at}/2$, appearing successively after each collapse point $\varepsilon(m_S)$ and in good agreement with the appearance of multiple peaks in the Wigner distributions. This implies the existence of $2s+1$ different symmetry sectors, which we relate to the number of possible dressed-states ladders. However, the symmetry was not characterized explicitly and, thus, remains an open question. The signatures in the system indicate a discrete Z_n symmetry that should be revealed by a generalization of the single-atom results in Ref. [115] but was not immediately trivially seen in our numerical investigations.

A full characterization of the symmetries in the few-emitter regime of the driven-dissipative Cummings model would be a valuable contribution that could provide theoretical insights into the role of the competition between coherent and incoherent processes in settling the system's behavior. An important part of this investigation would be to look at other decay channels, including individual, and collective spontaneous emission from the emitters. This could not only help in relating the results of Paper Cto the seemingly different correlations between the field and the emitters that were shown in Paper A. It could also help bridge the gap between one, a few, and many emitters and connect the breakdown of photon blockade to optical bistability and collective resonance fluorescence.

[1]The Liouviliian eigenvalues are negative to ensure decay to a steady state. The eigenvalues are, moreover, complex. As our system does not have the symmetries required to have oscillating coherence – eigenvalues with zero real part and non-zero imaginary part – the imaginary parts of the biggest eigenvalues are zero in our case.

Part II
Identical harmonic emitters

The second part of this thesis is dedicated to the intriguing properties of polaritons in the strong- and ultrastrong-coupling regimes. In particular, we are interested in polaritons formed with a single light mode of a microcavity and the collective bright mode of an array of identical metallic nanoparticles that sustain surface plasmon polaritons. This is the model system of Paper D whose main results will be discussed in Chapter 8. While our study was performed on this particular plasmon-microcavity system, our results are also relevant for a big family of polaritonic platforms where a Lorentzian permittivity can describe the matter component. A Lorentzian approximation has, for example, been applied to an ensemble of atoms [120], phonons in a crystal [121], excitons and phonons in a 2D crystal [122], and excitons in organic molecules [123].

Chapter 8 will additionally give a quantum description of this model system for cavity-polaritons, which was described classically in Paper D. To this end, the Hopfield model for coupled bosonic modes described by quadratic Hamiltonians is introduced in Chapter 7. The Hopfield model is a versatile tool for coupled modes that can be modeled as harmonic oscillators described by bosonic creation and annihilation operators. Even though the observed phenomena in Paper D are essentially classical, the quantum description provides further insight into the effects of the light-matter interaction.

Chapter 7

The Hopfield model

The modern formulation of the Hopfield model describes the coupling between the electromagnetic field and a generic matter field whose excitation and deexcitation can be described by bosonic creation and excitation operators. In Chapter 8, we will apply the Hopfield model to the plasmon-microcavity of Paper D to explore the effects of the RWA and the $\mathbf{A}^2$-term on the polaritonic decay rates. As a primer for that study, Section 7.2 of this chapter will discuss the diagonalization of the Hopfield Hamiltonian, and provide expressions for the polaritonic operators in terms of the so-called Hopfield coefficients. But first, the original formulation from Hopfield will be briefly introduced below. This will give context to the great versatility of the Hopfield model. Then, in Section 7.1, we will move on to discuss the equivalence between the Coulomb and dipole gauge formulations, as this has recently been a topic of heated discussions in the context of ultrastrong coupling.

The Hopfield model originates back to Hopfield's seminal work on exciton-polaritons formed due to light-matter interaction in a bulk dielectric, published in 1958 [44]. In this work, Hopfield demonstrates that it is necessary to also include the interaction with light when describing excitons in a 3D crystal. In particular, Hopfield describes the excitation of excitons in a uniform dispersionless dielectric as approximate bosonic modes and uses a coupled-boson Hamiltonian for the light-matter interaction between these collective matter modes and the electromagnetic field. Since then, this model has been generalized and applied to many different interacting light-matter systems where the light and matter modes can be described by Lorenztian bosonic fields including quantum wells [124], cavity polaritons [125], phonon polaritons [126, 127], and plasmon polaritons [13, 128].

Following the original formulation, the Hopfield Hamiltonian in the Coulomb gauge ($\nabla \cdot \mathbf{A} = 0$) can be written as

$$\begin{aligned}\hat{H}_{\mathrm{hop}} = &\sum_{\mathbf{k},\sigma} \hbar\omega_{\mathbf{k},\sigma}\left(\hat{a}^{\dagger}_{\mathbf{k},\sigma}\hat{a}_{\mathbf{k},\sigma} + \frac{1}{2}\right) + \hbar\omega_0 \sum_{\mathbf{k},\sigma}\left(\hat{b}^{\dagger}_{\mathbf{k},\sigma}\hat{b}_{\mathbf{k},\sigma} + \frac{1}{2}\right) \\ &+ i\hbar\omega_0 \sum_{\mathbf{k},\sigma} \lambda_k\left(\hat{a}_{\mathbf{k},\sigma} + \hat{a}^{\dagger}_{-\mathbf{k},\sigma}\right)\left(\hat{b}_{\mathbf{k},\sigma} - \hat{b}^{\dagger}_{-\mathbf{k},\sigma}\right) \\ &+ \hbar\omega_0 \sum_{\mathbf{k},\sigma} \lambda_k^2\left(\hat{a}_{\mathbf{k},\sigma} + \hat{a}^{\dagger}_{-\mathbf{k},\sigma}\right)^2,\end{aligned} \tag{7.1}$$

where the index $\mathbf{k}$ labels the wave vector, and σ labels the two transverse polarization directions defined by the polarization unit vectors $\mathbf{e}_{\mathbf{k},\sigma}$. The first line in the Hamiltonian describes the bare light and matter modes without the light-matter interaction. The terms on the second and third lines arise from the minimal coupling replacement $(\mathbf{p} + e\mathbf{A})^2$ and describe, respectively, the light-matter coupling with coupling parameter $\omega_0\lambda_k$ and the $\mathbf{A}^2$-term. The operators $\hat{a}_{\mathbf{k},\sigma}$ are the standard bosonic annihilation operators for the electromagnetic field with dispersion $\omega_{\mathbf{k},\sigma}$, and the $\hat{b}_{\mathbf{k},\sigma}$ operators are bosonic annihilation operators for the matter excitations with frequency ω_0. As in Hopfield's formulation, the matter frequency ω_0 is fixed assuming dispersionless matter excitation and the field and matter operators obey the bosonic commutation relations $[\hat{a}_{\mathbf{k},\sigma}, \hat{a}_{\mathbf{k}'\sigma'}] = [\hat{b}_{\mathbf{k},\sigma}, \hat{b}_{\mathbf{k}'\sigma'}] = \delta_{\mathbf{k},\mathbf{k}'}\delta_{\sigma,\sigma'}$, where $\delta_{x,x'}$, $\{x = \mathbf{k}, \sigma\}$ is the Kronecker delta.

7.1 Equivalence of the dipole and Coulomb gauges

In recent years, an old discussion about the subtleties [129, 130] of gauge invariance in quantum light-matter Hamiltonians was reignited by ambiguous results found in the Coulomb and dipole gauges in the ultrastrong coupling regime [131, 132]. Most of the issues were related to an inappropriate application of the two-level approximation and a consistent transformation between the two gauges was shortly resolved [39, 133–135]. Yet, the discussion about gauge invariance is still ongoing [133, 136, 137].

As the Hopfield model does not rely on a two-level approximation, it has generally been considered protected from the discussed gauge ambiguities, even though it is known that the parameters that enter the interaction Hamiltonian are gauge-dependent and cannot be directly compared. The benefit of writing the Hopfield Hamiltonian on the form in Eq. (7.1) is that the coupling parameter λ_k remains invariant [32] under the unitary Power-Zienau-Woolley (PZW) transformation [133], taking the Coulomb gauge Hamiltonian into the dipole gauge Hamiltonian. One should not forget, however, that by

choosing a gauge, one also chooses constraints that are included in the field and matter operators, which *are* gauge-dependent. Choosing a gauge does not change observables, but the different constraints are the reason for the different forms of the interaction parameters. This fact can be exemplified by noting that the Hopfield Hamiltonian in the Coulomb gauge can be written as [32]

$$\hat{H}_{\mathrm{C}} = \hat{H}_a + \hat{U}\hat{H}_b\hat{U}^\dagger, \tag{7.2}$$

with $\hat{U} = \exp[i\sum_{\mathbf{k},\sigma}\lambda_k(\hat{a}_{\mathbf{k},\sigma}+\hat{a}^\dagger_{-\mathbf{k},\sigma})(\hat{b}_{\mathbf{k},\sigma}-\hat{b}^\dagger_{-\mathbf{k},\sigma})]$, and $\hat{H}_a$ and $\hat{H}_b$ being the bare light and matter Hamiltonians, respectively. Similarly, the dipole gauge Hamiltonian can be written as

$$\hat{H}_{\mathrm{D}} = \hat{U}\hat{H}_a\hat{U}^\dagger + \hat{H}_b. \tag{7.3}$$

For an electromagnetic field and generic polarization field associated with the matter excitation described by

$$\hat{\mathbf{A}}(\mathbf{r}) = \sum_{\mathbf{k},\sigma} A_{k,0}\mathbf{e}_{\mathbf{k},\sigma}\left(\hat{a}_{\mathbf{k},\sigma} + \hat{a}^\dagger_{-\mathbf{k},\sigma}\right)\mathrm{e}^{i\mathbf{kr}}, \tag{7.4}$$

$$\hat{\mathbf{P}}(\mathbf{r}) = P_0\sum_{\mathbf{k},\sigma} \mathbf{e}_{\mathbf{k},\sigma}\left(\hat{b}_{\mathbf{k},\sigma} + \hat{b}^\dagger_{-\mathbf{k},\sigma}\right)\mathrm{e}^{i\mathbf{kr}}, \tag{7.5}$$

the unitary operator $\hat{U}$ coincide with the PZW transformation

$$\begin{aligned}\hat{T} &= \exp\left[\frac{i}{\hbar}\int_{\mathbf{r}} \mathrm{d}\mathbf{r}\ \hat{\mathbf{A}}(\mathbf{r})\hat{\mathbf{P}}(\mathbf{r})\right], \\ &= \exp\left[i\sum_{\mathbf{k},\sigma}\lambda_k(\hat{a}_{\mathbf{k},\sigma} + \hat{a}^\dagger_{-\mathbf{k},\sigma})(\hat{b}_{\mathbf{k},\sigma} - \hat{b}^\dagger_{-\mathbf{k},\sigma})\right]\end{aligned} \tag{7.6}$$

with $\lambda_k = VA_{k,0}P_0$ and V the quantization volume. Thus, applying the PZW transformation, one finds that the Coulomb gauge representation of the bare matter operators is given by $\hat{b}_{\mathrm{C}} = \hat{T}\hat{b}\hat{T}^\dagger$, and conversely the dipole gauge representation of the bare field operators is given by $\hat{a}_{\mathrm{D}} = \hat{T}\hat{a}\hat{T}^\dagger$. The physical interpretation of $\hat{a}_{\mathrm{D}}$ and $\hat{b}_{\mathrm{C}}$ is that they represent the physical light-like and matter-like fields, respectively, that describe the annihilation of the physical quanta of the fields [32, 138]. The index $\mathbf{k}, \sigma$ has been dropped here and in the rest of the section for better readability.

For most practical applications of the Hopfield model, one can use the Coulomb and dipole gauges interchangeably without knowledge of $\hat{a}_{\mathrm{D}}$ and $\hat{b}_{\mathrm{C}}$ and still get the correct results. So why go through all this trouble? In addition to gaining insight into the meaning of physical (measurable) fields and gauge invariance, the motivation for this thesis is the recent publication [138]. This work showcased that one obtains ambiguous values for the dephasing rates in an open Hopfield model if the bare operators $\hat{a}$ and $\hat{b}$

are erroneously used in the perturbation Hamiltonian in the dipole and Coulomb gauges, respectively. With the formulation in Eqs. (7.2) and (7.3), it is easy to see how these ambiguities arise as $\hat{a}^\dagger\hat{a} \neq \hat{T}\hat{a}^\dagger\hat{a}\hat{T}^\dagger$ and $\hat{b}^\dagger\hat{b} \neq \hat{T}\hat{b}^\dagger\hat{b}\hat{T}^\dagger$.

In the next chapter, we consider another open Hopfield model to find expressions for the polaritonic decay rates in a quantum description. Therefore, we went through this somewhat lengthy discussion to make sure that the dissipation model employed is appropriate for our purposes. In our case, we use the Coulomb gauge representation and are interested in single-photon loss which for the matter mode is modeled by the system-reservoir interaction Hamiltonian $\hat{H}_{\mathrm{SR}} = \sum_j(\hat{b} + \hat{b}^\dagger)(\kappa_j\hat{r}_j + \kappa_j^*\hat{r}_j^\dagger)$. Using the explicit expression for $\hat{T}$ from Eq. (7.6), and after performing some algebra, it is easy to see that the dissipation model for single-photon loss is invariant under the PZW transformation $(\hat{b} + \hat{b}^\dagger) = \hat{T}(\hat{b} + \hat{b}^\dagger)\hat{T}^\dagger$. Hence, the bare matter operators $\hat{b}$ and $\hat{b}^\dagger$ can safely be used without loss of generality.

7.2 Polaritonic eigenenegergies and eigenoperators

As preparation for Chapter 8 on polaritonic decay rates, this section presents the eigenenergies and eigenoperators for the Hopfield Hamiltonian. The eigenenergies and eigenoperators correspond to the polaritonic resonances and their bosonic annihilation and creation operators. As the Hopfield Hamiltonian is bilinear and at most quadratic, the solution can be obtained analytically by a bosonic Bogoliubov transformation [139, 140].

In the following, a two-mode version of the Hopfield Hamiltonian (7.1) will be considered. This reduction of the problem will make for easier readability and suffices for describing the interaction between a single-mode electromagnetic resonator and a bosonic matter field that models certain collective matter excitations, also Hopfield's original formulation naturally reduces to a two-mode version for each $|\mathbf{k}|$ when modes with different $\mathbf{k}$ and σ don't couple [44]. The bosonic Bogoliubov transformation technique is, nevertheless, not restricted to two modes as long as the mode couplings remain bilinear.

Let $\hat{a}$ and $\hat{a}^\dagger$ represent the annihilation and creation operators for the light mode, and $\hat{b}$ and $\hat{b}^\dagger$ represent the (bosonic) annihilation and creation operators for the matter mode. Then, the two-mode Hopfield Hamiltonian is

$$\begin{aligned}\hat{H}_{ab} =& \hbar\omega_a\left(\hat{a}^\dagger\hat{a} + \frac{1}{2}\right) + \hbar\omega_b\left(\hat{b}^\dagger\hat{b} + \frac{1}{2}\right) \\ &+ i\hbar\omega_b\lambda\left(\hat{a} + \hat{a}^\dagger\right)\left(\hat{b} - \hat{b}^\dagger\right) + \hbar\omega_b\lambda^2\left(\hat{a} + \hat{a}^\dagger\right)^2\end{aligned} \tag{7.7}$$

It is possible to diagonalize $\hat{H}_{ab}$ directly, but it is instructive to perform the diagonal-

ization in two steps: first, a single-mode Bogoliubov rotation to get rid of the quadratic term, and secondly a two-mode Bogoliubov rotation on the resulting Hamiltonian that now only have linear terms. The transformation of a general single-mode Hamiltonian and a general two-mode Hamiltonian with no self-quadratic terms are shown in Box 1 and Box 2, respectively.

BOX 1

SINGLE-MODE QUADRATIC HAMILTONIAN

$$\tfrac{1}{\hbar}\hat{H} = w\hat{a}^\dagger\hat{a} + w\hat{a}\hat{a}^\dagger + v\hat{a}^\dagger\hat{a}^\dagger + v\hat{a}\hat{a}, \quad w, v \in \mathbb{R}$$
$$\Rightarrow \quad \tfrac{1}{\hbar}\tilde{H} = \tilde{\omega}\left(\tilde{a}^\dagger\tilde{a} + \frac{1}{2}\right)$$

$$\tilde{\omega} = 2\Omega = 2\sqrt{w^2 - v^2}, \quad \text{condition: } w^2 > v^2$$

$$\begin{bmatrix}\tilde{a}\\ \tilde{a}^\dagger\end{bmatrix} = U\begin{bmatrix}\hat{a}\\ \hat{a}^\dagger\end{bmatrix}, \qquad \begin{bmatrix}\hat{a}\\ \hat{a}^\dagger\end{bmatrix} = U^{-1}\begin{bmatrix}\tilde{a}\\ \tilde{a}^\dagger\end{bmatrix}$$

$$U = \begin{bmatrix}u_1 & u_2\\ u_2 & u_1\end{bmatrix}, \qquad U^{-1} = \begin{bmatrix}u_1 & -u_2\\ -u_2 & u_1\end{bmatrix}$$

$$u_1 = \frac{\sqrt{w+\Omega}}{\sqrt{2\Omega}}, \qquad u_2 = \frac{\sqrt{w-\Omega}}{\sqrt{2\Omega}}, \quad \text{constraint: } |u_1|^2 - |u_2|^2 = 1$$

STEP 1: The Hamiltonian for the light mode only can be written in matrix form as

$$\frac{\hat{H}_a}{\hbar} = \begin{bmatrix}\hat{a}^\dagger & \hat{a}\end{bmatrix}\begin{bmatrix}\frac{\omega_a}{2} + \omega_b\lambda^2 & \omega_b\lambda^2\\ \omega_b\lambda^2 & \frac{\omega_a}{2} + \omega_b\lambda^2\end{bmatrix}\begin{bmatrix}\hat{a}\\ \hat{a}^\dagger\end{bmatrix} = \langle\mathbf{a}|\, M\, |\mathbf{a}\rangle\,. \tag{7.8}$$

A Bogoliubov transformation takes the matrix M to its diagonal form and ensures that the new eigenoperators obey bosonic commutation relations. The details will not be presented here, but the results from a general single-mode transformation with real matrix elements are found in Box 1. Note that a standard matrix diagonalization of M would not automatically ensure bosonic commutation relations.

The diagonal form of the light mode Hamiltonian is

$$\boxed{\hat{H}_{\tilde{a}} = \hbar\tilde{\omega}_a\left(\tilde{a}^\dagger\tilde{a} + \frac{1}{2}\right),} \tag{7.9}$$

$$\boxed{\tilde{\omega}_a = \sqrt{\omega_a^2 + 4\omega_a\omega_b\lambda^2},} \tag{7.10}$$

and the diagonal-form operators are

$$\boxed{\tilde{a} = u_1\hat{a} + u_2\hat{a}^\dagger,} \tag{7.11}$$

$$\boxed{\tilde{a}^\dagger = u_2\hat{a} + u_1\hat{a}^\dagger,} \tag{7.12}$$

with the coefficients obeying the constraint $|u_1|^2 - |u_2|^2 = 1$, which ensures the bosonic commutation reltation $\left[\tilde{a}, \tilde{a}^\dagger\right] = 1$. The inverse transformation gives the bare operators in terms of the new ones as,

$$\boxed{\hat{a} = u_1\tilde{a} - u_2\tilde{a}^\dagger,} \tag{7.13}$$

$$\boxed{\hat{a}^\dagger = -u_2\tilde{a} + u_1\tilde{a}^\dagger.} \tag{7.14}$$

Equation (7.10) displays how the resonance frequency for the light mode is shifted due to the light-matter interaction. Hence, if the bare frequencies of the two modes were initially tuned $\omega_a = \omega_b \equiv \omega_0$, the light-matter interaction will make them slightly detuned $\tilde{\omega}_a - \omega_0 \approx 2\omega_0\lambda^2$, assuming $4\lambda^2 \ll 1$. The detuning is approximately the strength of the diamagnetic ($\mathbf{A}^2$) term and can, in general, be neglected when λ is small, e.g., in the strong-coupling regime.

A common gauge-related misconception is a belief that this light-matter-induced detuning could be avoided in the dipole gauge where the quadratic term instead involves the matter operators. This is not true, and performing an analogous Bogoliubov transformation on the matter mode in the dipole gauge would instead give a shifted matter frequency $\tilde{\omega}_b = \sqrt{\omega_b^2 + 4\omega_a\omega_b\lambda^2}$. Here, we also see another example of the benefit of writing the light-matter coupling parameter in terms of the coulomb-dipole-gauge invariant parameter λ which makes the expressions in the two gauges symmetric with respect to the resonance frequencies.

Interestingly, $\tilde{\omega}_a$ ($\tilde{\omega}_b$) coincides with the resonance of the upper polariton found in the limit $k \to 0$ in the case of bulk polaritons, which additionally defines the upper edge of the polaritonic gap [141]. That is: a region of forbidden frequencies for light propagation. This region has been interpreted as the so-called Reststrahlen band, wherein the real part of the permittivity becomes negative, thus forbidding the propagation of plane waves [44]. Consequently, the results of this partial diagonalization of the Hopfield Hamiltonian provide a connection between the opening of a polaritonic gap and the effect of the diamagnetic term in the light-matter interaction Hamiltonian.

BOX 2

TWO-MODE BILINEAR HAMILTONIAN

$$\tfrac{1}{\hbar}\hat{H} = w_{11}\Big(\hat{a}^\dagger\hat{a} + \hat{a}\hat{a}^\dagger\Big) + w_{22}\Big(\hat{b}^\dagger\hat{b} + \hat{b}\hat{b}^\dagger\Big) + w_{12}\Big(\hat{a}^\dagger\hat{b} + \hat{b}\hat{a}^\dagger\Big) + w_{12}^*\Big(\hat{a}\hat{b}^\dagger + \hat{b}^\dagger\hat{a}\Big)$$
$$+v_{12}\Big(\hat{a}\hat{b} + \hat{b}\hat{a}\Big) + v_{12}^*\Big(\hat{a}^\dagger\hat{b}^\dagger + \hat{b}^\dagger\hat{a}^\dagger\Big), \quad w_{11}, w_{22} \in \mathbb{R}, \quad w_{12}, v_{12} \in \mathbb{C},$$
$$\Rightarrow \quad \tfrac{1}{\hbar}\tilde{H} = \omega_A\left(A^\dagger A + \frac{1}{2}\right) + \omega_B\left(B^\dagger B + \frac{1}{2}\right).$$

$$\omega_A = 2\sqrt{C_1/2 + \sqrt{C_1^2/4 - C_2}}, \qquad \omega_B = 2\sqrt{C_1/2 - \sqrt{C_1^2/4 - C_2}},$$
$$C_1 = w_{11}^2 + w_{22}^2,$$
$$C_2 = w_{11}^2 w_{22}^2 - 2w_{11}w_{22}\big(|w_{12}|^2 + |v12|^2\big)$$
$$+|w_{12}|^2 + |v_{12}|^2 - 2|w_{12}|^2|v_{12}|^2.$$

$$\begin{bmatrix} A \\ B \\ A^\dagger \\ B^\dagger \end{bmatrix} = T^\dagger \begin{bmatrix} \hat{a} \\ \hat{b} \\ \hat{a}^\dagger \\ \hat{b}^\dagger \end{bmatrix}, \qquad \begin{bmatrix} \hat{a} \\ \hat{b} \\ \hat{a}^\dagger \\ \hat{b}^\dagger \end{bmatrix} = JTJ \begin{bmatrix} A \\ B \\ A^\dagger \\ B^\dagger \end{bmatrix}.$$

$$T_{4\times4} = \begin{bmatrix} T_1 & T_2 \\ T_2^* & T_1^* \end{bmatrix}, \qquad J_{4\times4} = \begin{bmatrix} \mathbb{1}_{2\times2} & 0 \\ 0 & -\mathbb{1}_{2\times2} \end{bmatrix},$$
$$T_1 = \begin{bmatrix} c_1 & d_1 \\ c_2 & d_2 \end{bmatrix}, \qquad T_2 = \begin{bmatrix} c_3^* & d_3^* \\ c_4^* & d_4^* \end{bmatrix}.$$

$$\mathbf{c} = \begin{bmatrix} c_1 & c_2 & c_3 & c_4 \end{bmatrix}^{\mathrm{T}} = \frac{\mathbf{v}_A}{\|\mathbf{v}_A\|_p}, \quad \mathbf{d} = \begin{bmatrix} d_1 & d_2 & d_3 & d_4 \end{bmatrix}^{\mathrm{T}} = \frac{\mathbf{v}_B}{\|\mathbf{v}_B\|_p},$$

where $\mathbf{v}_{A,B}$ are the eigenvectors corresponding to $\omega_{A,B}$ and the paranorm is

$$\|\mathbf{v}\|_p = \mathbf{v}^\dagger J \mathbf{v} = |v_1|^2 + |v_2|^2 - |v_3|^2 - |v_4|^2$$

STEP 2: The transformation above presents the light mode Hamiltonian in its (coulomb gauge) diagonal form, including the effects of the $\mathbf{A}^2$ term that arises due to the light-matter interaction. This shifted light mode with resonance frequency $\tilde{\omega}_a$ interacts with the matter mode with the coupling parameter $\tilde{\lambda} = \lambda(u_1 - u_2)$, where λ is the coupling parameter from Eq. (7.7), and u_1 and u_2 are the coefficients from the single-mode transformation above.

Analogous to the single-mode Hamiltonian, we can write the two-mode Hamiltonian in matrix form,

$$\frac{\hat{H}_{\tilde{a}b}}{\hbar} = \left[\begin{array}{cc:cc} \tilde{a}^\dagger & \hat{b}^\dagger & \tilde{a} & \hat{b} \end{array}\right] \frac{1}{2} \left[\begin{array}{cc:cc} \tilde{\omega}_a & i\omega_b\tilde{\lambda} & 0 & -i\omega_b\tilde{\lambda} \\ -i\omega_b\tilde{\lambda} & \omega_b & -i\omega_b\tilde{\lambda} & 0 \\ \hdashline 0 & i\omega_b\tilde{\lambda} & \omega_a & -i\omega_b\tilde{\lambda} \\ i\omega_b\tilde{\lambda} & 0 & i\omega_b\tilde{\lambda} & \omega_b \end{array}\right] \left[\begin{array}{c} \tilde{a} \\ \hat{b} \\ \hdashline \tilde{a}^\dagger \\ \hat{b}^\dagger \end{array}\right]. \tag{7.15}$$

Following the prescription in Box 2, the solution can be found as

$$\boxed{\hat{H}_{\text{pol}} = \hbar\omega_+\left(\hat{P}_+^\dagger\hat{P}_+ + \frac{1}{2}\right) + \hbar\omega_-\left(\hat{P}_-^\dagger\hat{P}_- + \frac{1}{2}\right),} \tag{7.16}$$

$$\boxed{\omega_\pm = \frac{1}{\sqrt{2}}\sqrt{\tilde{\omega}_a^2 + \omega_b^2 \pm \sqrt{\left(\tilde{\omega}_a^2 - \omega_b^2\right)^2 + 16\tilde{\omega}_a\omega_b|i\omega_b\tilde{\lambda}|^2},}} \tag{7.17}$$

with the polaritonic annihilation operators given by

$$\boxed{\hat{P}_+ = c_1\tilde{a} + c_2\hat{b} + c_3\tilde{a}^\dagger + c_4\hat{b}^\dagger,} \tag{7.18}$$

$$\boxed{\hat{P}_- = d_1\tilde{a} + d_2\hat{b} + d_3\tilde{a}^\dagger + d_4\hat{b}^\dagger.} \tag{7.19}$$

The coefficients c_i and d_i with $i = \{1, 2, 3, 4\}$ are often referred to as the Hopfield coefficients in the strong-coupling community. Here, the coefficients are allowed to be complex and they obey the constraints $|x_1|^2 + |x_2|^2 - |x_3|^2 - |x_4|^2 = 1$ for $x = \{c, d\}$. These constraints ensure that the new polaritonic operators obey the bosonic commutation relations $\left[\hat{P}_+, \hat{P}_+^\dagger\right] = \left[\hat{P}_-, \hat{P}_-^\dagger\right] = 1$. Continuing, the inverse transformation gives

$$\boxed{\tilde{a} = c_1^*\hat{P}_+ + d_1^*\hat{P}_- - c_3\hat{P}_+^\dagger - d_3\hat{P}_-^\dagger,} \tag{7.20}$$

$$\boxed{\hat{b} = c_2^*\hat{P}_+ + d_2^*\hat{P}_- - c_4\hat{P}_+^\dagger - d_4\hat{P}_-^\dagger.} \tag{7.21}$$

In the next chapter, we want to find expressions for the polaritonic decay rates using a Hopfield model for the plasmon-microcavity system from Paper D and the master equation formalism.

Chapter 8

Polaritonic decay rate asymmetry

Technical advancements over the last decade have significantly improved our control over the interaction between light and matter. As discussed in Section 1.2, photons interacting strongly with a material resonance form hybrid light-matter states called polaritons. Polaritons formed due to strong and ultrastrong light-matter coupling have gained significant attention because of their intriguing properties and their potential to modify and manipulate material properties, such as conductivity [142], energy transport [143], photochemistry [144], and chemical reaction rates [145, 146].

Despite intense research, the dissipative properties of polaritons in the strong and ultrastrong coupling regimes remain less explored. In Paper D, we experimentally and numerically demonstrate a linewidth asymmetry in a plasmon-microcavity system that challenges previous expectations of equal line widths at zero detuning [21, 147, 148]. According to previous descriptions of polaritons formed in the strong-coupling regime, the decay rates of both upper and lower polaritons are expected to equal the average of the uncoupled decay rates [21] when the light-matter system is tuned on resonance. A linewidth asymmetry only occurs at nonzero detuning [147].

Asymmetric linewidths have been previously observed in experiments on exciton-polaritons [149–151]. Several theoretical studies performed in the 90s attributed this to disorder and motional narrowing [149, 151–156]. Linewidth asymmetries continue to be observed in modern experiments [18, 150, 157–159], including the experiments presented in Paper D. These asymmetries are often attributed to the disorder proposed in the earlier theoretical studies. However, the model system in Paper D is homogeneous under the effective Lorentzian-permittivity approximation of the collective nanoparticle response and thus is disorder-free. Our results, moreover, suggest that the observed linewidth asymmetry is a general classical electromagnetism phenomenon that could be observed in other experimental platforms whose matter components can be approximated by a Lorenztian permittivity.

Even though the method used in Paper D can determine the linewidths without

detailed knowledge about the system's microscopic properties and refrains from phenomenological descriptions such as non-Hermitian Hamiltonians based on coupled-oscillator models. The study left open questions about the meaning of zero detuning and the connections to the light-matter interaction terms arising in a quantum mechanical description. For example: In Paper D, it was found that the interband transitions (IBTs) in the gold mirrors enhanced the linewidth asymmetry by broadening the upper polariton for higher angles and coupling strengths where they start to overlap spectrally. However, considering mirrors without IBTs showed that the asymmetry persists at zero detuning, but now, the polaritons share the same linewidth at a higher detuning[1]. Moreover, Paper D showed that the linewidth asymmetry also remains in the case of bulk polaritons, and in this case, it is found that the polaritonic linewidths become equal when the detuning equals the frequency shift associated with the polaritonic gap.

The preliminary results presented in Section 8.3 below display our efforts to provide insights into these questions from a quantum perspective. In contrast to a classical description based on Maxwelll's equations, a quantum description has the power to study the effects of different physical processes separately, by choosing which coherent and incoherent interactions to include. The former corresponds to the interaction terms included in the Hamiltonian, and the latter corresponds to dissipation channels included in an open quantum system treatment. This study was mainly developed in parallel with the study presented in Paper D and guided us in the discussions. As the quantum description builds on the study in Paper D, the model plasmon-microcavity system will first be briefly introduced below.

8.1 A model system for cavity-polaritons

The experimental platform considered in Paper D was constituted by an array of gold nanodisks sustaining localized surface plasmons in a Fabry–Pérot microcavity. The setup is shown schematically in Fig. 8.1(a). From an experimental perspective, this is a unique platform for cavity-polaritons as it has the potential to span all coupling regimes due to the large and tunable oscillator strength of the plasmonic nanoparticles, and the tunability of the collective coupling to the cavity mode through changes in the pitch of the array, and the diameter of the nanoparticles. Figure 8.1(c) shows experimental data for the described system for varying pitch Λ.

The localized surface plasmon modes in the nanoparticles will form collective modes when organized in an array. Depending on the pitch Λ, these modes can display a complex mode structure [160, 161]. Here and in Paper D, we are interested in a regime where the array sustains a distinct collective bright mode that can be described by an effective permittivity composed of a single Lorenztian. This was confirmed in Paper D by

[1] See Fig. S13 in the supplementary material to Paper D [14].

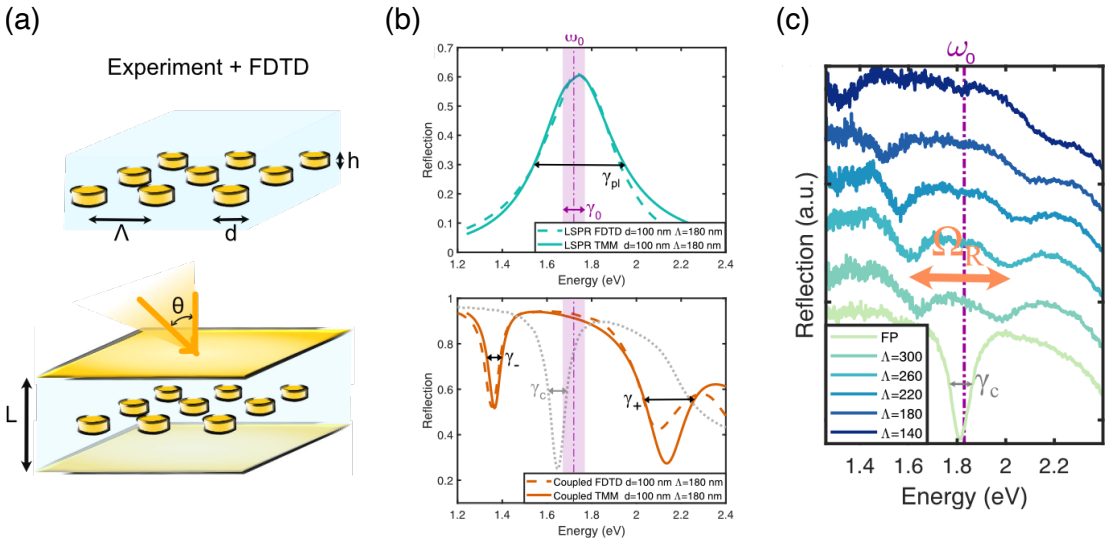

Figure 8.1: (a) Schematic illustration of the plasmonic nanoparticle array outside [top panel] and inside [bottom panel] the cavity. (b) Numerical simulations of the reflection spectrum from the plasmonic nanoparticle array [top panel] and the plasmon-micro cavity system [bottom panel]. (c) Experimental reflection spectra for increasing coupling strength ($\propto 1/\Lambda$). The figures are adapted from Paper D [14].

a comparison between exact FDTD simulations and a transfer-matrix-method (TMM) using an effective permittivity[2]. The collective mode of the particles outside the cavity is shown in the top panel of Fig. 8.1(b). When the particle array is placed inside a resonant or near-resonant cavity, the two modes hybridize and one can see the formation of two distinct polaritons, as shown in the bottom panel of Fig. 8.1(b).

8.2 Quantum description

The plasmon-microcavity system described above can be modeled by a simplified two-mode Hopfield Hamiltonian. The first mode represents the first-order Fabry–Pérot mode of the cavity, and the second mode represents the collective bright mode of the plasmonic nanoparticle array. Tuned in resonance, the coupling between these modes will be the dominant coupling mechanism in the system.

Letting the cavity and plasmon modes be represented by the pairs of bosonic annihilation and creation operators $\hat{a}, \hat{a}^\dagger$, and $\hat{b}, \hat{b}^\dagger$, respectively, the two-mode Hopfield Hamiltonian introduced in Eq. (7.7) can be written as

$$\hat{H}_{\mathrm{hop}} = \hbar\omega_c\left(\hat{a}^\dagger\hat{a} + \frac{1}{2}\right) + \hbar\omega_0\left(\hat{b}^\dagger\hat{b} + \frac{1}{2}\right) \tag{8.1}$$

$$- i\hbar g_C\left(\hat{a} + \hat{a}^\dagger\right)\left(\hat{b} - \hat{b}^\dagger\right) + \hbar\frac{g_C^2}{\omega_0}\left(\hat{a}^\dagger + \hat{a}\right)^2. \tag{8.2}$$

The first two terms describe the bare evolution of the cavity mode with resonance frequency ω_c and the plasmonic mode with resonance frequency ω_0, respectively. The third term describes the light-matter coupling with the Coulomb gauge coupling strength $g_C \equiv \omega_0\lambda$, with λ being the gauge-invariant coupling strength discussed in Section 7.1. In this system, λ will be proportional to the cavity field amplitude and the collective polarization field of the plasmonic nanoparticles. The last term is the A^2 term. By keeping the A^2 term and refraining from the RWA, this Hamiltonian is suitable for the ultrastrong-coupling regime.

The polaritonic resonance frequencies $\omega_\pm$ are given by Eq. (7.17). Expressed in terms of the Coulomb gauge coupling strength g_C they are

$$\omega_\pm = \frac{1}{\sqrt{2}}\sqrt{\tilde{\omega}_c^2 + \omega_0^2 \pm \sqrt{\left(\tilde{\omega}_c^2 - \omega_0^2\right)^2 + 16\omega_0\omega_c g_C^2}}. \tag{8.3}$$

with $\tilde{\omega}_c = \sqrt{\omega_c^2 + 4\frac{\omega_c}{\omega_0}g_C^2}$ being the shifted cavity frequency due to the A^2 term, as explained in Section 7.2. The shift of the cavity frequency due to A^2 makes the initially tuned system, $\omega_c = \omega_0$, detuned by the amount $\delta\omega = (\tilde{\omega}_c - \omega_0)|_{\omega_c=\omega_0}$. For

[2]See Paper D for details on the theoretical methods.

$4g_C^2/(\omega_c\omega_0) \ll 1$, this detuning is $\delta\omega \approx 2g_C^2/\omega_0$. Interestingly, this value coincides with the polaritonic gap found for bulk polaritions [141] in a classical description. But, in the case of the polaritonic gap for bulk polaritons, the shift is found in the material resonance $\tilde{\omega}_0$ in the limit $k \to 0$. The behavior of the corresponding polaritonic decay rates obtained in this quantum description will be studied in the next section.

8.3 Decay rate asymmetry in the open Hopfield model

The polaritonic decay rates associated with the dressed eigenmodes of the Hopfield model presented above can be found within the Born and Markov approximations by employing the Lindblad master-equation formalism introduced in Chapter 3. We are interested in investigating the dissipative properties of the polaritons in the strong and ultrastrong-coupling regimes. In particular, we are interested in the effects of approximations made in the light-matter interaction Hamiltonian. Therefore, we employ the dressed master equation for bosonic modes introduced in Section 3.3.

The dressed master equation for the two polaritonic modes is given by Eq. (3.13) with the bare modes labeled by $n = \{c, 0\}$ for the cavity and plasmon modes, respectively, and the dressed modes labeled by $m = \{+, -\}$:

$$\dot{\hat{\rho}}(t) = -\frac{i}{\hbar}\Big[\hat{H}_{\rm Hop}, \hat{\rho}(t)\Big] + \big[\Gamma_c(\omega_+) + \Gamma_0(\omega_+)\big]\mathcal{D}[\hat{P}_+]\hat{\rho} + \big[\Gamma_c(\omega_-) + \Gamma_0(\omega_-)\big]\mathcal{D}[\hat{P}_-]\hat{\rho},$$

with the superoperator $\mathcal{D}[\hat{o}]\cdot = \hat{o}\cdot\hat{o}^\dagger - \frac{1}{2}\{\hat{o}^\dagger\hat{o}, \cdot\}$ having the standard Lindblad form. Recalling the relationship $\Gamma_n(\omega_m) = \gamma_n(\omega_m)|c_{nm}|^2$ given in Eq. (3.16), the polaritonic decay rates can be identified as

Polaritonic decay rates:

$$\gamma_+ = \gamma_c(\omega_+)|c_{c+}|^2 + \gamma_0(\omega_+)|c_{0+}|^2, \tag{8.4}$$

$$\gamma_- = \gamma_c(\omega_-)|c_{c-}|^2 + \gamma_0(\omega_-)|c_{0-}|, \tag{8.5}$$

where the coefficients $|c_{c\pm}|$ and $|c_{0\pm}|$ are given by Eq. (3.15),

$$c_{c\pm} = \langle 0, \pm|\hat{a} + \hat{a}^\dagger|1, \pm\rangle\,, \tag{8.6}$$

$$c_{0\pm} = \langle 0, \pm|-i(\hat{b} - \hat{b}^\dagger)|1, \pm\rangle\,. \tag{8.7}$$

The states $|n_{ex}, \pm\rangle$ are dressed states containg $n_{ex} = \{0, 1\}$ excitations in the polaritonic modes labeled by $\{+, -\}$. The latter equation is obtained with the system operator

$(\hat{s}_n + \hat{s}_n^\dagger) = -i(\hat{b} - \hat{b}^\dagger)$, interacting with the environment. This choice is consistent with the form of the Hamiltonian in Eq. (8.1).

The frequency-dependent decay rates $\gamma_n(\omega) = 2\pi D_n(\omega)|\kappa_n(\omega)|^2$, $n = \{c, 0\}$ are determined by the density of states $D_n(\omega)$ and the coupling to the environment with strength $\kappa_n(\omega)$, assuming local white noise[3]. Evaluated at the bare resonance frequencies, they correspond to the bare decay rates: $\gamma_c(\omega_c) = \gamma_c$, and $\gamma_0(\omega_0) = \gamma_0$. In the following, it will be assumed that the decay rates $\gamma_n(\omega)$ have the same values at the two resonances, $\gamma_c(\omega_\pm) = \gamma_c$ and $\gamma_0(\omega_\pm) = \gamma_0$. As in Paper D, γ_c is the decay rate of the bare cavity and γ_0 is the intrinsic loss of the plasmon mode. In free space, the total decay rate of the bare plasmon mode would be given by $\gamma = \gamma_r + \gamma_0$ where γ_r is the radiative decay rate, that is proportional to the particle's oscillator strength [14]. However, inside the cavity, the radiative decay of the plasmon mode mainly occurs through the coupling to the cavity[4]. Thus, the radiative decay to modes other than the cavity is neglected. Nevertheless, the master equation formalism allows for absorbing additional decay channels into the parameter γ_0 if the system operators involved in the decay process are the same.

In Fig. 8.2, the polaritonic decay rates are shown as a function of the cavity-emitter detuning. The results obtained making the RWA (dash-dotted curves) again agree with the expectation of equal decay rates at zero detuning. The decay rates of the full Hopfield Hamiltonian (solid curves), on the other hand, display a large decay rate asymmetry at zero detuning. Instead, they cross at a non-zero detuning. It is tempting to attribute the crossing at a non-zero detuning to the A^2 related shift of the cavity resonance $\delta\omega$. However, as is clearly illustrated by the vertical dashed-dotted line in Fig. 8.2, this shift only accounts for a small fraction of the detuning for the new crossing point with this set of parameters, even though a considerable coupling strength ($g_C/\omega_0 = 0.15$) was chosen. Empirically varying the values of the bare decay rates show that the new crossing point strongly depends on the difference $\gamma_c - \gamma_0$, but no exact parameter dependence was determined. Similar observations were made in Fig. S13 in the supplementary material to Paper D with fully classical caluclations.

Figure 8.3 instead shows the polaritonic decay rates γ_+ and γ_- for increasing coupling strength g_C at zero detuning $\omega_c = \omega_0$. The results are obtained with Eqs. (8.4) and (8.5) using the full Hopfield Hamiltonian (8.1) [Fig. 8.3(a) (solid curves)], including all light-matter interaction terms, and within the RWA [Fig. 8.3(b) (solid curves)]. The decay rates are normalized by the average of the bare decay rates, $\gamma_{\text{avg}} = (\gamma_c + \gamma_0)/2$, to illustrate the emergence of a linewidth asymmetry that deviates from previous strong-coupling predictions. The dash-dotted curves in both panels correspond to the exclusion of the A^2 term.

[3] See Section 3.3

[4] This is the same argument as the Purcell effect in the weak-coupling regime, which leads to Purcell enhancement of the radiative decay in the resonant case.

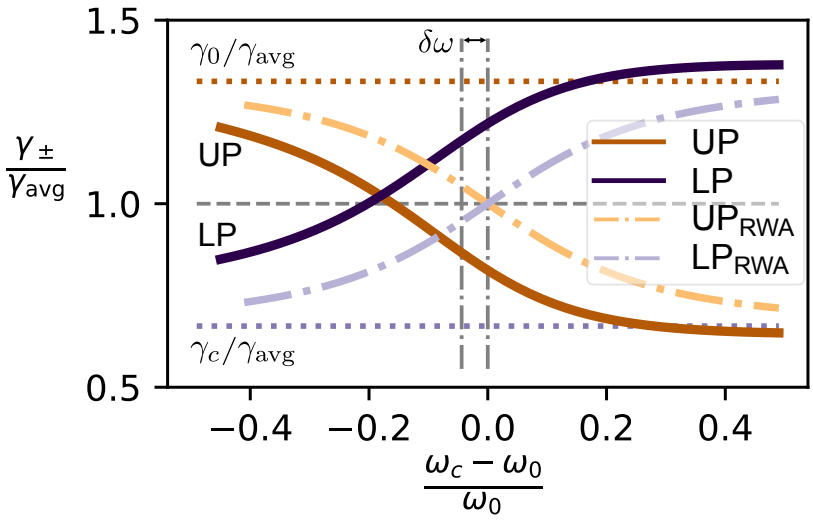

Figure 8.2: The decay rates γ_+ and γ_- as a function of the cavity-plasmon detuning. The decay rates obtained with the full Hopfield Hamiltonian (solid curves) display a large linewidth asymmetry at zero detuning and equal linewidths at negative detuning. On the other hand, the decay rates obtained within the RWA and neglecting the A^2 term (dash-dotted curves) display equal line widths at zero detuning, in agreement with previous expectations in the strong-coupling regime. The vertical dashed-dotted line marks the shift of the cavity frequency $\delta\omega$, due to the A^2 term. The coupling strength used to produce this figure was $g_C/\omega_0 = 0.15$, the other parameter was the same as in Fig. 8.3 [$\omega_c = \omega_0$, $\gamma_0/\omega_0 = 0.17$,$\gamma_c/\omega_0 = 0.08$].

The results in Fig. 8.3(b) show that making the RWA gives equal polaritonic linewidths at all coupling strengths. This result confirms the previous predictions in the strong-coupling regime [21, 147] and can be understood by the Hopfield coefficients being equal within the RWA, $|c_{c\pm}|^2_{\text{RWA}} = |c_{0\pm}|^2_{\text{RWA}} = 1/2$. The latter corresponds to the polaritons being equal mixtures of the light and matter modes at zero detuning, which agrees with the standard descriptions of polaritons within the RWA[5]. However, Fig. 8.3(a), which is obtained including all light-matter interaction terms, contrarily demonstrates a linewidth asymmetry that is very sensitive to changes in the coupling strength. The results show that the asymmetry can be significant at coupling strengths before the ultrastrong-coupling regime ($g_C/\omega_0 < 0.1$), similar to the results presented in Paper D. However, strangely enough, the behaviors of the two polariton branches are inverted, with the upper polariton taking the role of the lower polariton and vice versa. The discrepancy between the two descriptions could be understood by considering a fully plas-

[5]Thus, this result further supports the argumentation about labeling the different light-matter coupling regimes by the level of approximation posed in Section 2.3.3

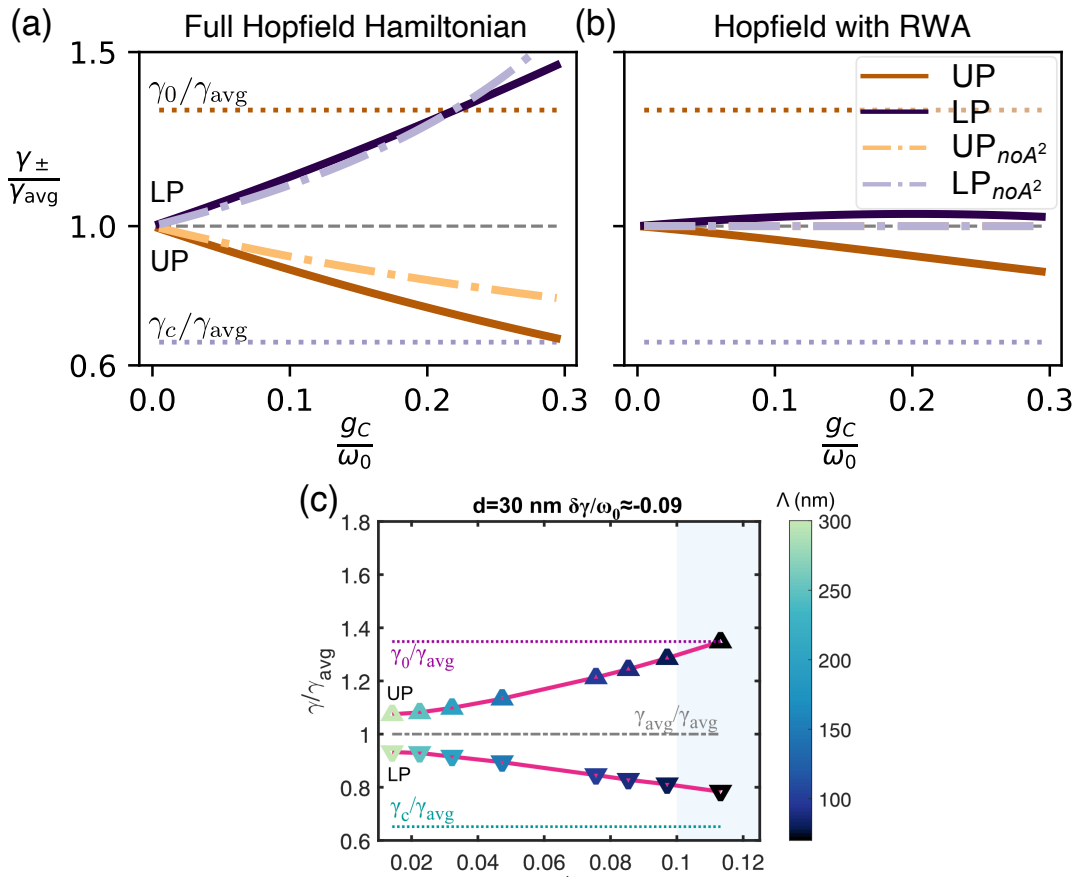

Figure 8.3: Plots of the polaritonic decay rates γ_+ and γ_-, corresponding to the decay of the upper (UP) and lower (LP) polaritons, respectively. Panel (a) shows the decay rates found with the full Hopfield Hamiltonian (solid curves), and neglecting A^2 (dash-dotted curves). Panel (b) shows the decay rates found in the RWA with A^2 (solid curves), and without A^2 (dash-dotted curves). The parameters used for panel (a) and (b) were $\omega_c = \omega_0$, $\gamma_0/\omega_0 = 0.17$, and $\gamma_c/\omega_0 = 0.08$. These parameters correspond to Fig. 4 in Paper D and are realistic for the plasmon-cavity system. Panel (c) shows classical results from Paper D. The behavior is qualitatively the same, but curiously the behaviors of the polaritonic branches are reversed.

monic system with two identical nanodisks. In this situation, the dissipative behaviors of the two polaritons can be swapped, depending on their configuration. The change of behaviors, in this case, occurs as the two coupled modes can align or anti-align in phase, and depending on the configuration, one or the other is energetically more favorable, thus, changing the roles of the upper and lower polaritons. The translation of this scenario to the Hopfield model could resolve the issue.

8.3.1 Outlook

The results presented in this work regarding the Hopfield diagonalization are consistent with other works employing a quantum description of polaritons modeled with the Hopfield model [57, 124, 162–164]. However, with the current numerical results, it is hard to see if a similar phase dependence is absorbed in the parameters of the Hopfield model, as in the classically described example of two coupled plasmons. The numerical results also hide how the polaritonic decay rates depend on the bare decay rates explicitly, as noted above. Therefore, it would be interesting to derive the Hopfield coefficients explicitly, which in turn would additionally give analytical expressions for the polaritonic decay rates expressed in the system parameters. The latter would help elucidate the mechanism governing linewidth asymmetries in homogeneous systems, without disorder. Expressions for the decay rates in terms of the Hopfield coefficients are given at the end of this chapter.

It is also interesting to note that a similar behavior to the results in Fig. 8.2 has been observed with exciton-polaritons [150]. In that case, the linewidth asymmetry at zero-detuning was attributed to a cross-damping term in a phenomenological non-Hermitian Hamiltonian. The fact that we can reproduce a similar asymmetry by just keeping the full form of the Hamiltonian, could shine new light on their empirical study.

That being said, there is also an analog to cross-damping within the Lindblad master-equation formalism. As was discussed in Section 3.2, dissipative coupling can arise between different subsystems when they are coupled to the same environment. Thus, the formalism presented here has the potential to be extended to such systems. On this note, it would also be interesting to connect their cross-damping Hamiltonian to an effective non-Hermitian Hamiltonian by neglecting the jump terms in a Lindblad master equation. A systematic study, combining the effects of dissipative and coherent (as presented here) light-matter interactions could elucidate the mechanism behind the dissipative properties of polaritons in a broad range of polaritonic platforms, provided that an appropriate Hamiltonian formulation can be motivated. Such systematic mapping could then be used as a roadmap for engineering polaritonic resonances at will.

Decay rates in terms of the Hopfield coefficients

A Bogoliubov transformation solves the considered two-mode Hopfield Hamiltonian. The eigenfrequencies were already given in Eq. (8.3) and the corresponding polariton operators are given by Eqs. (7.18) and (7.19). But here, we are interested in the inverse Bogoliubov transformation given by Eqs. (7.20) and (7.21), repeated here for clarity,

$$\tilde{a} = c_1^* \hat{P}_+ + d_1^* \hat{P}_- - c_3 \hat{P}_+^\dagger - d_3 \hat{P}_-^\dagger, \tag{8.8}$$

$$\hat{b} = c_2^* \hat{P}_+ + d_2^* \hat{P}_- - c_4 \hat{P}_+^\dagger - d_4 \hat{P}_-^\dagger. \tag{8.9}$$

Note that the annihilation operator $\tilde{a}$ is the rotated operator obtained after diagonalizing the cavity part of Eq. (8.1). The bare cavity annihilation operator $\hat{a}$ is given by Eq. (7.13) in terms of the single-mode Hopfield coefficient u_1 and u_2:

$$\hat{a} = u_1 \tilde{a} - u_2 \tilde{a}^\dagger. \tag{8.10}$$

Employing Eqs. (8.8)-(8.10) it is possible to evaluate the expectation values in Eqs. 8.6 and 8.7 analytically to obtain the decay rates in terms of the Hopfield coefficients

$$\boxed{\gamma_+ = \gamma_c(\omega_+)|u_1 - u_2|^2 |c_1^* - c_3^*|^2 + \gamma_0(\omega_+)|c_2^* + c_4^*|,} \tag{8.11}$$

$$\boxed{\gamma_- = \gamma_c(\omega_-)|u_1 - u_2|^2 |d_1^* - d_3^*|^2 + \gamma_0(\omega_+)|d_2^* + d_4^*|.} \tag{8.12}$$

The single-mode coefficients u_1, u_2 are given explicitly in Box 1 in Chapter 7. With the Hopfield Hamiltonian used here, the scalar numbers w and v can be identified as $w = \omega_c/2 + g_C^2/\omega_0$ and $v = g_C^2/\omega_0$. Thus, the absolute value of the difference can be evaluated as $|u_1 - u_2|^2 = [1 + 4g_C^2/(\omega_0\omega_c)]^{-1/2}$. Explicit expressions for the Hopfield coefficients $\{c_i^*, d_i^*\}$, $i = 1, 2, 3, 4$, expressed in terms of the system parameters, are attainable with the Bogoliubov transform outlined in Box 2 in Chapter 7. It will be an interesting investigation for future work to see if these expressions can provide deeper insights into the exact parameter dependencies governing the observed behaviors of the polaritonic decay rates. For example, such an investigation could elucidate the new detuning condition where the decay rates are equal, as well as provide insight into the potential for engineering resonances that are narrower, or broader than the bare decay rates.

Chapter 9

Concluding remarks

This thesis has presented a theoretical exploration of the intriguing effects of light-matter interactions with identical emitters of light in new regimes of cavity QED that are attainable in state-of-the-art experiments. In particular, this thesis has focused on the *few-emitter* regime, where correlations between the emitters and the field are tractable, and on the exciting properties of polaritons formed in the strong and *ultrastrong* coupling regimes. As the interaction with the environment is unavoidable in any realistic setting, all the presented works have taken an open-quantum-system approach to include the effects of dissipation.

Throughout the appended Papers A to D, it is clear that the environment and dissipation play a key role in settling the system's behavior. Notably, the results of Paper A and Paper C are two illustrative examples where dissipation does not destroy the correlations that form between the emitters and the light field, contrary to common beliefs. In Paper A, the competition between coherent external driving, collective coupling to N emitters, and dissipation to the environment leads to a fascinating interference effect with multiphoton absorption in the cavity that is directly related to the emitter number. This work also shows that including a small spontaneous emission rate changes the behavior of the system in the weak-drive regime. With spontaneous emission, the response in this regime is that of two lossy coupled oscillators. However, without it, emitters would act as perfect mirrors up to N photons, which would extend the behavior seen in region II in Fig. 5.4 to the weak drive regime. In Paper C, on the other hand, it is not interference but the fact that coherent states are eigenstates to the decay operator $\hat{a}$ that keeps the correlations between the emitters and the field. In this case, dissipation stabilizes the system, driven far from equilibrium, in one of the parallel quasiharmonic ladders corresponding to a different m_S projection of the collective pseudospin.

The work in Paper D has a different character, dealing with an essentially classical system, but is the work that dives the deepest into losses. In this work, we show the potential for engineering of narrow or broad polaritonic resonances that can have very

different properties than the bare constituents that form them. Nevertheless, even though our study shows that linewidth asymmetry is a classical electromagnetism phenomenon, the quantum description of the polaritonic system given in Chapter 8 provides a complimentary perspective that showcases the close interconnection between light and matter interaction and the dissipative properties of polaritons.

Bibliography

[1] S. A. Maier, *Plasmonics: fundamentals and applications*, repr. ed. (Springer, New York, 2007).

[2] L. Novotny and B. Hecht, "Principles of nano-optics" (Cambridge University Press, Cambridge; New York, 2006) Chap. 12.

[3] D. E. Chang, A. S. Sørensen, P. R. Hemmer, and M. D. Lukin, "Quantum Optics with Surface Plasmons", Physical Review Letters **97**, 053002 (2006).

[4] M. S. Tame, K. R. McEnery, S. K. Özdemir, J. Lee, S. A. Maier, and M. S. Kim, "Quantum plasmonics", Nature Physics **9**, 329–340 (2013).

[5] B. Rousseaux, D. G. Baranov, M. Käll, T. Shegai, and G. Johansson, "Quantum description and emergence of nonlinearities in strongly coupled single-emitter nanoantenna systems", Physical Review B **98**, 045435 (2018).

[6] J.-B. You, X. Xiong, P. Bai, Z.-K. Zhou, R.-M. Ma, W.-L. Yang, Y.-K. Lu, Y.-F. Xiao, C. E. Png, F. J. Garcia-Vidal, C.-W. Qiu, and L. Wu, "Reconfigurable Photon Sources Based on Quantum Plexcitonic Systems", Nano Letters **20**, 4645–4652 (2020).

[7] R. Sáez-Blázquez, J. Feist, A. I. Fernández-Domínguez, and F. J. García-Vidal, "Enhancing photon correlations through plasmonic strong coupling", Optica **4**, 1363 (2017).

[8] P. Lalanne, W. Yan, K. Vynck, C. Sauvan, and J.-P. Hugonin, "Light Interaction with Photonic and Plasmonic Resonances", Laser & Photonics Reviews **12**, 1700113 (2018).

[9] S. Franke, S. Hughes, M. K. Dezfouli, P. T. Kristensen, K. Busch, A. Knorr, and M. Richter, "Quantization of Quasinormal Modes for Open Cavities and Plas-

monic Cavity Quantum Electrodynamics", Physical Review Letters **122**, 213901 (2019).

[10] I. Medina, F. J. García-Vidal, A. I. Fernández-Domínguez, and J. Feist, "Few-Mode Field Quantization of Arbitrary Electromagnetic Spectral Densities", Physical Review Letters **126**, 093601 (2021).

[11] E. Waks and D. Sridharan, "Cavity QED treatment of interactions between a metal nanoparticle and a dipole emitter", Physical Review A **82**, 043845 (2010).

[12] A. Frisk Kockum, A. Miranowicz, S. De Liberato, S. Savasta, and F. Nori, "Ultrastrong coupling between light and matter", Nature Reviews Physics **1**, 19–40 (2019).

[13] D. G. Baranov, B. Munkhbat, E. Zhukova, A. Bisht, A. Canales, B. Rousseaux, G. Johansson, T. J. Antosiewicz, and T. Shegai, "Ultrastrong coupling between nanoparticle plasmons and cavity photons at ambient conditions", Nature Communications **11**, 2715 (2020).

[14] A. Canales, T. Karmstrand, D. G. Baranov, T. J. Antosiewicz, and T. O. Shegai, "Polaritonic linewidth asymmetry in the strong and ultrastrong coupling regime", Nanophotonics **12**, 4073–4086 (2023).

[15] S. De Liberato, "Virtual photons in the ground state of a dissipative system", Nature Communications **8**, 1465 (2017).

[16] F. Todisco, M. De Giorgi, M. Esposito, L. De Marco, A. Zizzari, M. Bianco, L. Dominici, D. Ballarini, V. Arima, G. Gigli, and D. Sanvitto, "Ultrastrong Plasmon–Exciton Coupling by Dynamic Molecular Aggregation", ACS Photonics **5**, 143–150 (2018).

[17] D. G. Baranov, M. Wersäll, J. Cuadra, T. J. Antosiewicz, and T. Shegai, "Novel Nanostructures and Materials for Strong Light–Matter Interactions", ACS Photonics **5**, 24–42 (2018).

[18] A. Bisht, J. Cuadra, M. Wersäll, A. Canales, T. J. Antosiewicz, and T. Shegai, "Collective Strong Light-Matter Coupling in Hierarchical Microcavity-Plasmon-Exciton Systems", Nano Letters **19**, 189–196 (2019).

[19] M. Stührenberg, B. Munkhbat, D. G. Baranov, J. Cuadra, A. B. Yankovich, T. J. Antosiewicz, E. Olsson, and T. Shegai, "Strong Light–Matter Coupling between Plasmons in Individual Gold Bi-pyramids and Excitons in Mono- and Multilayer WSe_2", Nano Letters **18**, 5938–5945 (2018).

[20] O. S. Ojambati, R. Chikkaraddy, W. D. Deacon, M. Horton, D. Kos, V. A. Turek, U. F. Keyser, and J. J. Baumberg, "Quantum electrodynamics at room temperature coupling a single vibrating molecule with a plasmonic nanocavity", Nature Communications **10**, 1049 (2019).

[21] P. Törmä and W. L. Barnes, "Strong coupling between surface plasmon polaritons and emitters: a review", Reports on Progress in Physics **78**, 013901 (2015).

[22] L. Novotny, "Strong coupling, energy splitting, and level crossings: A classical perspective", American Journal of Physics **78**, 1199–1202 (2010).

[23] E. Altewischer, M. P. van Exter, and J. P. Woerdman, "Plasmon-assisted transmission of entangled photons", Nature **418**, 304–306 (2002).

[24] A. Huck, S. Smolka, P. Lodahl, A. S. Sørensen, A. Boltasseva, J. Janousek, and U. L. Andersen, "Demonstration of Quadrature-Squeezed Surface Plasmons in a Gold Waveguide", Physical Review Letters **102**, 246802 (2009).

[25] R. Chikkaraddy, B. de Nijs, F. Benz, S. J. Barrow, O. A. Scherman, E. Rosta, A. Demetriadou, P. Fox, O. Hess, and J. J. Baumberg, "Single-molecule strong coupling at room temperature in plasmonic nanocavities", Nature **535**, 127–130 (2016).

[26] C. Anton-Solanas, M. Waldherr, M. Klaas, H. Suchomel, T. H. Harder, H. Cai, E. Sedov, S. Klembt, A. V. Kavokin, S. Tongay, K. Watanabe, T. Taniguchi, S. Höfling, and C. Schneider, "Bosonic condensation of exciton–polaritons in an atomically thin crystal", Nature Materials **20**, 1233–1239 (2021).

[27] T. K. Hakala, A. J. Moilanen, A. I. Väkeväinen, R. Guo, J.-P. Martikainen, K. S. Daskalakis, H. T. Rekola, A. Julku, and P. Törmä, "Bose–Einstein condensation in a plasmonic lattice", Nature Physics **14**, 739–744 (2018).

[28] J. D. Jackson, *Classical electrodynamics*, 3rd ed. (Wiley, Hoboken, NY, 2009).

[29] D. J. Griffiths, *Introduction to electrodynamics*, 4th ed., Always learning (Pearson, Boston, 2013).

[30] C. Cohen-Tannoudji, J. Dupont-Roc, and G. Grynberg, *Photons and atoms: introduction to quantum electrodynamics*, Physics textbook (Wiley, Weinheim, 2004).

[31] W. Schleich, *Quantum optics in phase space*, 1st ed. (Wiley-VCH, Berlin; New York, 2001).

[32] L. Garziano, A. Settineri, O. Di Stefano, S. Savasta, and F. Nori, "Gauge invariance of the Dicke and Hopfield models", Physical Review A **102**, 023718 (2020).

[33] M. S. Rider and W. L. Barnes, "Something from nothing: linking molecules with virtual light", Contemporary Physics **62**, 217–232 (2021).

[34] R. J. Thompson, G. Rempe, and H. J. Kimble, "Observation of normal-mode splitting for an atom in an optical cavity", Physical Review Letters **68**, 1132–1135 (1992).

[35] M. F. Limonov, M. V. Rybin, A. N. Poddubny, and Y. S. Kivshar, "Fano resonances in photonics", Nature Photonics **11**, 543–554 (2017).

[36] I. I. Rabi, "Space Quantization in a Gyrating Magnetic Field", Physical Review **51**, 652–654 (1937).

[37] E. M. Purcell, H. C. Torrey, and R. V. Pound, "Resonance Absorption by Nuclear Magnetic Moments in a Solid", Physical Review **69**, 37–38 (1946).

[38] H. Carmichael, "Statistical methods in quantum optics 2: non-classical fields" (Springer, Berlin, 2008) Chap. 13.

[39] O. Di Stefano, A. Settineri, V. Macrì, L. Garziano, R. Stassi, S. Savasta, and F. Nori, "Resolution of Gauge Ambiguities in Ultrastrong-Coupling Cavity QED", Nature Physics **15**, 803–808 (2019).

[40] E. Jaynes and F. Cummings, "Comparison of quantum and semiclassical radiation theories with application to the beam maser", Proceedings of the IEEE **51**, 89–109 (1963).

[41] C. C. Gerry and P. Knight, *Introductory quantum optics* (Cambridge University Press, Cambridge, UK; New York, 2005).

[42] F. Beaudoin, J. M. Gambetta, and A. Blais, "Dissipation and Ultrastrong Coupling in Circuit QED", Physical Review A **84**, 043832 (2011).

[43] D. Braak, "Integrability of the Rabi Model", Physical Review Letters **107**, 100401 (2011).

[44] J. J. Hopfield, "Theory of the Contribution of Excitons to the Complex Dielectric Constant of Crystals", Physical Review **112**, 1555–1567 (1958).

[45] C. Tserkezis, A. I. Fernández-Domínguez, P. A. D. Gonçalves, F. Todisco, J. D. Cox, K. Busch, N. Stenger, S. I. Bozhevolnyi, N. A. Mortensen, and C. Wolff, "On the applicability of quantum-optical concepts in strong-coupling nanophotonics", Reports on Progress in Physics **83**, 082401 (2020).

[46] J. Fregoni, F. J. Garcia-Vidal, and J. Feist, "Theoretical Challenges in Polaritonic Chemistry", ACS Photonics **9**, 1096–1107 (2022).

[47] F. Minganti, A. Miranowicz, R. W. Chhajlany, and F. Nori, "Quantum exceptional points of non-Hermitian Hamiltonians and Liouvillians: The effects of quantum jumps", Physical Review A **100**, 062131 (2019).

[48] K. Özdemir, S. Rotter, F. Nori, and L. Yang, "Parity–time symmetry and exceptional points in photonics", Nature Materials **18**, 783–798 (2019).

[49] M.-A. Miri and A. Alù, "Exceptional points in optics and photonics", Science **363**, eaar7709 (2019).

[50] G. Lindblad, "On the generators of quantum dynamical semigroups", Communications in Mathematical Physics **48**, 119–130 (1976).

[51] C. W. Gardiner and P. Zoller, *Quantum noise: a handbook of Markovian and non-Markovian quantum stochastic methods with applications to quantum optics*, 3rd ed., Springer series in synergetics (Springer, Berlin; New York, 2004).

[52] H.-P. Breuer and F. Petruccione, *The theory of open quantum systems* (Clarendon Press, Oxford, 2010).

[53] H. Carmichael, *Statistical methods in quantum optics 1: master equations and Fokker-Planck equations*, Vol. 1 (Springer, Berlin; London, 2011).

[54] M. Gross and S. Haroche, "Superradiance: An essay on the theory of collective spontaneous emission", Physics Reports **93**, 301–396 (1982).

[55] A. Settineri, V. Macrí, A. Ridolfo, O. Di Stefano, A. F. Kockum, F. Nori, and S. Savasta, "Dissipation and thermal noise in hybrid quantum systems in the ultrastrong-coupling regime", Physical Review A **98**, 053834 (2018).

[56] A. Mercurio, *Cavity QED: unconventional phenomena and new perspectives on quantum technologies*, Phd thesis, Messina U. (2023), available at `https://inspirehep.net/literature/2746558f`.

[57] S. De Liberato, "Light-Matter Decoupling in the Deep Strong Coupling Regime: The Breakdown of the Purcell Effect", Physical Review Letters **112**, 016401 (2014).

[58] H. M. Wiseman and G. J. Milburn, *Quantum measurement and control*, first paperback edition ed. (Cambridge University Press, Cambridge, 2014).

[59] F. Minganti, A. Miranowicz, R. W. Chhajlany, I. I. Arkhipov, and F. Nori, "Hybrid-Liouvillian formalism connecting exceptional points of non-Hermitian Hamiltonians and Liouvillians via postselection of quantum trajectories", Physical Review A **101**, 062112 (2020).

[60] R. H. Dicke, "Coherence in Spontaneous Radiation Processes", Physical Review **93**, 99–110 (1954).

[61] S. De Léséleuc, V. Lienhard, P. Scholl, D. Barredo, S. Weber, N. Lang, H. P. Büchler, T. Lahaye, and A. Browaeys, "Observation of a symmetry-protected topological phase of interacting bosons with Rydberg atoms", Science **365**, 775–780 (2019).

[62] J. Rui, D. Wei, A. Rubio-Abadal, S. Hollerith, J. Zeiher, D. M. Stamper-Kurn, C. Gross, and I. Bloch, "A subradiant optical mirror formed by a single structured atomic layer", Nature **583**, 369–374 (2020).

[63] M. Zanner, T. Orell, C. M. F. Schneider, R. Albert, S. Oleschko, M. L. Juan, M. Silveri, and G. Kirchmair, "Coherent control of a multi-qubit dark state in waveguide quantum electrodynamics", Nature Physics **18**, 538–543 (2022).

[64] Z. Wang, H. Li, W. Feng, X. Song, C. Song, W. Liu, Q. Guo, X. Zhang, H. Dong, D. Zheng, H. Wang, and D.-W. Wang, "Controllable Switching between Superradiant and Subradiant States in a 10-qubit Superconducting Circuit", Physical Review Letters **124**, 013601 (2020).

[65] O. Katz, L. Feng, A. Risinger, C. Monroe, and M. Cetina, "Demonstration of three- and four-body interactions between trapped-ion spins", Nature Physics **19**, 1452–1458 (2023).

[66] C. M. Holland, Y. Lu, and L. W. Cheuk, "On-demand entanglement of molecules in a reconfigurable optical tweezer array", Science **382**, 1143–1147 (2023).

[67] N. B. Vilas, P. Robichaud, C. Hallas, G. K. Li, L. Anderegg, and J. M. Doyle, "An optical tweezer array of ultracold polyatomic molecules", Nature **628**, 282–286 (2024).

[68] J. Heintz, N. Markešević, E. Y. Gayet, N. Bonod, and S. Bidault, "Few-Molecule Strong Coupling with Dimers of Plasmonic Nanoparticles Assembled on DNA", ACS Nano , acsnano.1c04552 (2021).

[69] K. Santhosh, O. Bitton, L. Chuntonov, and G. Haran, "Vacuum Rabi splitting in a plasmonic cavity at the single quantum emitter limit", Nature Communications **7**, ncomms11823 (2016).

[70] G. Zengin, M. Wersäll, S. Nilsson, T. J. Antosiewicz, M. Käll, and T. Shegai, "Realizing strong light-matter interactions between single nanoparticle plasmons and molecular excitons at ambient conditions", Physical Review Letters **114**, 157401 (2015).

[71] M. Wersäll, J. Cuadra, T. J. Antosiewicz, S. Balci, and T. Shegai, "Observation of Mode Splitting in Photoluminescence of Individual Plasmonic Nanoparticles Strongly Coupled to Molecular Excitons", Nano Letters **17**, 551–558 (2017).

[72] J. M. Fink, R. Bianchetti, M. Baur, M. Göppl, L. Steffen, S. Filipp, P. J. Leek, A. Blais, and A. Wallraff, "Dressed Collective Qubit States and the Tavis-Cummings Model in Circuit QED", Physical Review Letters **103**, 083601 (2009).

[73] Y. Liu, Z. Wang, P. Yang, Q. Wang, Q. Fan, S. Guan, G. Li, P. Zhang, and T. Zhang, "Realization of Strong Coupling between Deterministic Single-Atom Arrays and a High-Finesse Miniature Optical Cavity", Physical Review Letters **130**, 173601 (2023).

[74] Z. Yan, J. Ho, Y.-H. Lu, S. J. Masson, A. Asenjo-Garcia, and D. M. Stamper-Kurn, "Superradiant and Subradiant Cavity Scattering by Atom Arrays", Physical Review Letters **131**, 253603 (2023).

[75] R. Reimann, W. Alt, T. Kampschulte, T. Macha, L. Ratschbacher, N. Thau, S. Yoon, and D. Meschede, "Cavity-Modified Collective Rayleigh Scattering of Two Atoms", Physical Review Letters **114**, 023601 (2015).

[76] A. Neuzner, M. Körber, O. Morin, S. Ritter, and G. Rempe, "Interference and dynamics of light from a distance-controlled atom pair in an optical cavity", Nature Photonics **10**, 303–306 (2016).

[77] B. Casabone, K. Friebe, B. Brandstätter, K. Schüppert, R. Blatt, and T. Northup, "Enhanced Quantum Interface with Collective Ion-Cavity Coupling", Physical Review Letters **114**, 023602 (2015).

[78] S. Begley, M. Vogt, G. K. Gulati, H. Takahashi, and M. Keller, "Optimized Multi-Ion Cavity Coupling", Physical Review Letters **116**, 223001 (2016).

[79] M. Reitz, C. Sommer, and C. Genes, "Cooperative Quantum Phenomena in Light-Matter Platforms", PRX Quantum **3**, 010201 (2022).

[80] M. Tavis and F. W. Cummings, "Exact Solution for an N -Molecule—Radiation-Field Hamiltonian", Physical Review **170**, 379–384 (1968).

[81] F. Bloch, "Nuclear Induction", Physical Review **70**, 460–474 (1946).

[82] R. P. Feynman, F. L. Vernon, and R. W. Hellwarth, "Geometrical Representation of the Schrödinger Equation for Solving Maser Problems", Journal of Applied Physics **28**, 49–52 (1957).

[83] J. J. Sakurai and S. F. Tuan, *Modern quantum mechanics*, rev. ed ed. (Addison-Wesley Pub. Co, Reading, MA, 1994).

[84] E. Merzbacher, *Quantum mechanics*, 3rd ed. (Wiley, New York, 1998).

[85] G. Scharf, "On a quantum mechanical maser model", Helvetica Physica Acta **43**, 806–828 (1970).

[86] L. M. Narducci, M. Orszag, and R. A. Tuft, "Energy Spectrum of the Dicke Hamiltonian", Physical Review A **8**, 1892–1906 (1973).

[87] I. M. Palstra, H. M. Doeleman, and A. F. Koenderink, "Hybrid cavity-antenna systems for quantum optics outside the cryostat?", Nanophotonics **8**, 1513–1531 (2019).

[88] D. E. Chang, A. S. Sørensen, E. A. Demler, and M. D. Lukin, "A single-photon transistor using nanoscale surface plasmons", Nature Physics **3**, 807–812 (2007).

[89] A. V. Zasedatelev, A. V. Baranikov, D. Urbonas, F. Scafirimuto, U. Scherf, T. Stöferle, R. F. Mahrt, and P. G. Lagoudakis, "A room-temperature organic polariton transistor", Nature Photonics **13**, 378–383 (2019).

[90] A. I. Lvovsky, B. C. Sanders, and W. Tittel, "Optical quantum memory", Nature Photonics **3**, 706–714 (2009).

[91] W. Chen, K. M. Beck, R. Bücker, M. Gullans, M. D. Lukin, H. Tanji-Suzuki, and V. Vuletić, "All-Optical Switch and Transistor Gated by One Stored Photon", Science **341**, 768–770 (2013).

[92] D. F. Phillips, A. Fleischhauer, A. Mair, R. L. Walsworth, and M. D. Lukin, "Storage of Light in Atomic Vapor", Physical Review Letters **86**, 783–786 (2001).

[93] C. Liu, Z. Dutton, C. H. Behroozi, and L. V. Hau, "Observation of coherent optical information storage in an atomic medium using halted light pulses", Nature **409**, 490–493 (2001).

[94] C. L. Alzar G. et al., M. A. G. Martinez, and P. Nussenzveig, "Classical analog of electromagnetically induced transparency", American Journal of Physics **70**, 37–41 (2002).

[95] R. D. Artuso and G. W. Bryant, "Strongly coupled quantum dot-metal nanoparticle systems: Exciton-induced transparency, discontinuous response, and suppression as driven quantum oscillator effects", Physical Review B **82**, 195419 (2010).

[96] M. Pelton, S. D. Storm, and H. Leng, "Strong coupling of emitters to single plasmonic nanoparticles: exciton-induced transparency and Rabi splitting", Nanoscale **11**, 14540–14552 (2019).

[97] A. Ridolfo, O. Di Stefano, N. Fina, R. Saija, and S. Savasta, "Quantum Plasmonics with Quantum Dot-Metal Nanoparticle Molecules: Influence of the Fano Effect on Photon Statistics", Physical Review Letters **105**, 263601 (2010).

[98] R. A. Shah, N. F. Scherer, M. Pelton, and S. K. Gray, "Ultrafast reversal of a Fano resonance in a plasmon-exciton system", Physical Review B **88**, 075411 (2013).

[99] X. Wu, S. K. Gray, and M. Pelton, "Quantum-dot-induced transparency in a nanoscale plasmonic resonator", Optics Express **18**, 23633 (2010).

[100] P. Rice and R. Brecha, "Cavity induced transparency", Optics Communications **126**, 230–235 (1996).

[101] P. R. Rice and H. J. Carmichael, "Photon statistics of a cavity-QED laser: A comment on the laser–phase-transition analogy", Physical Review A **50**, 4318–4329 (1994).

[102] D. F. Walls, P. D. Drummond, S. S. Hassan, and H. J. Carmichael, "Non-Equilibrium Phase Transitions in Cooperative Atomic Systems", Progress of Theoretical Physics Supplement **64**, 307–320 (1978).

[103] J. J. Sanchez-Mondragon, N. B. Narozhny, and J. H. Eberly, "Theory of Spontaneous-Emission Line Shape in an Ideal Cavity", Physical Review Letters **51**, 550–553 (1983).

[104] R. Loudon, *The quantum theory of light*, 3rd ed., Oxford science publications (Oxford University Press, Oxford; New York, 2000).

[105] R. J. Glauber, "Coherent and Incoherent States of the Radiation Field", Physical Review **131**, 2766–2788 (1963).

[106] R. Bonifacio, M. Gronchi, and L. A. Lugiato, "Photon statistics of a bistable absorber", Physical Review A **18**, 2266–2279 (1978).

[107] T. Shirai, S. Todo, H. de Raedt, and S. Miyashita, "Optical bistability in a low-photon-density regime", Physical Review A **98**, 043802 (2018).

[108] D. O. Krimer, M. Zens, and S. Rotter, "Critical phenomena and nonlinear dynamics in a spin ensemble strongly coupled to a cavity. I. Semiclassical approach", Physical Review A **100**, 013855 (2019).

[109] C. Savage and H. Carmichael, "Single atom optical bistability", IEEE Journal of Quantum Electronics **24**, 1495–1498 (1988).

[110] S. Sarkar and J. S. Satchell, "Optical Bistability with Small Numbers of Atoms", Europhysics Letters (EPL) **3**, 797–801 (1987).

[111] P. Alsing and H. J. Carmichael, "Spontaneous dressed-state polarization of a coupled atom and cavity mode", Quantum Optics: Journal of the European Optical Society Part B **3**, 13–32 (1991).

[112] P. Alsing, D.-S. Guo, and H. J. Carmichael, "Dynamic Stark effect for the Jaynes-Cummings system", Physical Review A **45**, 5135–5143 (1992).

[113] H. Carmichael, "Breakdown of Photon Blockade: A Dissipative Quantum Phase Transition in Zero Dimensions", Physical Review X **5**, 031028 (2015).

[114] A. R. R. Carvalho, P. Milman, R. L. De Matos Filho, and L. Davidovich, "Decoherence, Pointer Engineering, and Quantum State Protection", Physical Review Letters **86**, 4988–4991 (2001).

[115] J. B. Curtis, I. Boettcher, J. T. Young, M. F. Maghrebi, H. Carmichael, A. V. Gorshkov, and M. Foss-Feig, "Critical theory for the breakdown of photon blockade", Physical Review Research **3**, 023062 (2021).

[116] F. Minganti, A. Biella, N. Bartolo, and C. Ciuti, "Spectral theory of Liouvillians for dissipative phase transitions", Physical Review A **98**, 042118 (2018).

[117] V. V. Albert and L. Jiang, "Symmetries and conserved quantities in Lindblad master equations", Physical Review A **89**, 022118 (2014).

[118] L. Sá, P. Ribeiro, and T. Prosen, "Symmetry Classification of Many-Body Lindbladians: Tenfold Way and Beyond", Physical Review X **13**, 031019 (2023).

[119] F. Minganti, V. Savona, and A. Biella, "Dissipative phase transitions in n -photon driven quantum nonlinear resonators", Quantum **7**, 1170 (2023).

[120] Y. Zhu, D. J. Gauthier, S. E. Morin, Q. Wu, H. J. Carmichael, and T. W. Mossberg, "Vacuum Rabi splitting as a feature of linear-dispersion theory: Analysis and experimental observations", Physical Review Letters **64**, 2499–2502 (1990).

[121] U. Fano, "Atomic Theory of Electromagnetic Interactions in Dense Materials", Physical Review **103**, 1202–1218 (1956).

[122] B. Munkhbat, D. G. Baranov, M. Stührenberg, M. Wersäll, A. Bisht, and T. Shegai, "Self-Hybridized Exciton-Polaritons in Multilayers of Transition Metal Dichalcogenides for Efficient Light Absorption", ACS Photonics **6**, 139–147 (2019).

[123] M. Balasubrahmaniyam, C. Genet, and T. Schwartz, "Coupling and decoupling of polaritonic states in multimode cavities", Physical Review B **103**, L241407 (2021).

[124] C. Ciuti, G. Bastard, and I. Carusotto, "Quantum vacuum properties of the intersubband cavity polariton field", Physical Review B **72**, 115303 (2005).

[125] V. Savona, Z. Hradil, A. Quattropani, and P. Schwendimann, "Quantum theory of quantum-well polaritons in semiconductor microcavities", Physical Review B **49**, 8774–8779 (1994).

[126] C. R. Gubbin, F. Martini, A. Politi, S. A. Maier, and S. De Liberato, "Strong and Coherent Coupling between Localized and Propagating Phonon Polaritons", Physical Review Letters **116**, 246402 (2016).

[127] M. A. Sentef, M. Ruggenthaler, and A. Rubio, "Cavity quantum-electrodynamical polaritonically enhanced electron-phonon coupling and its influence on superconductivity", Science Advances **4**, eaau6969 (2018).

[128] S. Lamowski, C.-R. Mann, F. Hellbach, E. Mariani, G. Weick, and F. Pauly, "Plasmon polaritons in cubic lattices of spherical metallic nanoparticles", Physical Review B **97**, 125409 (2018).

[129] W. E. Lamb, "Fine Structure of the Hydrogen Atom. III", Physical Review **85**, 259–276 (1952).

[130] K.-H. Yang, "Gauge transformations and quantum mechanics I. Gauge invariant interpretation of quantum mechanics", Annals of Physics **101**, 62–96 (1976).

[131] D. De Bernardis, P. Pilar, T. Jaako, S. De Liberato, and P. Rabl, "Breakdown of gauge invariance in ultrastrong-coupling cavity QED", Physical Review A **98**, 053819 (2018).

[132] A. Stokes and A. Nazir, "Gauge ambiguities imply Jaynes-Cummings physics remains valid in ultrastrong coupling QED", Nature Communications **10**, 499 (2019).

[133] D. L. Andrews, G. A. Jones, A. Salam, and R. G. Woolley, "Perspective: Quantum Hamiltonians for Optical Interactions", The Journal of Chemical Physics **148**, 040901 (2018).

[134] D. M. Rouse, B. W. Lovett, E. M. Gauger, and N. Westerberg, "Avoiding gauge ambiguities in cavity quantum electrodynamics", Scientific Reports **11**, 4281 (2021).

[135] S. Savasta, O. Di Stefano, A. Settineri, D. Zueco, S. Hughes, and F. Nori, "Gauge principle and gauge invariance in two-level systems", Physical Review A **103**, 053703 (2021).

[136] E. Rousseau and D. Felbacq, "The quantum-optics Hamiltonian in the Multipolar gauge", Scientific Reports **7**, 11115 (2017).

[137] A. Vukics, G. Kónya, and P. Domokos, "The gauge-invariant Lagrangian, the Power–Zienau–Woolley picture, and the choices of field momenta in nonrelativistic quantum electrodynamics", Scientific Reports **11**, 16337 (2021).

[138] A. Mercurio, S. Abo, F. Mauceri, E. Russo, V. Macrì, A. Miranowicz, S. Savasta, and O. Di Stefano, "Pure Dephasing of Light-Matter Systems in the Ultrastrong and Deep-Strong Coupling Regimes", Physical Review Letters **130**, 123601 (2023).

[139] C. Tsallis, "Diagonalization methods for the general bilinear Hamiltonian of an assembly of bosons", Journal of Mathematical Physics **19**, 277–286 (1978).

[140] J. Colpa, "Diagonalization of the quadratic boson hamiltonian", Physica A: Statistical Mechanics and its Applications **93**, 327–353 (1978).

[141] A. Canales, D. G. Baranov, T. J. Antosiewicz, and T. Shegai, "Abundance of cavity-free polaritonic states in resonant materials and nanostructures", The Journal of Chemical Physics **154**, 024701 (2021).

[142] P. Bhatt, K. Kaur, and J. George, "Enhanced Charge Transport in Two-Dimensional Materials through Light–Matter Strong Coupling", ACS Nano **15**, 13616–13622 (2021).

[143] D. M. Coles, N. Somaschi, P. Michetti, C. Clark, P. G. Lagoudakis, P. G. Savvidis, and D. G. Lidzey, "Polariton-mediated energy transfer between organic dyes in a strongly coupled optical microcavity", Nature Materials **13**, 712–719 (2014).

[144] B. Munkhbat, M. Wersäll, D. G. Baranov, T. J. Antosiewicz, and T. Shegai, "Suppression of photo-oxidation of organic chromophores by strong coupling to plasmonic nanoantennas", Science Advances **4**, eaas9552 (2018).

[145] J. A. Hutchison, T. Schwartz, C. Genet, E. Devaux, and T. W. Ebbesen, "Modifying Chemical Landscapes by Coupling to Vacuum Fields", Angewandte Chemie International Edition **51**, 1592–1596 (2012).

[146] J. Feist, J. Galego, and F. J. Garcia-Vidal, "Polaritonic Chemistry with Organic Molecules", ACS Photonics **5**, 205–216 (2018).

[147] M. G. Raizen, R. J. Thompson, R. J. Brecha, H. J. Kimble, and H. J. Carmichael, "Normal-mode splitting and linewidth averaging for two-state atoms in an optical cavity", Physical Review Letters **63**, 240–243 (1989).

[148] J. P. Reithmaier, G. Sek, A. Löffler, C. Hofmann, S. Kuhn, S. Reitzenstein, L. V. Keldysh, V. D. Kulakovskii, T. L. Reinecke, and A. Forchel, "Strong coupling in a single quantum dot–semiconductor microcavity system", Nature **432**, 197–200 (2004).

[149] D. M. Whittaker, P. Kinsler, T. A. Fisher, M. S. Skolnick, A. Armitage, A. M. Afshar, M. D. Sturge, and J. S. Roberts, "Motional Narrowing in Semiconductor Microcavities", Phys. Rev. Lett. **77**, 4792–4795 (1996).

[150] W. Wang, P. Vasa, R. Pomraenke, R. Vogelgesang, A. De Sio, E. Sommer, M. Maiuri, C. Manzoni, G. Cerullo, and C. Lienau, "Interplay between Strong Coupling and Radiative Damping of Excitons and Surface Plasmon Polaritons in Hybrid Nanostructures", ACS Nano **8**, 1056–1064 (2014).

[151] A. V. Kavokin and J. J. Baumberg, "Exciton-light coupling in quantum wells: From motional narrowing to superradiance", Physical Review B **57**, R12697–R12700 (1998).

[152] D. M. Whittaker, "What Determines Inhomogeneous Linewidths in Semiconductor Microcavities?", Physical Review Letters **80**, 4791–4794 (1998).

[153] C. Ell, J. Prineas, T. R. Nelson, S. Park, H. M. Gibbs, G. Khitrova, S. W. Koch, and R. Houdré, "Influence of Structural Disorder and Light Coupling on the Excitonic Response of Semiconductor Microcavities", Physical Review Letters **80**, 4795–4798 (1998).

[154] V. Savona, C. Piermarocchi, A. Quattropani, F. Tassone, and P. Schwendimann, "Microscopic Theory of Motional Narrowing of Microcavity Polaritons in a Disordered Potential", Physical Review Letters **78**, 4470–4473 (1997).

[155] A. V. Kavokin, "Motional narrowing of inhomogeneously broadened excitons in a semiconductor microcavity: Semiclassical treatment", Physical Review B **57**, 3757–3760 (1998).

[156] M. Litinskaia, G. La Rocca, and V. Agranovich, "Inhomogeneous broadening of polaritons in high-quality microcavities and weak localization", Physical Review B **64**, 165316 (2001).

[157] W. Gao, X. Li, M. Bamba, and J. Kono, "Continuous transition between weak and ultrastrong coupling through exceptional points in carbon nanotube microcavity exciton–polaritons", Nature Photonics **12**, 362–367 (2018).

[158] S. Gambino, M. Mazzeo, A. Genco, O. Di Stefano, S. Savasta, S. Patanè, D. Ballarini, F. Mangione, G. Lerario, D. Sanvitto, and G. Gigli, "Exploring Light–Matter Interaction Phenomena under Ultrastrong Coupling Regime", ACS Photonics **1**, 1042–1048 (2014).

[159] M. Wurdack, E. Estrecho, S. Todd, T. Yun, M. Pieczarka, S. K. Earl, J. A. Davis, C. Schneider, A. G. Truscott, and E. A. Ostrovskaya, "Motional narrowing, ballistic transport, and trapping of room-temperature exciton polaritons in an atomically-thin semiconductor", Nature Communications **12**, 5366 (2021).

[160] B. Auguié and W. L. Barnes, "Collective Resonances in Gold Nanoparticle Arrays", Physical Review Letters **101**, 143902 (2008).

[161] V. G. Kravets, A. V. Kabashin, W. L. Barnes, and A. N. Grigorenko, "Plasmonic Surface Lattice Resonances: A Review of Properties and Applications", Chemical Reviews **118**, 5912–5951 (2018).

[162] E. Cortese and S. De Liberato, "Exact solution of polaritonic systems with arbitrary light and matter frequency-dependent losses", The Journal of Chemical Physics **156**, 084106 (2022).

[163] C. A. Downing, E. Mariani, and G. Weick, "Radiative frequency shifts in nanoplasmonic dimers", Physical Review B **96**, 155421 (2017).

[164] A. Brandstetter-Kunc, G. Weick, D. Weinmann, and R. A. Jalabert, "Decay of dark and bright plasmonic modes in a metallic nanoparticle dimer", Physical Review B **91**, 035431 (2015).